UNIVERSITY OF BIRMINGHAM

PREPARATION OF CARBON FIBRE PREFORM FROM ACETYLATED CELLULOSE AND NANO-CRYSTALLINE CELLULOSE

By

MAHYUNI HARAHAP

A thesis submitted to the University of Birmingham for the degree of MASTER OF SCIENCE (MSc) by Research

Sensor and Composites Group

School of Metallurgy and Materials

College of Engineering and Physical Sciences

University of Birmingham

April 2018

Abstract

The search for precursors that are bio-based, renewable and biodegradable has attracted significant attention due to increased environmental awareness. Recently, nano-crystalline cellulose (NCC) has been considered as a potential precursor for the production of carbon fibre owing to its high crystallinity and excellent mechanical properties. However, its crystallinity and strong hydrogen bonding in the NCC structure prevents it from being dissolved in common solvents, making it difficult to process. The main aims of this study were: (i) to acetylate NCC to improve its solubility in DMSO (dimethylsulfoxide); (ii) to electro-spin NCC suspension using polyacrylonitrile (PAN) as the "carrier" polymer; (iii) to extrude NCC and acetylated NCC gel via wet-spinning; and (iv) to pyrolyse the wet-spun NCC fibres. In this study, the rod-like particles of NCC with diameters in the range 2.0 - 4.8 nm and lengths of 46 - 114 nm were characterised using a transmission electron microscope (TEM). The surface acetylation of NCC was achieved and the degree of substitution (DS) was determined using ^{13}C solid-state nuclear magnetic resonance (NMR) spectroscopy. The DS obtained were between 0.01 and 0.07. The viscosity of the NCC before and after acetylation were 0.20 Pa.s and 0.40 Pa.s respectively. In addition, the crystallinity of NCC was characterised before and after acetylation using X-ray diffraction. The crystallinity indicates of the NCC before and after acetylation were 78% and 68% respectively.

The introduction of PAN, dissolved in DMSO, into NCC increased the conductivity of the solution from 15.41 µS/cm to 21.59 µS/cm. This solution was electro-spun to obtain fibres diameters in the range 500 to 200 nm. Wet-spun NCC fibres from unacetylated and acetylated NCC was pyrolysed at 900 ºC in an inert atmosphere. The heating rate, from room temperature to 400 ºC, was carried out at 0.5 K.minute^{-1}. The sample was held at 400 ºC for 1 hour and heated to 900 ºC at 1.0 K.minute^{-1} in order to carbonise the fibres. The morphologies and the cross-section areas of the spun-fibres before and after pyrolysis were investigated using an environmental scanning electron microscope (ESEM). They were found to be void-free. Raman spectroscopy was used to characterise the carbonised fibres. The 'G' and 'D' bands in the Raman spectrum were used to obtain the I_D/I_G ratio; this was 0.83 - 0.84.

The feasibility of using NCC to manufacture fibres via electro-spinning and wet-spinning was demonstrated.

Declaration

I declare that the work described herein was performed entirely by myself during the course of my MSc by Research studies at The University of Birmingham.

Mahyuni Harahap

Acknowledgements

I would like to express my grateful thanks to my supervisor Professor Gerard Fernando for his patience and generous and valuable advice during my Master's programme.

I would also like to thank to my co-supervisor Dr Surya Pandita and my colleagues, Inam and Kate who helped me with fibre formation. I also wish to thank Frank, Dan, Paul and Jeff for their patience in training me to use all the analytical equipment in the laboratory. My grateful thanks also go to the staff at the School of Metallurgy and Materials, University of Birmingham. Furthermore, I also wish to give special thanks to Dr Saharman Gea, Department of Chemistry, University of Sumatera Utara, Indonesia for providing me with valuable advice.

Financial support was received from the Indonesian Government through the Indonesian Endowment Fund for Education (LPDP).

Last but not least, I would like to express my special thanks and gratitude to my dearest parents, Hotmatua Harahap and Fatima Sari.

Table of Contents

List of Figures

Figure Page

List of Tables

Table Page

List of Equations

Abbreviations

AFM	Atomic force microscope
AmimCl	1-allyl-3-methylimidazolium chloride
CC	Cellulose carabamate
CO	Carbon monoxide
CO_2	Carbon dioxide
$C_6H_{12}O_6$	Cellulose
DCM	Dichloromethane
DMAc	Dimethylacetamide
DMF	Dimethylformamide
DMSO	Dimethyl sulfoxide
DP	Degree of polymerisation
DS	Degree of substitution
DTG	Differential thermal gravimetry
ESEM	Environmental scanning electron microscope
FTIR	Fourier transmission infrared
HBr	Hydrobromic acid
HCl	Hydrochloric acid
HM	High modulus
HT	High tensile
HTT	High temperature
H_3PO_4	Phosphoric acid
H_2SO_4	Sulphuric acid
H_2O	Water
IHT	Intermediate temperature
IM	Intermediate modulus
KBr	Potassium bromide
K_2CO_3	Potassium carbonate
LiCl	Lithium chloride
MES	Mechano-electro-spinner
$MgCl_2$	Magnesium chloride

Mw	Molecular weight
NaCl	Sodium chloride
NaOH	Sodium hydroxide
NCC	Nano-crystalline cellulose
NCC-Ac	Acetylated nano-crystalline cellulose
NMR	Nuclear magnetic resonance
PAA	Polyacrylic acid
PAN	Polyacrylonitrile
PCl	Polycaprolactone
PEO	Polyetylene oxide
PHB	Polyhydroxyl butyrate
PLA	Polylactic acid
PMMA	Polymethyl methacrylate
PVA	Polyvinyl alcohol
PS	Polystyrene
PTFE	Polytetrafluoroethylene
SEM	Scanning electron microscope
TBAF	Tetrabutylammonium fluoride chloride trihydrate
TEM	Transmission electron microscope
T_g	Glass transition temperature
TGA	Thermal gravimetric analysis
TsCl	p-toluenesulfonyl chloride
UHM	Ultra high modulus
XRD	X-Ray diffraction
δ	Hildebrand solubility parameter

CHAPTER 1
INTRODUCTION

1.1 Background

Carbon fibres are defined as consisting of at least 92% carbon by weight, a definition that is based on data obtained via the pyrolysis of carbon precursors [1]. The fibres are normally produced by extruding the precursor [2]. Carbon fibre is a lightweight material with a high tensile strength, tensile modulus and low density. The mechanical properties of carbon fibre are higher than those of steel and aluminium. Selected commercial properties of these three materials are summarised in Table 1.1.

Table 1.1 The mechanical properties of carbon fibre, steel and aluminium.

No.	Materials	Elastic modulus (GPa)	Tensile strength (MPa)	Density (g/cm^3)	Sources
1	Carbon fibre T700S	230	4,900	1.8	[3]
2	Annealed S15700 stainless steel	220	1,190	7.8	[4]
3	7005-T5 aluminium	71	400	2.9	[4]

These properties make carbon fibre an attractive material for high-value applications in sporting goods, aerospace and other engineering fields [5]. For example, the Boeing 777 uses over 50% by weight of carbon fibre composite in its structure [6]. The global application of carbon fibres is presented in Figure 1.1. Owing to the broad application of carbon fibres, the demand for these materials has increased significantly from

approximately 33 thousand tonnes in 2010 to around 64 thousand tonnes in 2016, and it is projected to experience an increase to roughly 120 thousand tonnes in 2022 [7].

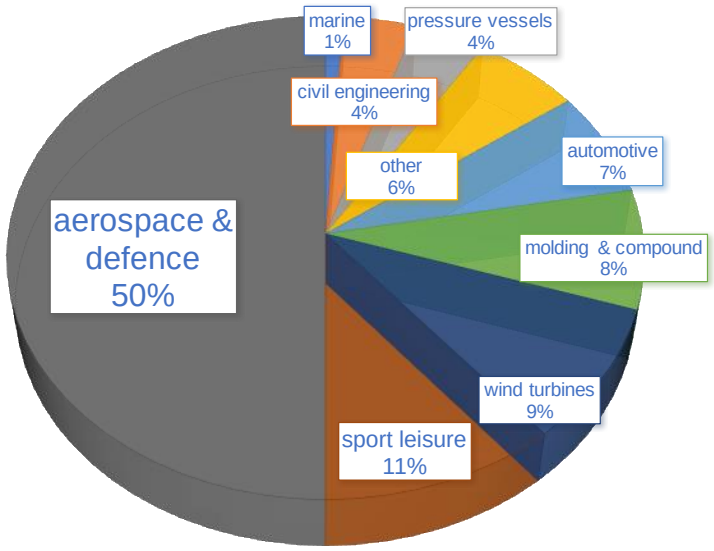

Figure 1.1 Global application of carbon fibres based on applications [8].

Nowadays, the dominant precursor for the production of carbon fibre is polyacrylonitrile (PAN) followed by pitch; both of which are petroleum-based [9]. Increasing environmental awareness has resulted in a renewed interest in materials that are produced from biorenewable polymers. Hence, there is significant merit in developing precursors for carbon fibres that are derived from renewal and biobased resources such as cellulose.

Cellulose is the most abundant natural biopolymer in the world. It is renewable, biodegradable and non-toxic [10]. It has attracted significant attention with regard to its suitability as a precursor for the production of carbon fibres [11]. Furthermore, cellulose has a crystalline structure that makes this material a promising precursor for the production of carbon fibre [12]. A higher crystalline content can be found in nano-crystalline cellulose (NCC), which can be extracted by acid hydrolysis of cellulose [13].

NCC has attracted much interest from industry and academia because in general, polymeric materials with high crystallinity enhance abrasion resistance, chemical resistance, hardness, glass transition temperature (T_g) and tensile strength [14].

Compared with cellulose fibres, NCC has several benefits, and selected properties for the two classes of materials are presented in Appendix 1 [15].

In the context of the current research project, the overall aim was to investigate the conditions required to obtain fibres based on NCC. In order to render this material processable, it is necessary to modify it chemically by acetylation to enable it to be dissolved. In the current research project, the hydroxyl groups in NCC were substituted by acetyl function groups.

There are several methods that have been reported by previous studies to acetylate cellulose, including: (i) dissolving cellulose in phosphoric acid [16]; (ii) using an ionic liquid to dissolve cellulose and applying acetyl chloride and acetic anhydride as the acetylating reagent [17]; (iii) applying acetic anhydride in a solution of cellulose with N,N-dimethylacetamide (DMAc)/lithium chloride (LiCl) [18]; and (iv) dissolving cellulose in DMAc/LiCl using various acetylating reagents such as acetyl chloride, dimethyl sulfoxide (DMSO)/tetrabutylammonium fluoride chloride trihydrate (TBAF), and lauric acid/p-toluenesulfonyl chloride (Tos-Cl) [19]. Moreover, inhomogeneous reactions have been applied to modify the surface of cellulose. For example: (i) dispersing cellulose in glacial acetic acid in the presence of sulfuric acid (H_2SO_4) as the catalyst [20]; (ii) solvent exchange using water, acetone and toluene before acetylating with acetic anhydride [21]; and (iii) dispersing cellulose in alkenyl succinic anhydride [22].

Recently, the acetylation reaction has been applied to NCC to modify the surface of NCC to improve its dispersion in organic solvents [15]. The reaction condition for NCC is not the same as that used for cellulose because NCC is highly ordered [23]. Hence, the acetylation of NCC requires a longer reaction times, higher temperatures and concentrations of the acetylating agent [23]. Table 1.2 presents a summary of the process of acetylation for NCC as reported from previous studies.

Table 1.2 Selected method for acetylation NCC.

Solvents	**Acetylating agent**	**Temperature (ºC)**	**Time (hours)**	**References**
Pyridine and p-toluenesulfonyl chloride (TsCl)	Carboxylic acid	50	4	[24]
Dimethylformamide (DMF) and potasium carbonate (K_2CO_3)	Vinyl acetate	94	24	[25]
Citric acid	Acetic anhydride	120	3	[26]
DMAc and pyridine	Acetic anhydride	80	14	[27]
Acetic acid and H_2SO_4	Acetic anhydride	80	7	[28]
Anhydrous pyridine	Acetic anhydride	80	5	[29]

With reference to Table 1.2, the concentration of the acetylating agent, the temperature and the reaction time of the acetylation reaction affect the degree of substitution. However, to improve the degree of substitution of NCC, the requirement is not only with the three parameters mentioned above but also using sonication to increase the dispersion of the NCC. For example, Tang *et al.* [28] used an ultrasonic reactor operating at 40 kHz and 68 - 75 ºC under constant stirring (300 rpm) for 0 - 6 hours. Sonicating the solution for 3 hours at 70 ºC increased the yield from 51.87% to 77.38% when compared to the unsonicated material. It is therefore believed that ultrasonication assists the degradation of cellulose and promotes esterification [30]. Furthermore, it has been reported that sonication enabled the reagent to enter the interior regions of the crystal [28].

In the current study, a methodology for the chemical modification of NCC through acetylation was investigated. The acetylation of NCC in a gel form was performed by swelling the NCC in water. This was followed by the introduction of pyridine to the suspension with sonication. The acetic anhydride was added dropwise to solution under a nitrogen environment with stirring. Based on the previous literature, acetylation is known to give a higher acetyl content by dispersing cellulose in solution before introducing acetylating reagent to the solution. However, as stated previously, NCC does not dissolve in common solvents due to the extensive hydrogen bonding and its high crystallinity. NCC is dispersed in water owing to the surface charge on the NCC [15]. The polyelectrolyte of NCC will be discussed in the next chapter.

1.2 Aims

The aims of the current study areas are follows.

i. To investigate microstructure of NCC using transmission electron microscopy.
ii. To characterise as-received NCC and cellulose, and acetylated NCC using a range of analytical techniques, including environmental scanning electron microscopy, X-Ray diffraction, thermogravimetric analysis, FTIR spectroscopy and nuclear magnetic resonance spectroscopy.
iii. To determine the viscosity of NCC before and after acetylation.
iv. To electrospin commercial cellulose acetate and to investigate the effect of the conductivity and temperature on electro-spinning.
v. To electrospin NCC with PAN as the “carrier polymer”.
vi. To produce spun fibres from NCC and acetylated NCC via wet-spinning.
vii. To pyrolyse wet-spun NCC fibre at 900 ºC and to characterise carbonised fibres using Raman spectroscopy and environmental scanning electron microscopy.

CHAPTER 2
LITERATURE REVIEW

2.1 Cellulose

Cellulose is the main constituent of plants and it is also found in micro-organisms such as fungi, bacteria, algae and tunicate [31]. Cellulose is a non-aromatic, cyclic polymer which is composed of D-anhydroglucopyranose units linked together by ether (-C-O-C), β-1-4 linkages as shown in Figure 2.1 [32]. Its chemical formula is $(C_6H_{10}O_5)_n$.

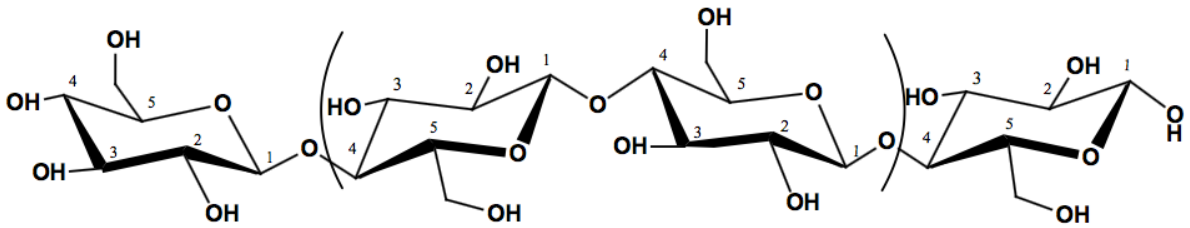

Figure 2.1 The structure of cellulose [33].

In nature, cellulose is bonded with lignin, hemicellulose and other compounds as the matrix. The removal of these substances is necessary to obtain pure cellulose [34]. Several studies have been undertaken for isolating cellulose from natural fibres and various procedures have been reported. For example, the extraction of cellulose from: (i) sugarcane bagasse by alkaline peroxide [35]; (ii) delignification followed by ultrasonic treatment of sugarcane bagasse [36]; (iii) wheat straw by the pulping method and steam explosion [37]; (iv) banana plants by chemical and mechanical treatment [38,39]; (v) wood chip using an ionic liquid such as 1-allyl-3-methylimidazolium chloride [40]; and rice husk using a Soxhlet apparatus [41].

With reference to Table 2.1, the highest concentration of cellulose is found in cotton with approximately 95% being reported. Table 2.1 also presents a summary of the primary composition of several naturally occurring fibres.

Table 2.1 Chemical composition of selected natural fibres [42].

Type of biofibre	**Composition (%)**				
	Source	**Cellulose**	**Hemicellulose**	**Lignin**	**Pectin, waxes, etc.**
Wood	Hardwood	43 - 47	25 - 35	16 - 24	2 - 8
	Softwood	40 - 44	25 - 29	25 - 31	1 - 5
Non-wood	Bagasse	40	30	20	10
	Coir	32 - 43	10 - 20	43 - 49	4
	Corn cobs	45	35	15	5
	Corn stalks	35	25	35	5
	Cotton	95	2	1	0.4
	Flax (retted)	71	21	2	6
	Flax (unretted)	63	12	3	13
	Hemp	70	22	6	2
	Henequen	78	4 - 8	13	4
	Istle	73	4 - 8	17	2
	Jute	71	14	13	2
	Kenaf	36	21	18	2
	Ramie	76	17	1	6
	Sisal	73	14	11	2
	Wheat straw	30	50	15	5

2.1.1 Crystallinity in cellulose

Polymorph of cellulose consists of cellulose-I, II, III and IV. Cellulose-I is the most stable form of cellulose and is found in nature, either in the form of 1α or 1β. Cellulose-1α is produced by primitive organisms, whist cellulose-1β is produced by higher plants [10]. Cellulose-II is converted from cellulose-I using two processes. The first method is the regeneration or solubilisation of cellulose-I in a solvent followed by dilution in water. The second is mercerisation by the swelling of native cellulose in sodium hydroxide

(NaOH) followed by coagulation and recrystallization [43]. Heat treatment of cellulose-I and cellulose-II with liquid ammonia generates cellulose-III_1 and III_2 respectively. Cellulose-IV_1 and IV_2 are obtained by heating cellulose-III_1 and III_2 in glycerol at 206 ºC [10]. The conversion of cellulose-I to cellulose-III_1 and cellulose-II to cellulose-III_2 is a reversible process [44]. A schematic illustration of the transformation for cellulose is illustrated in Figure 2.2.

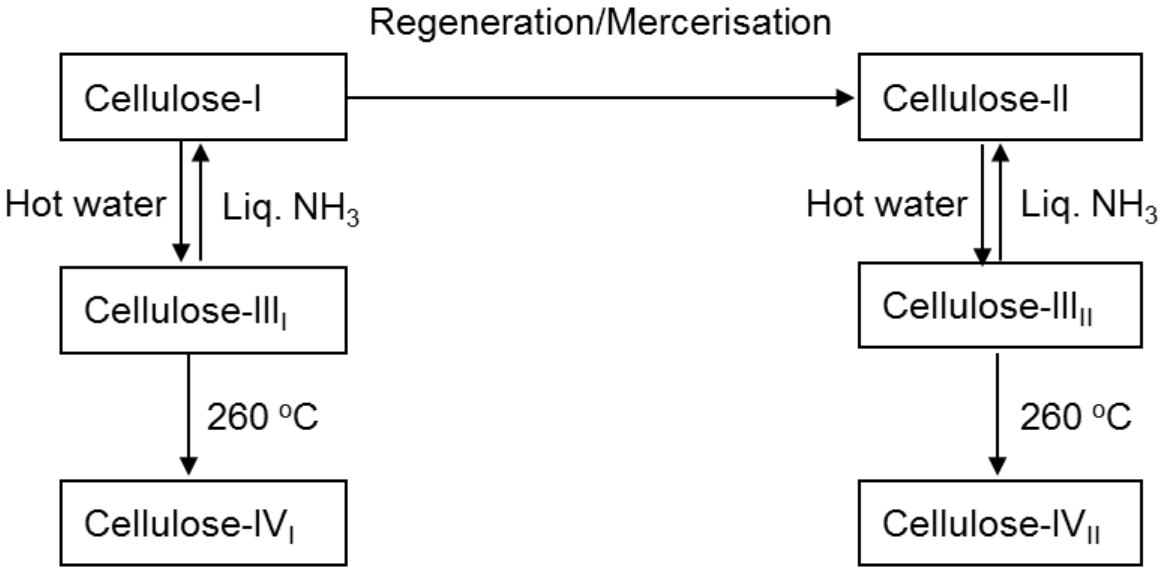

Figure 2.2 Interconversions of cellulose polymorphs [10].

Cellulose-Iα has a triclinic unit structure with unit cell parameters of a = 0.674 nm, b = 0.593 nm, c (chain axis) = 1.036 nm, and α the triclinic angle = 117º. Cellulose-Iβ has a monoclinic unit structure with a = 0.801 nm, b = 0.817 nm, c (chain axis) = 1.036 nm, and γ the monoclinic angle = 97.3º. The triclinic unit cell contains anti-parallel chains, while the monoclinic unit cell contains parallel chains [45]. Similarly, cellulose-II has unit parameters of a = 0.810 nm, b = 0.903 nm, c = 1.031 nm, and γ = 117.10º with anti-parallel chains [46]. The triclinic and the monoclinic structures are shown in Figure 2.3 (a and b).

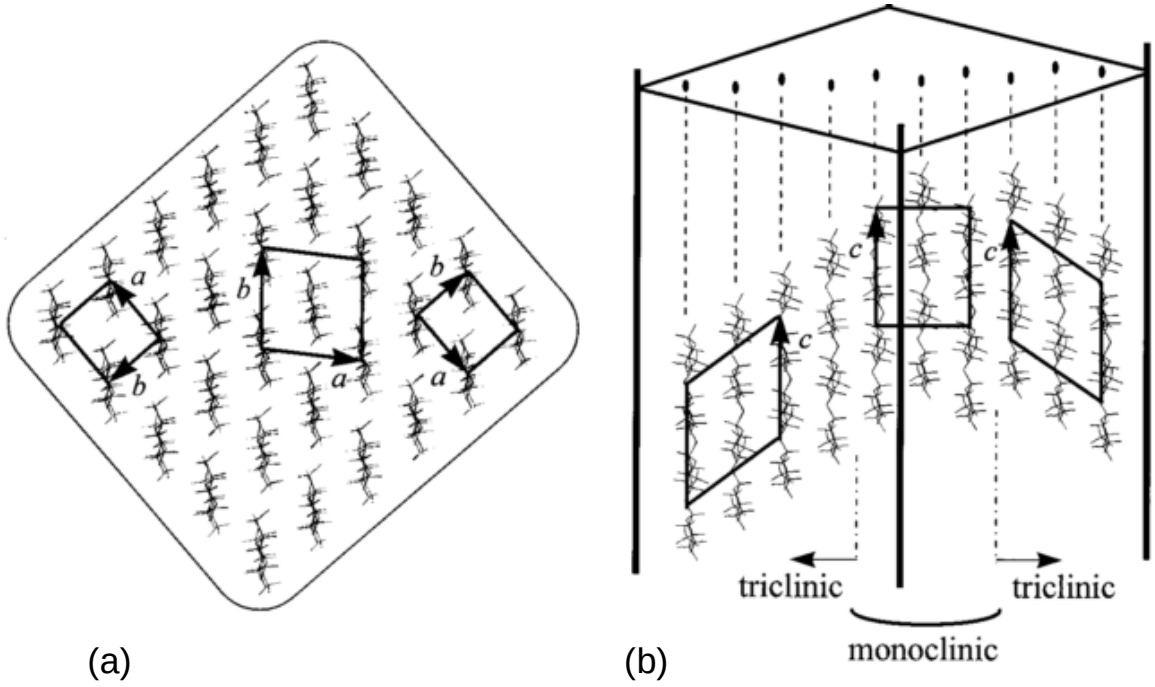

(a) (b)

Figure 2.3 Molecular sheet in a micro-fibril with triclinic and monoclinic domains: (a) view along the chain direction and (b) view along triclinic and monoclinic directions [47].

Native cellulose consists of low ordered (amorphous) and highly ordered (crystalline) regions. Compared to the crystalline regions, the amorphous parts have a lower density. Therefore, the amorphous region can be removed by acid hydrolysis which breaks down the amorphous components and releases the individual crystallites known as NCC [15].

2.1.2 Summary

Cellulose can be isolated from plants or micro-organisms. Several techniques have been reported to extract cellulose including pulping, grinding, soxhlet, chemical and mechanical methods. In the crystalline structure, cellulose consists of four types of cellulose, namely cellulose-I, II, III_1 and III_2, and IV_1 and IV_2. Native cellulose can be found in the form of cellulose-I. A highly ordered form of cellulose is known as NCC and it is extracted by acid hydrolysis. A brief review of NCC is provided in the next section.

2.2 Nano-crystalline cellulose

NCC is best described as rod-like or needle shape fibres whose diameters range from 5 nm to 20 nm and, in length, from 50 nm to several micrometres depending on its source and method of extraction [48]. It is also referred to as a 1D nanomaterial [49]. NCC is obtained by acid hydrolysis of cellulose which is said to remove the amorphous part of cellulose to produce a highly crystalline material [13]. For example, wood consists of 40 - 50% of cellulose of which half of it is nano-crystalline and the remainder is amorphous [50]. These crystalline regions are said to be 'defect-free' [51]. A schematic illustration of the crystalline and amorphous domains in cellulose fibre is shown in Figure 2.4.

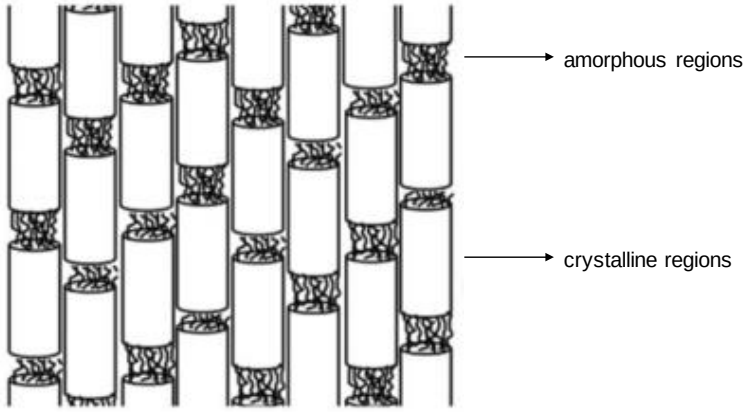

Figure 2.4 Schematic illustration depicting crystalline and amorphous regions in cellulose fibre [51].

Hydrolysis using 65% H_2SO_4 is a conventional method of extracting NCC [52]. During hydrolysis, the individual crystallites are released when the hydronium ions penetrate the amorphous region promoting the hydrolytic cleavage of the glyosidic bonds [53]. Acid hydrolysis of NCC using H_2SO_4 introduces a surface charge [15]. However, Fourier transmission infrared (FTIR) spectroscopy cannot detect the sulphate groups due to its low concentration. The absorbance of the sulphate groups is between 1400 - 1600 and 1200 cm^{-1} [54]. The anionic surface makes NCC to adopt the property of a polyelectrolyte and this improves its dispersion in water, and it forms a stable phase. Without the surface charge, NCC tends to aggregate because the rod-like fibres of NCC have extensive contact and interaction with each other [54,55].

The structure of NCC after acid hydrolysis using H_2SO_4 is depicted in Figure 2.5. It shows that the hydroxyl groups on the surface of NCC are partially substituted with sulphate groups of H_2SO_4 [56].

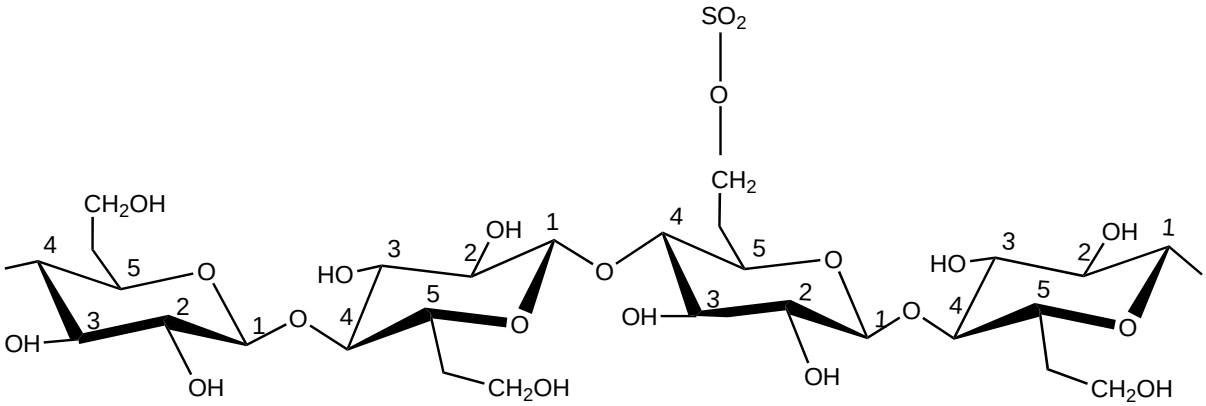

(a)

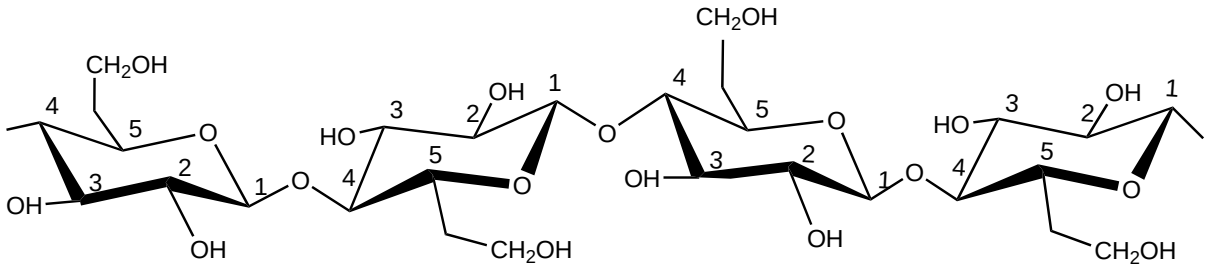

(b)

Figure 2.5 Structure of cellulose (a) surface crystalline and (b) inside crystalline after acid hydrolysis [57].

With reference to Table 2.2, there are several methods that have been reported to extract NCC including the use of H_2SO_4, hydrochloric acid (HCl), phosphoric acid (H_3PO_4), and hydrobromic acid (HBr). The surface charges of NCC produced using all the various techniques are not the same. In the case of hydrochloric acid, for example, the chloride ions are easy to remove during dialysis. Dialysis is the next process of acid hydrolysis of cellulose to remove other substances from the material. It depletes the NCC of electrostatic charge and they tend to agglomerate [58]. However, the extraction of NCC using H_2SO_4 has been reported to result in lower thermal stability when compared to treatment with other acids. For example, hydrolysis using H_3PO_4 was reported to produce NCC with higher thermal stability [59].

Table 2.2 A summary for the length and diameter of NCC from different resources that have been reported from previous studies.

No.	Samples	Method of extraction	Crystallinity (%)	Diameter (nm)	Length (nm)	Technique and Reference	Appearances
1	*Amorpha fruticosa Linn*	Mechanical treatment via grinding.	54.67	10	>100	TEM [49]	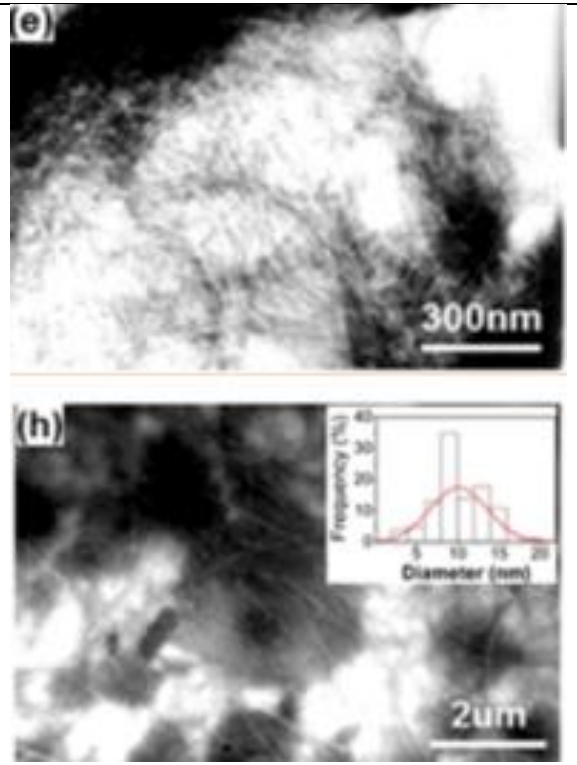

2	Eucalyptus wood flour (*Jiangmen Mujiangwei hua Inc*.)	Acid hydrolysis using 65% H_2SO_4 at 60 ºC for 30 minutes.	61	3 - 20	200 - 600	TEM [60]	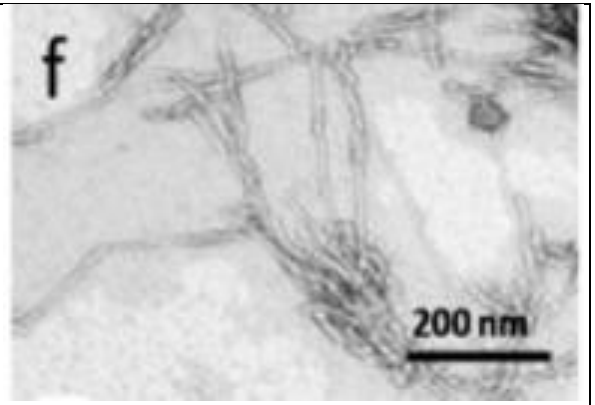
3	Filter paper	Acid hydrolysed using 64% H_2SO_4 at 45 ºC for 75 minutes.	89.1	15 ± 0.2	112 - 243	Atomic force microscope (AFM) [61]	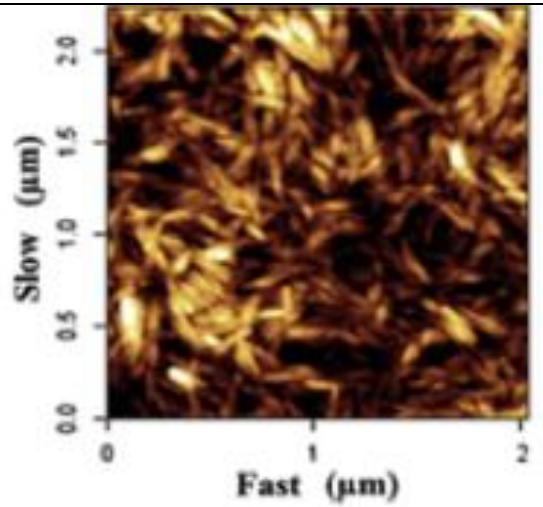

4	Garlic straw	Acid hydrolysis using 65% H_2SO_4 at 45 ºC for 40 minutes.	68	6	480	AFM/TEM [62]	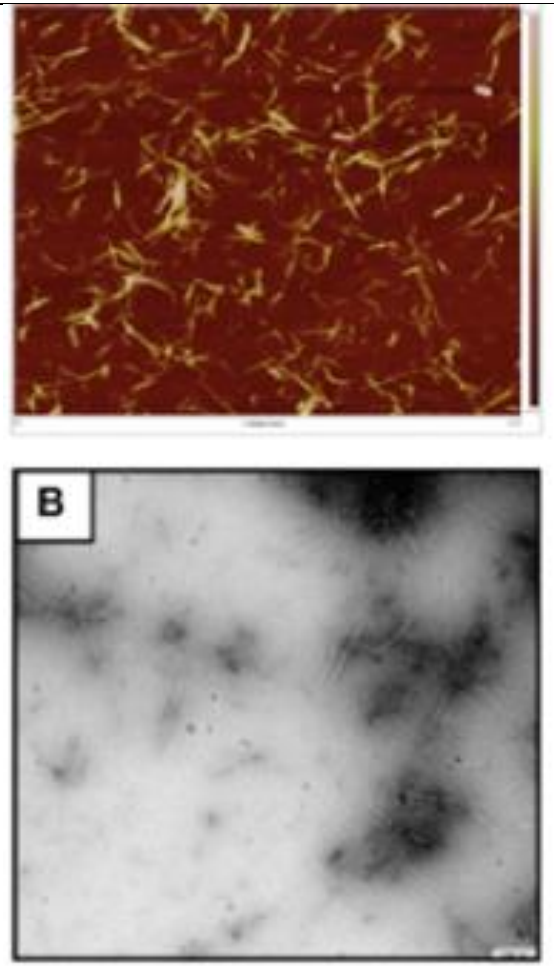

5	Sugarcane bagasse	Acid hydrolysis using 64% H_2SO_4 at 45 ºC for 60 minutes.	73	20 - 30	160 - 400	TEM [63]	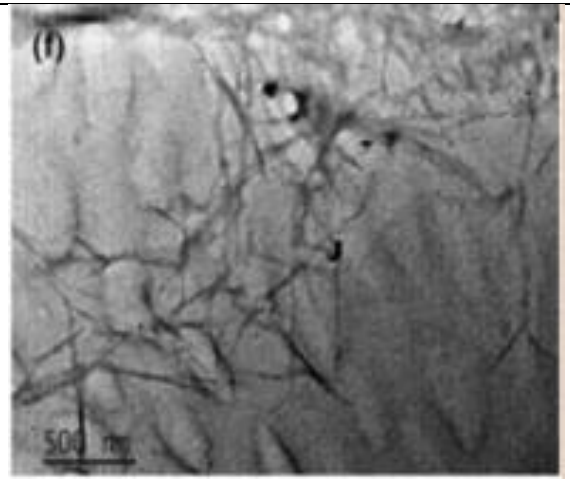
6	Oil palm trunk	Sulfuric acid hydrolysis assisted by the chemo-mechanical treatment using sodium hypochlorite as the bleaching agent.	74.81	3.58	82.81	TEM [64]	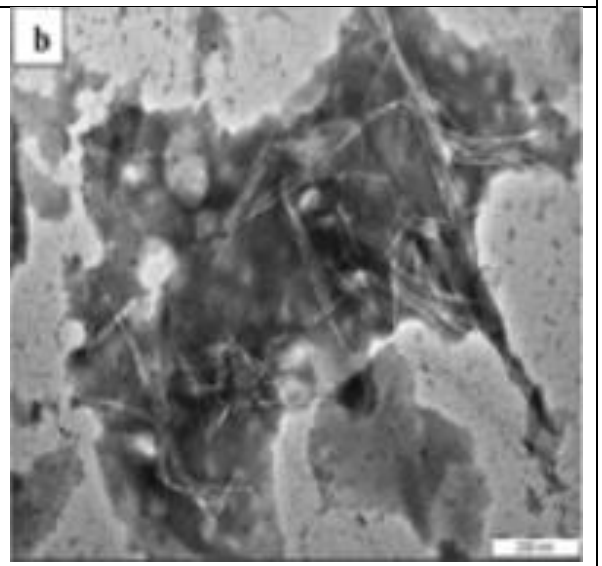

7	Whatman No. 1 filter paper	Acid hydrolysis using 85% H_3PO_4 at 100 ºC for 90 minutes.	81	31 ± 14	316 ± 127	TEM [59]	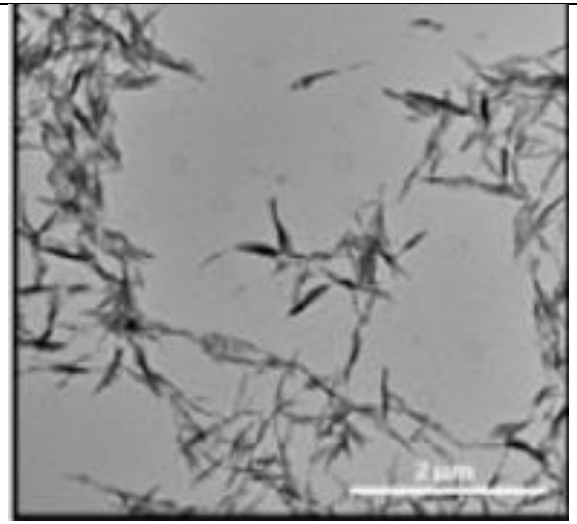

8	Tomato skins	Acid hydrolysis using 64% H_2SO_4 at 45 ºC for 30 minutes.	80.8	5 - 9	100 - 200	TEM/AFM [65]	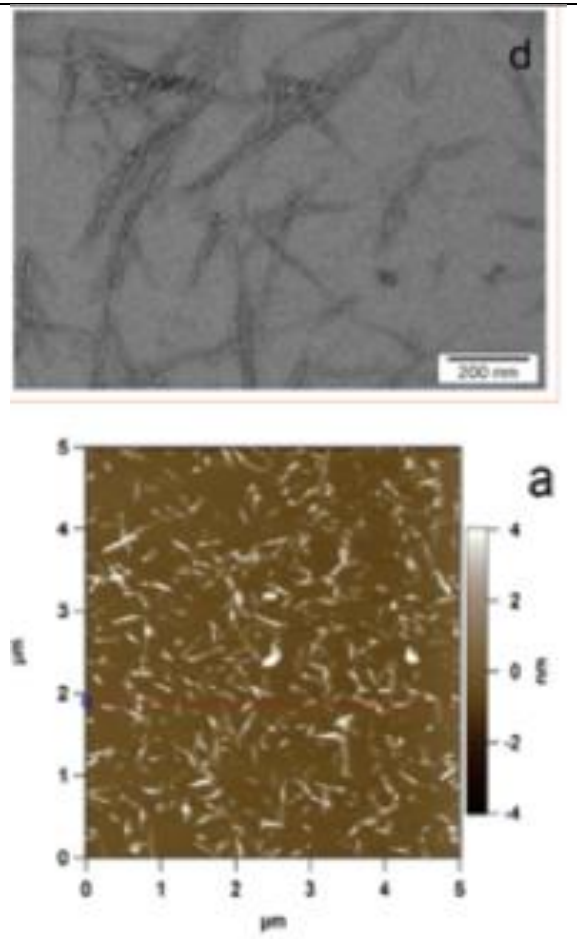

9	Corncob	Acid hydrolysis using 9.17 M H_2SO_4 at 45 ºC for 60 minutes.	83.7	4.15 ± 1.08	210.8 ± 44.2	AFM [66]	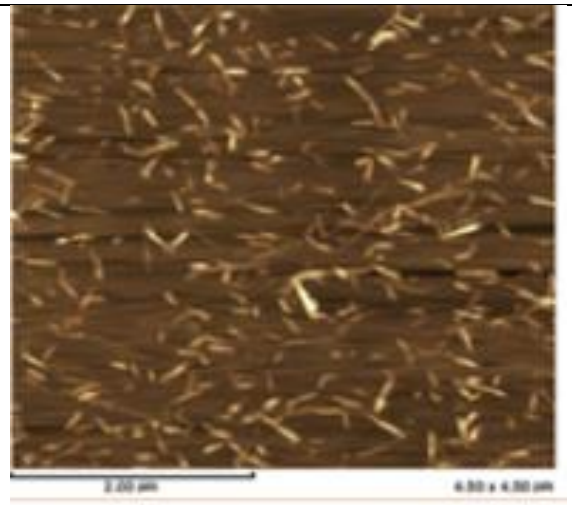
10	Syngonanthus nitens (*Capim Dourado*)	Acid hydrolysis using 65% H_2SO_4 at 50 ºC for about 60 minutes.	91	4.5	300	TEM [67]	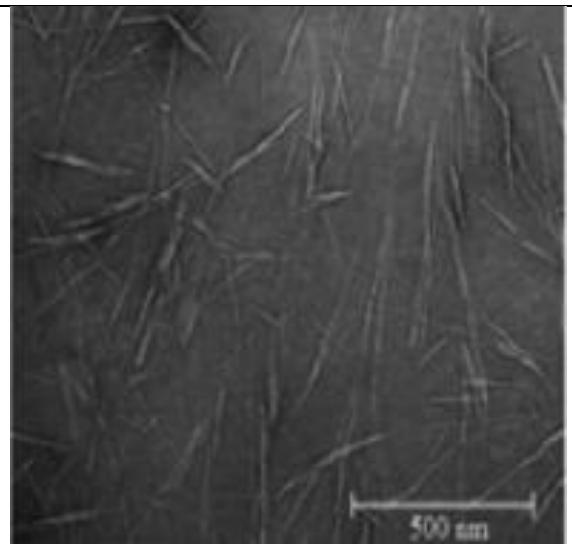

11	Soy hulls	Acid hydrolysis using 64% H_2SO_4 at 40 ºC for 30 minutes.	73.5	2.77 ± 0.67	122.66 ± 39.40	TEM [56]	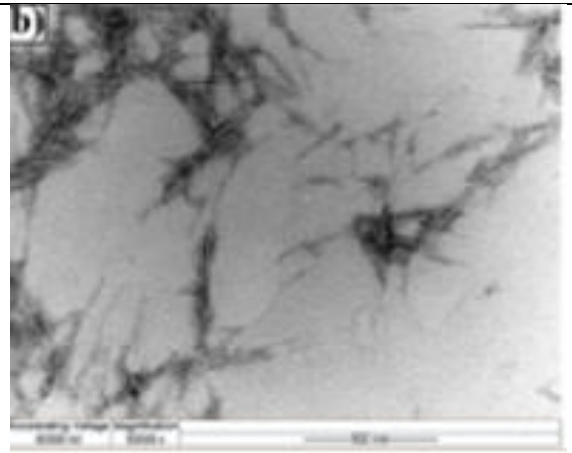
12	Cotton (*Gossypium hirsutum*) linters	Acid hydrolysis using 60% H_2SO_4 at 45 ºC for 60 minutes.	90.45	12	177	TEM [68]	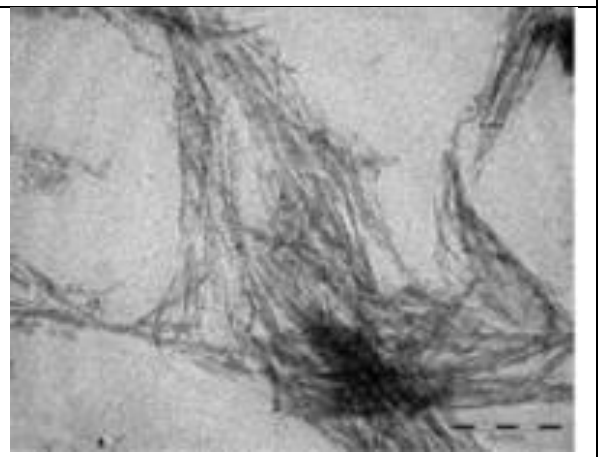

13	Pineapple leaf	Steam explosion.	73.6	5 - 60	200 - 300	TEM [69]	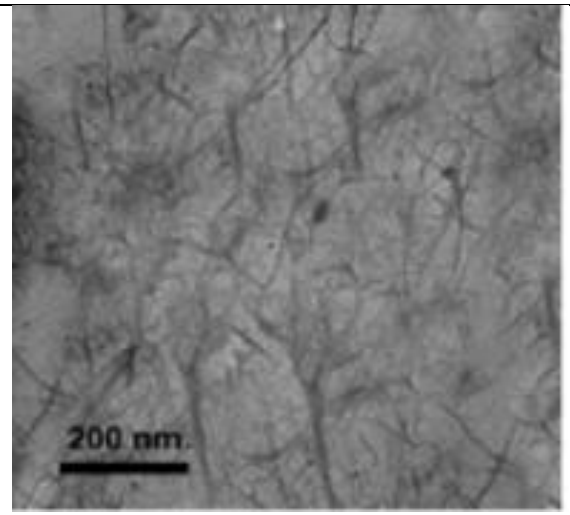
14	Curaua fibres	Acid hydrolysis using 36.5 % HCl at 45 ºC for 75 min.	74.0	6 - 10	80 - 170	TEM [58]	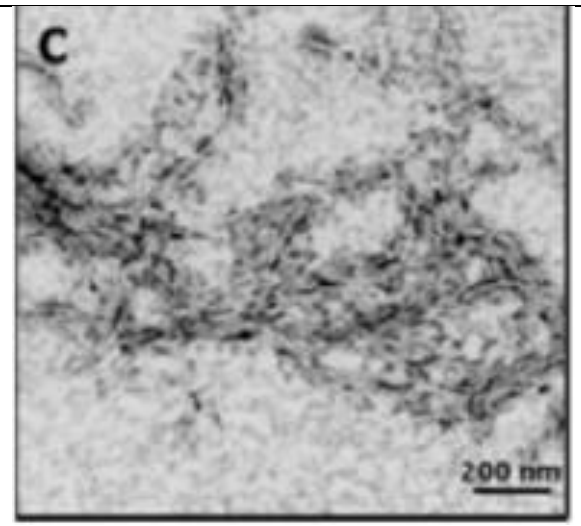

From Table 2.2, grinding is a simple method to extract NCC from cellulose. NCC with higher degree of purification displays the highest crystallinity due to the removal of the amorphous content along with the lignin and hemicellulose. However, the crystallinity of NCC has been reported to decrease with high-intensity shearing and impact forces. It causes the alignment of the cellulose chains to decrease and breaks the hydrogen bonds between the cellulose chains [49]. The conventional method of isolating NCC is by acid hydrolysis. Before the hydrolysis, it is important to bleach cellulose to remove other substances after delignification as this can enhance the crystallinity of NCC as compared to unbleached samples [64]. Similarly, the concentration of acid, temperature and extraction time during the hydrolysis are important parameters to produce the required diameter and length of NCC as well as the crystallinity. The concentration of H_2SO_4 between 60 - 65% has been reported to be optimal [70]. In addition, an optimum reaction time is required to produce the minimum diameter and length distribution of NCC. The isolation of NCC from rice straw, for example, produced smaller with width, thickness and length corresponding to 11.2, 5.06 and 117 nm particles respectively were produced when the reaction time was 45 minutes. However, when the reaction was reduced to 30 minutes, particles with an average width, thickness and length of 30.7, 5.95 and 270 nm particles respectively were produced [71].

NCC has attractive characteristics such as ability to be surface-modified (for example, via acetylation, esterification, Tempo-Media oxidation, polymer grafting, silytation and catonisation), large surface area and high aspect ratio and exhibiting gel-like characteristics in water and its hydrophilicity [72]. These properties have led to an increase in interest and the utilisation of NCC as a functional material over the past 20 years [73]. Some examples are, (i) biomedical applications [74], printed electronics [75], fillers in nano-composites [76] and as an adsorbent [77].

The fabrication of nano-fibres from NCC continues to attract significant attention including electro-spinning. Wanasekara *et al.* [78] have electro-spun polystyrene (PS) and polyvinyl alcohol (PVA) nanofibers containing NCC. From TEM studies, it was shown that NCC had little orientation along the direction parallel to the axis of the fibres

and random orientation of fibres in the cross-section direction. The mechanical properties of fibrous mats spun with NCC as the reinforcement were also reported. For example, the presence of NCC in PS spun-fibres improved the strength (elastic modulus) of the composite [79]. The mechanical properties and thermal stability of polycaprolactone (PCL) loaded NCC increased [80]. The thermal stability of polymethyl metacrylate (PMMA) increased with the addition of NCC [81]. In addition, Ago *et al.* [82] electro-spun lignin reinforced NCC. It had defect-free nanofibers with up to 90 wt% lignin and 15% NCC and the thermal stability of composite electro-spun fibres improved. Table 2.3 presents a summary of electro-spinning of NCC with various polymer solutions.

Table 2.3 A summary of selected reports on electro-spinning of NCC with different polymer/solvent combinations.

No.	**Polymer/solvent system**	**NCC content (%)**	**Focus**	**References**
1	PVA	0, 5, 10 and 15	The morphology and the mechanical properties of mat spun-fibres.	[83]
2	PVA	3 - 5	The morphology and the crystallinity of spun-fibres.	[84]
3	Cellulose acetate Acetic acid Acetone	0 - 5	The morphology and the crystallinity of spun-fibres.	[85]
4	Regenerated silk fibroin Formic acid	0 - 4	The morphology and the mechanical properties of nano-fibres.	[86]
5	Polyhydroxyl butyrate (PHB)	0, 5, 8, 12, 17 and 22	The effect of concentration of NCC	[87]

	Chloroform DMF		and the fibre diameter for the mechanical properties of nano-composite mats.	
6	Chitosan Polyethylene oxide (PEO)	N.A	The tensile strength and the tensile modulus of mat spun-fibres.	[88]
7	Polylactic acid (PLA) Chloroform DMF	5 - 10	The morphology, mechanical and thermal properties of spun-fibres.	[89]
8	PVA	0 - 15	The mechanical properties of nano-fibres.	[90]
9	PLA Chloroform Toluene Span 80 (as surfactant)	4, 5, and 7	The mechanical properties of electro-spun fibres.	[91]
10	Polyacrylic acid (PAA) Ethanol	5, 10, 12 and 20	Fibres diameter.	[92]
11	Cellulose acetate Acetone DMAc	5	Thermos-mechanical properties of spun-fibres.	[93]

As stated previously, NCC does not dissolve in common solvents. Similarly, the high surface area and the strong hydrogen bonding in NCC causes it to be agglomerated easily [72]. This makes NCC difficult to process and it has poor compatibility with common solvents.

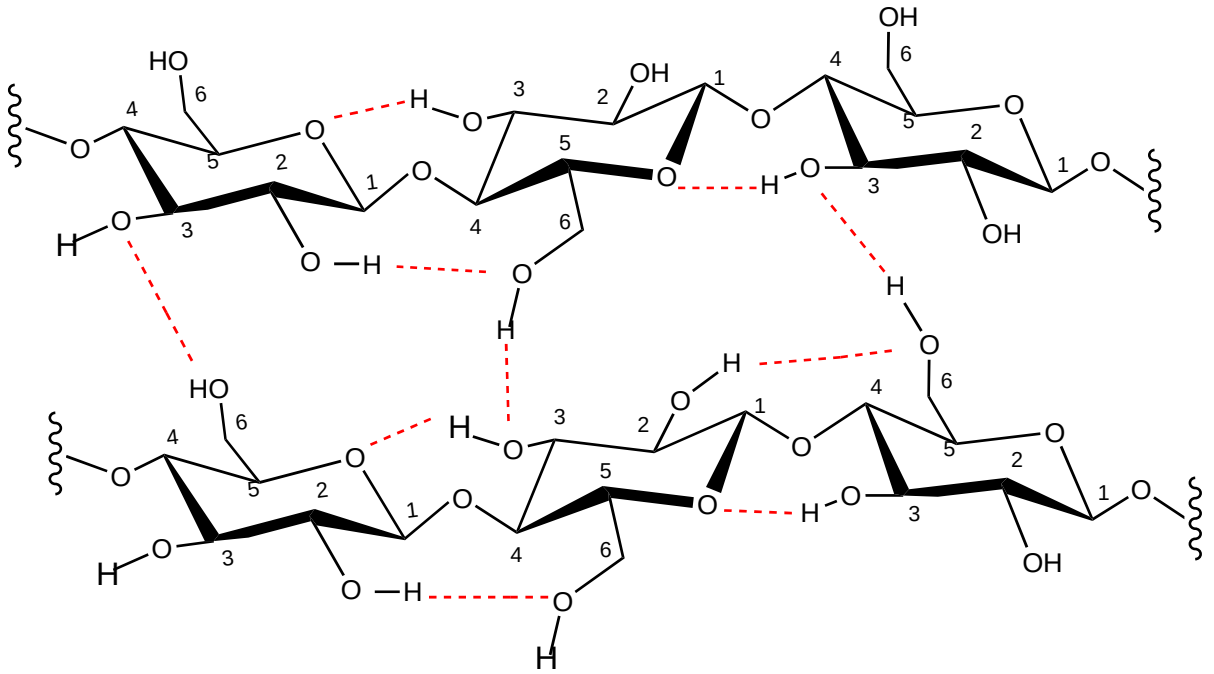

Figure 2.6 Illustration of hydrogen bonding in cellulose [72].

The bridging and the oxygen atom that connect cellulose chains with each other involve intra- and inter-molecular hydrogen bonding. The intramolecular hydrogen bonds are connected between OH group of the C_3 carbon cycle and oxygen from the adjacent ring (O_5) and between OH group of the C_6 carbon and oxygen from the carbon 2 hydroxyl of the adjacent ring. Similarly, the intermolecular hydrogen bonds are between the OH_6 primary hydroxyl and oxygen in position O_3 in a cycle of a neighbouring unit [94].

2.2.1 Summary

The extraction of NCC using H_2SO_4 is the most common preparation method to extract NCC compared with other acids such as HCl, H_3PO_4 and HBr. Hydrolysis using H_2SO_4 that produces NCC with high dispersibility in water. The utilisation of NCC has a significant interest in several applications due to its good mechanical properties including high crystallinity and surface area. However, NCC is difficult to process because it has poor solubility and compatibility with common solvents. One method to improve either its dispersion or solubility is to modify the hydrogen bonds of NCC by an acetylation reaction as described in the next section.

2.3 Acetylation

Cellulose acetate is a derivative of cellulose, which has better solubility in common solvents than cellulose. Cellulose acetate is a commercially important polymer and it is used for coatings, casting, formation of fibres, films and membranes [95]. Cellulose acetate is obtained by the acetylation of cellulose using acetic anhydride as the acetylating agent with a catalyst, for example, pyridine [29]. Modification of cellulose by acetylation is popular because of its simplicity [96].

With reference to Figure 2.6, each anhydroglucose unit of cellulose has hydroxyl groups at C_6, C_2 and C_3. The hydroxyl group at C_6 is a primary alcohol that is substituted first in reactions involving cellulose. In the acetylation reaction, for example, the hydrogen at C_6 is penetrated by an acetyl group followed by the reaction of the secondary alcohol at C_2 and C_3. This is due to fact that the primary alcohol of cellulose which is more reactive when compared to the secondary alcohol [97]. In addition, the reaction of cellulose occurs on the amorphous part, which means that solvent penetrates the material easily and breaks the chains at many points. This is because they are loosely packed together and there are few bonds between the chains. However, the crystalline regions are tightly packed and the solvent only penetrates the surface of the crystalline cellulose [97].

Fahma *et al.* [27] reported three situations associated with the acetylation of cellulose:

(i) The acetyl group is penetrated to the non-crystalline parts.
(ii) The reaction is partially on the surface of cellulose.
(iii) The surface of crystalline cellulose is completely acetylated.

One of the catalysts that is used in the acetylation reaction is pyridine. It facilitates the reaction between the hydroxyl groups of NCC and acetyl groups from acetic anhydride [98]. A mechanism of reaction between cellulose and acetic anhydride using pyridine as the catalyst is described in Figure 2.7.

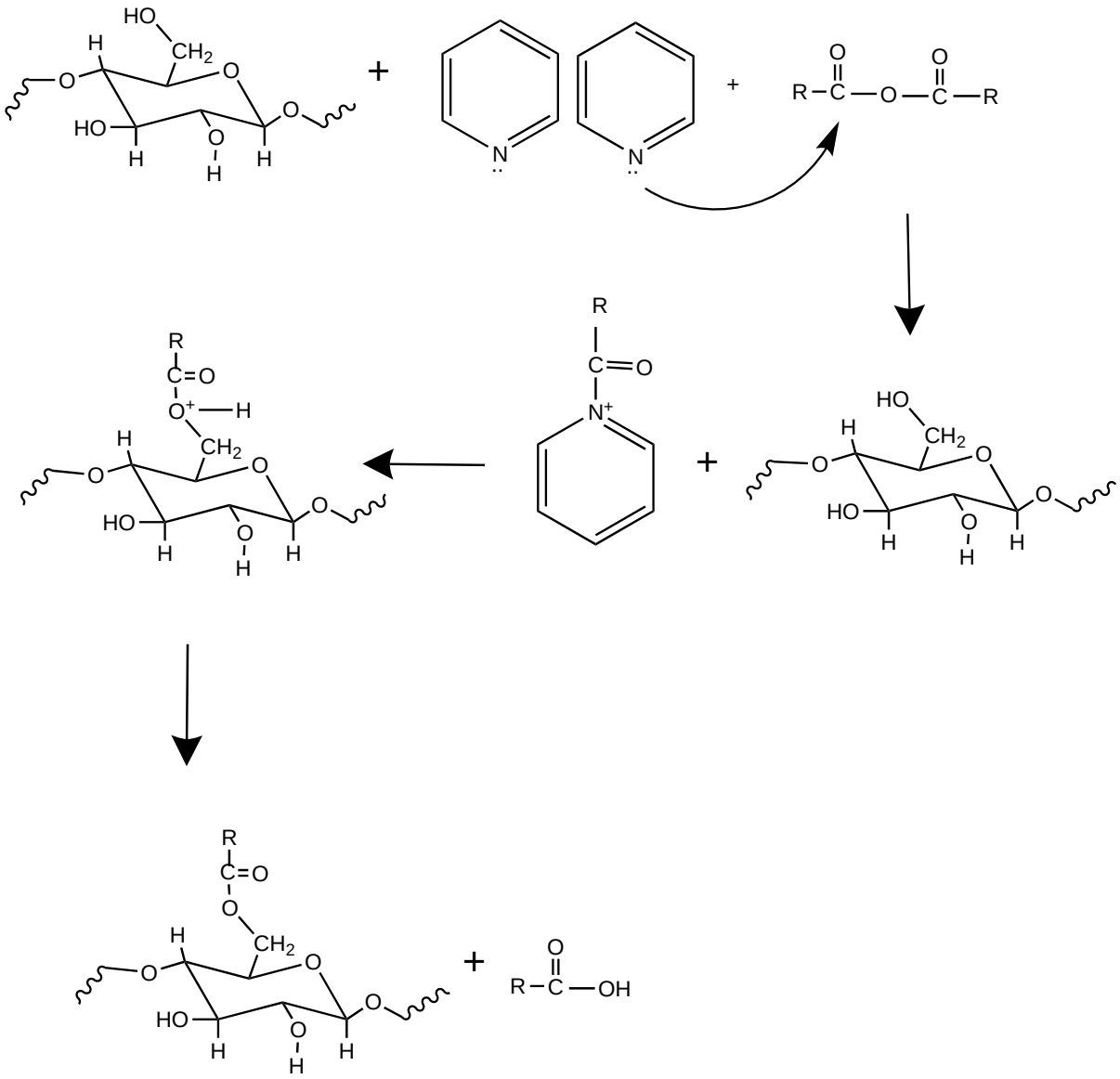

Figure 2.7 Reaction mechanisms for the acetylation of cellulose using pyridine as a catalyst [99].

With reference to Figure 2.7, there are certain factors that affect the degree of substitution [15] including the following: (i) Temperature: Acetylation at 50 ºC produced a higher degree of substitution compared to acetylation at room temperature under the same reaction conditions [99]. (ii) Concentration of the acetylating agent: Increasing the concentration of acetic anhydride leads to a greater degree of substitution of hydroxyl groups in cellulose [100]. These parameters can be adjusted to enable acetylation of the outer or inner surfaces of cellulose. A higher degree of substitution (> 0.38) is said to introduce acetyl groups within the core of the crystal structure [101].

It has been reported that prolonged acetylation, for example, eleven hours at 80 ºC, can reduce the degree of crystallinity [27].

The acetyl content of cellulose acetate and the molecular weight distribution are considered to influence its solubility in organic solvents. The maximum number of hydroxyl bonds that can be substituted is three per anhydroglucose. There are three kinds of cellulose acetates that can be produced from the acetylation of cellulose, namely monoacetate, diacetate and triacetate. The corresponding acetyl contents are 21.1%, 35% and 44.8% respectively [102]. Commercial cellulose acetates can be found with acetyl content between 35.8% and 41.5% and they are soluble in acetone. Cellulose triacetate is not soluble in acetone but dissolves in chloroform, tetrachlorethane, formic acid, acetic acid, nitro benzene, aniline and pyridine [102].

2.3.1 Summary

Cellulose acetate is obtained by the acetylation of cellulose with acetic anhydride. In this reaction, acetyl groups are introduced to the hydroxyl groups of cellulose either on the surface of crystalline cellulose or inside crystalline cellulose depending on the parameters and reaction conditions.

2.4 Electro-spinning

Electro-spinning is a method that is used to produce ultra-fine polymeric fibres with diameters ranging from nanometres to micrometres by dissolving polymer precursors in suitable solvents [103]. It was patented by Formhals in 1934 [104] in a work entitled ‘Process and apparatus for preparing artificial thread’ where cellulose acetate was dissolved in acetone and electro-spun in a strong electric field. The experimental set up for electro-spinning has five basic components, namely a power supply, syringe, spinneret or needle, liquid dispenser and collector as shown in Figure 2.8 [105].

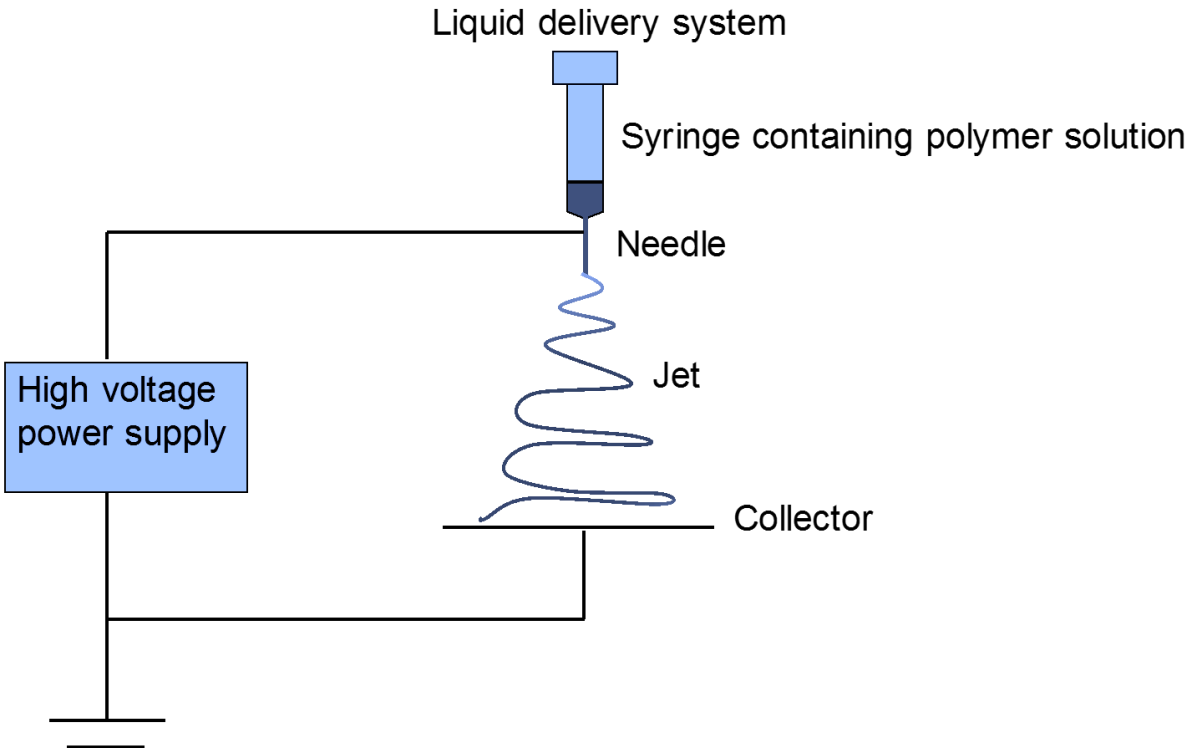

Figure 2.8 Experimental set up for electro-spinning.

In the electro-spinning process, a polymer solution is filled in a syringe and the droplet is maintained at the tip of a metal needle via a pump. An electric potential, from a high-voltage power supply, is applied between the needle and a metallic collector plate [106]. If the intensity of electric field overcomes the surface tension of the polymer solution, the droplet is transformed into a conical shape known as a 'Taylor cone' [107]. The formation of a Taylor cone is shown in Figure 2.9. When the electric field overcomes the surface tension of the solution a jet is ejected from the Taylor cone. The jet takes a spiral trajectory and a continue to whip towards the collector plate [108]. When this jet travels through air, the solvent evaporates from the solution. Thus, the polymer in fibrous form is deposited on the collector [109].

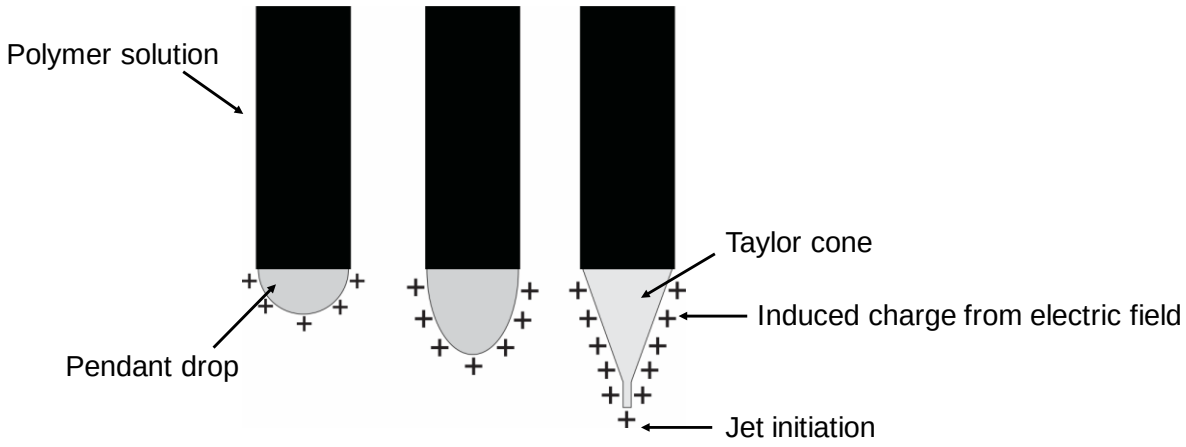

Figure 2.9 The formation of Taylor cone in the electro-spinning process [110].

Electro-spinning is the most widely technique to produce thin mats of polymer nano-fibres. Therefore, it has been used for several applications such as nano-sensor [111], ultrafiltration membrane [112], biomedical applications such as tissue engineering, drug delivery, implants and wound healing [113] and nano-composites [103]. Some polymers used for electro-spinning process are summarised in Table 2.3.

There are several parameters affecting the fibre formation for electro-spinning as reported in Section 2.4.1.

2.4.1 Solution parameters

2.4.1.1 Concentration and viscosity

The concentration and viscosity of the polymer solution is one of parameters that have a major influence on the ability to produce fine electro-spun fibres. At low concentrations (η < 1 Pa.s), beads will be formed instead of fibres. In addition, it has been observed that the higher the concentration, the fewer beads fibres will be formed. However, viscosities in the region of 20 Pa.s prohibits the formation of fibres due to the cohesiveness of the solution and this limits the followability of the polymer solution. Therefore, an appropriate concentration and viscosity should be used for each class of polymer to produce smooth fibres [114,115].

2.4.1.2 Molecular weight

Using higher molecular weight (M_w) polymer can increase the viscosity of polymer solutions as shown in Equation [2.1].

$$\eta = K M_w^a \qquad \text{Equation [2.1]}$$

where

η = viscosity.

K and a = constants.

M_w = molecular weight.

The fibre diameter decreases with decreasing of molecular weight of polymer solution. At low molecular weight, the rate of solvent evaporation is high and the fibres are dry before reaching the collector. The cross-section of spun-fibres is also circular at low molecular weight. By contrast, the fibre diameter increases and gradually shifts from circular to flat with increasing the molecular weight [116,117]. Similarly, fresh solution affects molecular weight of polymer solution. The freshly prepared polymeric solution will produce thicker fibres, whilst stored solution will obtain thinner solution. Store polymeric solution in longer time can degrade, hence decrease the viscosity of the solution [118]. The morphology of spun-fibres which was prepared from fresh solution and stored solution is demonstrated in Figure 2.10.

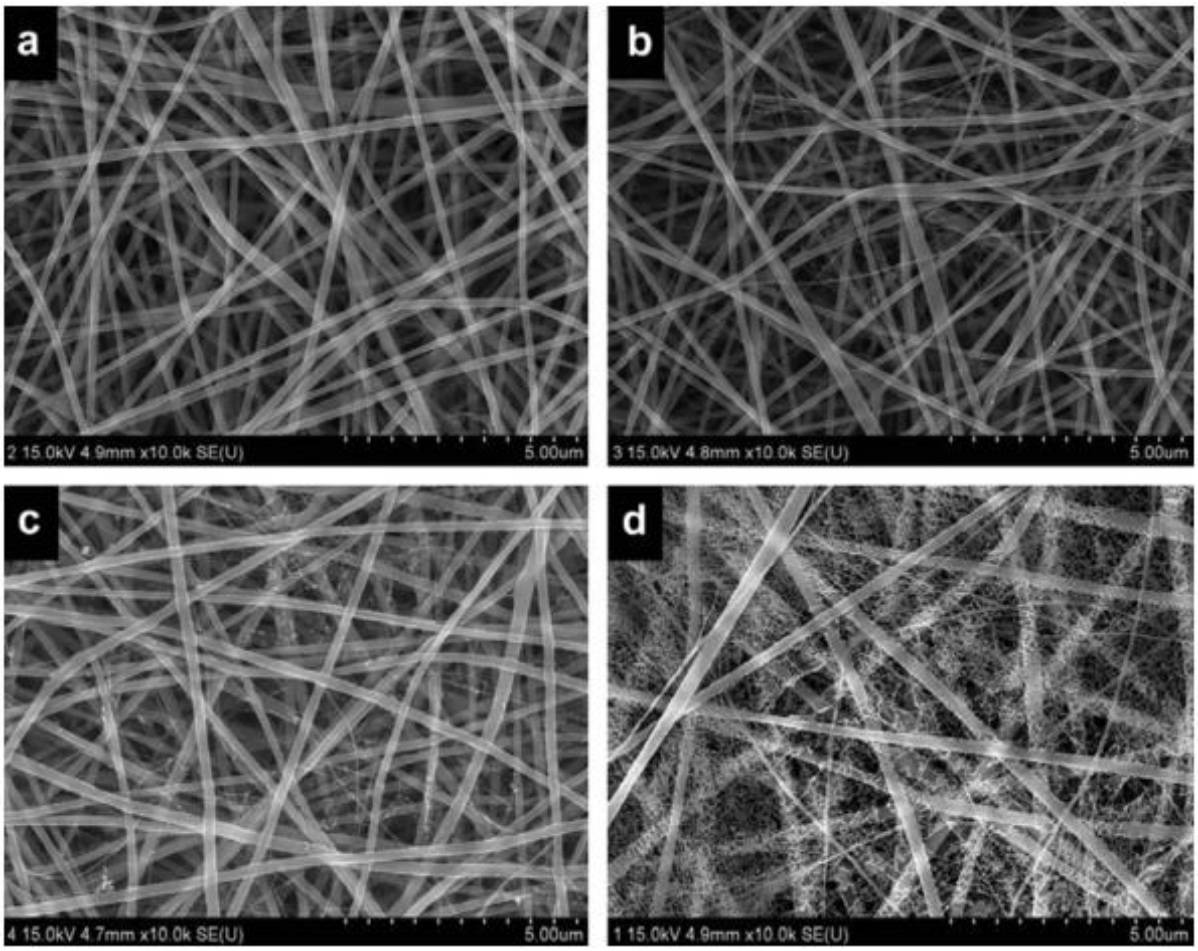

Figure 2.10 Scanning electron microscopy (SEM) images of electro-spun nylon-6 nanofibrous mats containing (a) 0, (b), 5, (c) 10 and (d) 20 wt% of solvent degrade solution in freshly prepared solution [118].

2.4.1.3 Surface tension

The surface tension of the polymer solution is another parameter that controls the production of bead-free fibres. An excess electric field improves the surface area to produce thinner fibres. Furthermore, low surface area favours the formation of fibres without beads [119]. Mixed solvents system can be used to adjust the surface tension of polymer solution [120].

2.4.1.4 Conductivity

Solution conductivity is one of the parameters that influences the production of fibres with a uniform cross-section. This is because the viscous polymer solution is stretched by the presence of charge on the surface of the solution [121]. Higher conductivity increases the electrostatic charge density of the polymer solution. When the conductivity is high, the elongation of the jet between the needle tip and collector become weaker, resulting in the fabrication of thicker fibres. The conductivity of the solution can be improved with the addition of salts to the solution, such as sodium chloride (NaCl), lithium chloride (LiCl) and magnesium chloride ($MgCl_2$) [122].

2.4.1.5 Volatility

In electro-spinning, evaporation of solvent is involved to separate solvent from solid fibre before reaching the collector. Hence, solvent volatility plays important role in the formation of fibres by determining the phase separation process [109]. Megelski *et al.* [123] reported the formation of PS spun-fibres using solvents with different volatility. High surface area of polymeric fibres were obtained and they reported that the formation of skin can be hindered with high-volatility solvents. However, too rapid evaporation of solvent prevents the formation of fibres. For example, cellulose acetate in acetone cannot be spun due to the low boiling point of the solution (56 ºC) and evaporate at room temperature. This causes clogging at the tip of the needle [124].

2.4.2 Processing parameters

2.4.2.1 Applied voltage

The effect of voltage depends on the concentration of polymer solution and the distance of collector [125]. When the two parameters are maintained, there is a slight increase in average fibre diameter with increasing applied voltage [126]. In addition, the uniformity of fibres is formed between 10 kV and 20 kV [127]. The trajectory of the jet also decreases at high voltage [128].

2.4.2.2 Liquid flow rate

Electrospray will be formed instead of electro-spinning if the flow rate is too high. This is due to a greater volume of solution being ejected from the tip of the needle, rendering the ejected solution unable to stretch. The electric field is also not able to stretch the ejected solution with increasing the flow rate at a constant voltage due to the insufficient charged ions [129]. Bead formation and fibre diameter also become prominent at high flow rates [130]. Bead formation in the spun fibres can be avoided by decreasing the flow rate. The lower the flow rate, solvent has much more time to evaporate before reaching the collector [131].

2.4.2.3 Tip-to-collector distance

Deposition time, evaporation rate and whipping or bending instability depend on the tip-to-collector distance [109]. Longer tip-to-collector distance and lower feed rates produce finer and smaller fibre in diameter [132]. This is due to the solvent having enough time to evaporate. However, if the distance is too great the effect of applied voltage is negligible: fibres will not be produced [125].

2.4.3 Processing environment

2.4.3.1 Temperature

Increasing temperature results thinner fibres. This is due to solidification of fibres formed before reaching the collector [122]. This also prevents the fibres from fusing together. Thus, it produces higher stretching rate and decreases the fibre diameter [133].

2.4.3.2 Humidity

A lower moisture content in the surrounding leads to the production of thicker fibres with a more homogeneous size distribution [134]. At higher relative humidity,

solidification more slowly to result thinner fibres [134]. However, if the humidity is too high, bead fibres will be formed as the capillary instability occurred before the jet solidifies [135]. Kim *et al.* [136] studied the effect of relative humidity on the pore formation of spun-fibres. They concluded that the pore size increased as the relative humidity increased.

2.4.3.3 Air-flow or turbulence

Air-flow influences fibre deposition. Increasing air-flow from 0 to 100 kPa increases the pore diameter fibres. However, when the air-flow is increased further between 200 and 400 kPa, the pore diameter decreases [137]. Air-flow system in electro-spinning system also accelerates the evaporation of solvent. Thus, it results thinner fibre. This is due to air-flow blowing the evaporated solvent to ambient areas and preventing the nano-fibres saturated with the solvents. [138].

2.4.4 Summary

Electro-spinning is a conventional technique used to produce nano-fibres by using a high electric field to eject fibres from a spinneret that contains a polymer solution. The simple apparatus for electro-spinning includes a high-voltage electric power supply, a syringe, a needle, a liquid delivery and a collector. The properties of fibres can also be controlled by several parameters including the solution parameters (concentration, molecular weight, surface tension, conductivity and volatility of polymer solution), processing parameters (applied voltage, liquid flow rate and distance of needle to collector) and processing environment (temperature and humidity).

2.5 Wet-spinning

Wet-spinning is a technique that is used to produce fibres, whereby the polymer solution is extruded into a bath containing a specified liquid. It is also a suitable method to extrude fibres from gels [139]. The concentration of the gel should be sufficient to produce spun-fibres via wet-spinning. For example, a concentration of below 1% and

above 10% cannot be spun [140]. Wet-spinning of NCC gel is prepared by dispersing NCC in water and using acetone as the coagulating bath. Acetone is able to dehydrate the spinning suspension rapidly. Hence, the fibrous structure of cellulose nano-fibres can be collected [141].

Wet-spinning has a benefit of producing fibres that can be evaluated mechanically in a single-fibre form [142]. It is also able to control the alignment of fibres that improves the mechanical properties of the spun-fibres. The maximum potential for the mechanical properties of fibres is achieved when the fibres are aligned. Aligned cellulose nano-fibres can be as strong as E-glass fibre (2000 MPa) and as stiff as Kevlar^{TM} [143]. Table 2.4 gives a summary of the mechanical properties of spun-fibre prepared by wet-spinning.

Table 2.4 Orientation and mechanical properties of spun-fibre prepared from wood cellulose nano-fibres by wet-spinning with different spinning rate [141].

Fibres	**Spinning rate (m/minute)**	**Young's modulus (GPa)**	**Tensile strength (MPa)**	**Elongation at break (%)**
Spun-fibre	0.1	8.4 $\pm$ 1.2	90 $\pm$ 22	1.5 $\pm$ 0.2
Spun-fibre	1	11.6 $\pm$ 2.1	192 $\pm$ 110	2.6 $\pm$ 1.8
Spun-fibre	10	19.1 $\pm$ 2.6	332 $\pm$ 93	3.1 $\pm$ 1.1
Spun-fibre	100	23.6 $\pm$ 2.1	321 $\pm$ 145	2.2 $\pm$ 1.2

With reference to Table 2.4, the extrusion rate affects the properties of the spun-fibres. It can be seen that the mechanical properties of spun-fibres increase with increasing the spinning rate. There is a tendency of shear forces in the spinneret to align fibrils along the filament axis at high spinning rate to produce a more oriented fibre structure [144]. At higher spinning rate, the number of voids spun-fibres per unit cross-section area also decreased. This is due to an increased extensional flow and a reduced retention time in the coagulation bath [145]. Coagulation bath is an important parameter used in wet-spinning technique as it affects the morphology of spun-fibre.

The utilisation of coagulation bath is prepared if the solution acts as a non-solvent for polymer solution [146].

2.5.1 Summary

Wet-spinning is a straightforward method to produce fibre by extruding a polymer solution into a coagulation bath where the fibres are drawn and solidified. Selected concentration, extrusion rate and the composition of the solution in the coagulation bath are important as these parameters can affect the morphology and the mechanical properties of the spun-fibres produced. One of the advantages of wet-spinning is that it can produce a single fibre that can be tested mechanically. In the case of electro-spinning, the spun-fibres are difficult to test mechanically in a single fibre form. Heat treatment of spun-fibres at high temperatures carbonises the preform to carbon fibre. A brief review on carbon fibres is given in Section 2.6.

2.6 Carbon fibre

Carbon fibres can be classified in several categories. In terms of their tensile modulus and strength, they are classified as; ultra-high modulus (UHM), with a modulus of > 500 GPa; high modulus (HM) with a modulus of between 350 and 450 GPa; intermediate modulus (IM), with a modulus of 250 to 350 GPa; low-modulus high-strength, with a modulus and strength of 100 GPa and > 3 GPa respectively; and high tensile (HT) with a strength of > 4 GPa [147]. Secondly, they are classified on the final heat-treatment temperature: (i) high temperature (HTT, type-I), heating above 2000 ºC and exhibiting high modulus; (ii) intermediate temperature (IHT, type-II), heat treatment above 1500 ºC (less than 2000 ºC) exhibiting high strength; and (iii) low temperature (type-III), heat treatment $\leq$ 1000 ºC obtaining low modulus and low strength [148].

Precursor for carbon fibre should have certain criteria, such as high strength, a circular cross-section, and a homogenous physical structure [149]. There are three general types of precursor for carbon fibres that have been reported:

(i) Polyacrylonitrile (PAN)-based carbon fibre

PAN is the dominant precursor for carbon fibre due to its high carbon yield, approximately 50 - 60%. The preparation of PAN-based carbon fibre involves spinning (wet, melt, dry, gel, dry-jet wet and electro-spinning), followed by thermal stabilisation, carbonisation and graphitisation [9].

(ii) Pitch-based carbon fibre

Pitch is the most widely used precursor after PAN. Pitch is available in specialised markets due to its unique properties: a tensile modulus of 960 GPa and axial thermal conductivity of 900 - 1100 W/m/K [150]. The production cost of pitch carbon fibre is high compared to PAN carbon fibre, hence, pitch-based carbon-fibres are used in general purpose carbon fibres such as construction materials, reinforced concrete and catalyst support [151].

(iii) Cellulose-based carbon fibre

Cellulose is a promising precursor for the production of carbon fibres because it has little impact on the environment since it is biodegradable, renewable and non-toxic [152]. The yield of volatile products produced during pyrolysis include water (H_2O), tars and fixed gases (CO, CO_2 and other substances such as alcohols as well as ketones) [153]. Theoretically, it has a carbon content of 44.4% with 6 residual atoms of carbon per anhydroglucose [154] and highly crystalline structure [155]. Besides, cellulose has low H content in the structure which is preferred as a good precursor for the production of carbon fibre. Low H content decreases the probability of the formation of by-products (amorphous carbon) [156].

A general mechanism of pyrolysis for a precursor has three stages: (i) stabilisation or the formation of rings; (ii) dehydrogenisation or elimination of water and other gases; (iii) carbonisation or removing other elements except carbon [157]. In the stabilisation process, a slow heating rate (1 $K.minute^{-1}$) is normally preferred to stabilise the precursor. The maximum ultimate tensile strength at 1000 ºC is obtained. Further heat treatment, greater than 2000 ºC is known as graphitisation [158]. Tang & Bacon, in 1964, proposed the mechanism of pyrolysis of cellulose as shown in Figure 2.11.

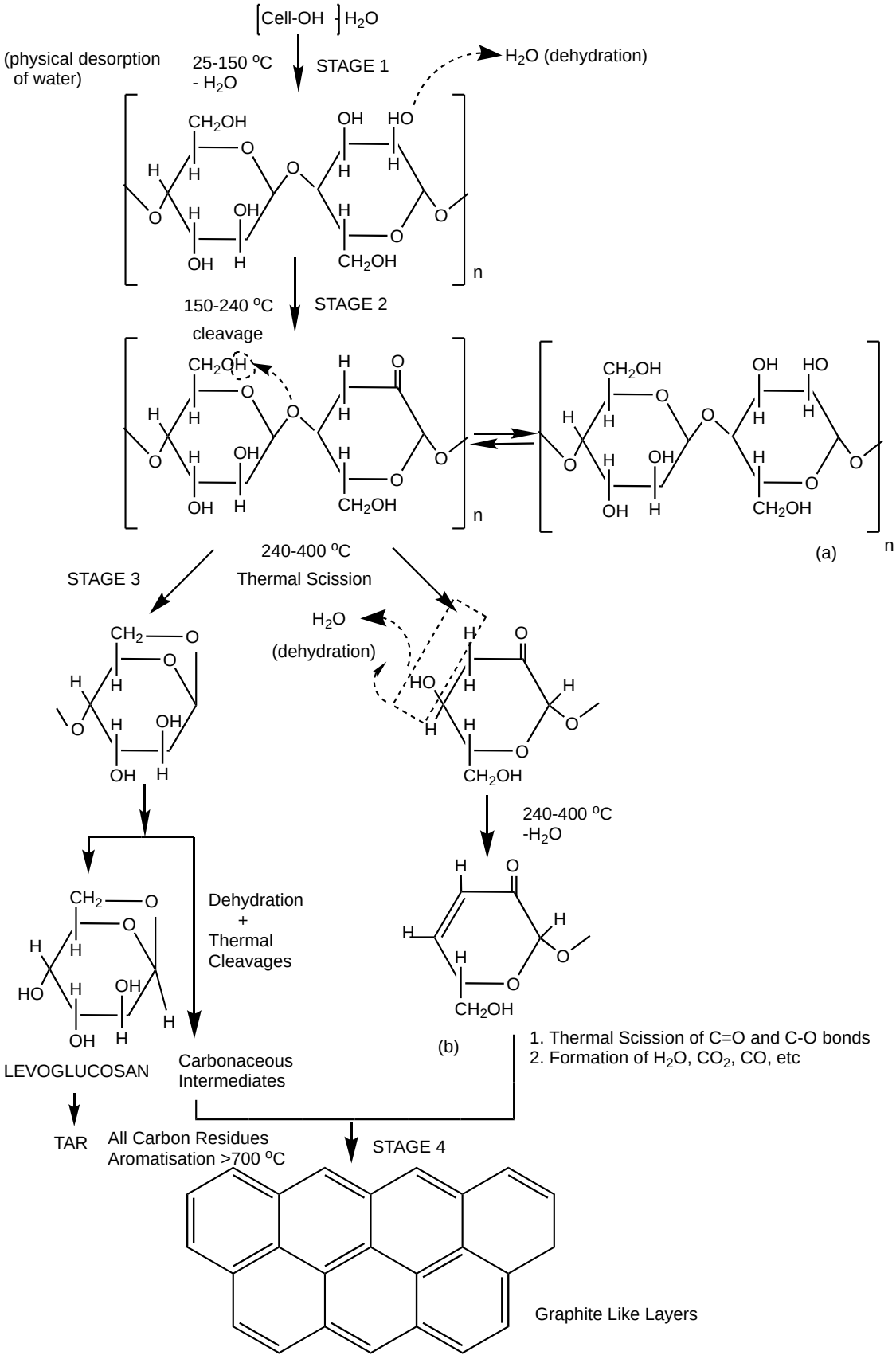

Figure 2.11 Reaction mechanism for the conversion of cellulose to carbon [153].

With reference to Figure 2.11, the mechanism of thermal decomposition of cellulose during pyrolysis based on Tang and Bacon's method is: (i) physical desorption of water at 25 - 150 ºC. This step is reversible and absorbs water by as much as 12%, (ii) dehydration of anhydroglucose at 150 - 240 ºC; (iii) thermal cleavage of the glycosidic linkage and scission of the other C-O bonds and some C-C bonds via a radical reaction at around 250 ºC. At this stage, a large amount of tar, H_2O, CO and CO_2 are formed; (iv) aromatisation deformation representing 4 residual carbon atoms per anhydroglucose above 400 ºC. The formation of carbon comes from C_3, C_4, C_5 and C_6. A yield of four carbons from each anhydroglucose corresponds to an ultimate weight loss of approximately 70%; and (v) complete aromatisation above 600 ºC. In this step, the ether linkages and aliphatic chains disappear.

Half a century later, the pyrolysis of cellulose was reviewed based on the formation of levoglucosan because this substance is the main product released during the carbonisation of cellulose, up to 60 wt% yield [159]. The mechanism for the pyrolysis of cellulose proposed by Mayes & Broadbelt [159] involves the formation of levoglucosan from methyl-cellobiose. Metyl-cellobiose is the smallest subunit of cellulose that contains a glycosidic bonding. The formation of levoglucosan is illustrated in Figure 2.12.

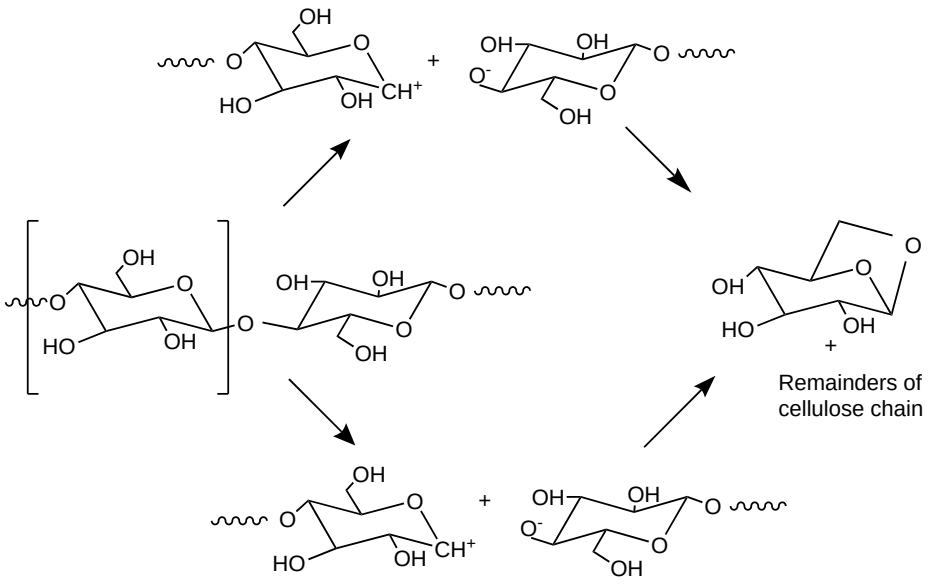

Figure 2.12 The formation of cellulose to levoglucosan [159].

The formation of levoglucosan starts with the initiation step and is followed by depropagation. In the second step, a molecule of levoglucosan is released from the chain-end of cellulose. This process repeats until the cellulose chain has fully decomposed into a levoglucosan molecule, see Figure 2.13 and 2.14.

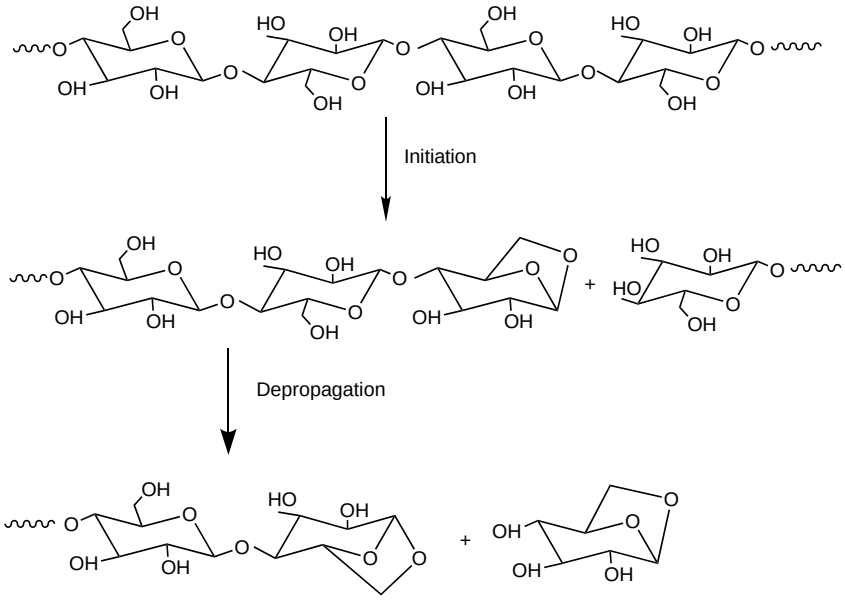

Figure 2.13 Mechanism for levoglucosan formation via the initiation and depropagation steps [159].

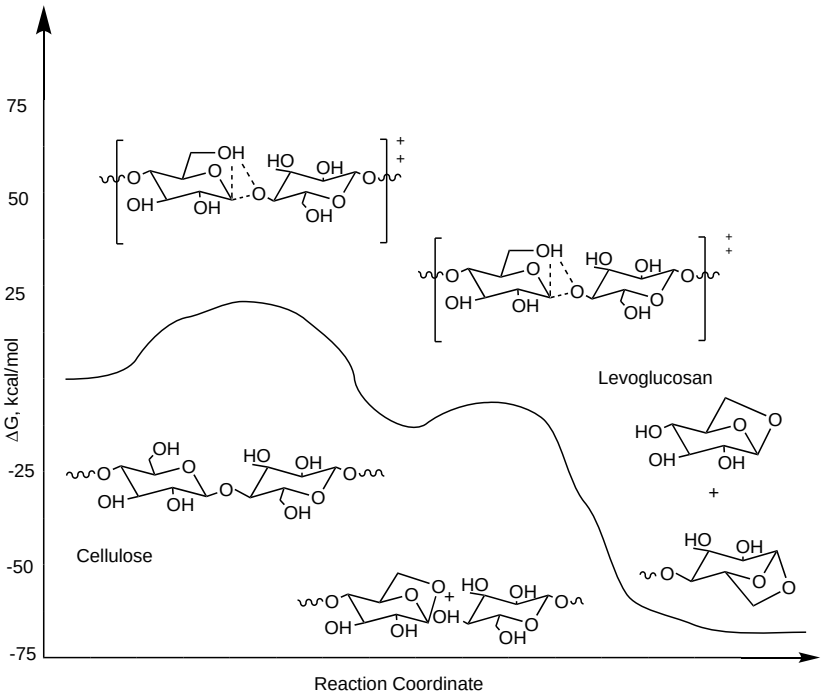

Figure 2.14 Free energy diagram for the glycosidic cleavage of methyl cellobiose [159].

The formation of levoglucosan during carbonisation reduces the carbon yield of cellulose. Therefore, a slow heating rate, oxidation and the use of flame retardants are carried out to prevent the excess formation of levoglucosan [160]. In addition, a slow heating rate can increase the mechanical properties of the resultant carbon fibre [160]. A summary for the mechanical properties of cellulose-based carbon fibres is displayed in Table 2.5.

Table 2.5 The mechanical properties of cellulose-based carbon fibres.

No.	**Precursors**	**Spinning method**	**Heating rate (ºC/minute)**	**Heat treatment (ºC)**	**Tensile strength (GPa)**	**Modulus (GPa)**	**References**
1	Cellulose	Melt-spinning	3	1000	1.01	116	[161]
2	Lyocell	Wet-spinning	N.A	1300	1.07	96.6	[162]
3	Rayon	Wet-spinning	N.A	1300	0.82	79.2	[162]
4	Lyocell	Wet-spinning	N.A	1300	0.90	0.81	[163]
5	Rayon	Wet-spinning	N.A	1300	0.99	0.90	[163]
6	Lyocell	Wet-spinning	N.A	1300	0.49	37.6	[164]
7	Lyocell filled 5% carbon black	Wet-spinning	N.A	1300	0.57	48.3	[164]
8	Lyocell filled 10%	Wet-spinning	N.A	1300	0.71	58.8	[164]

	carbon black						
9	Cellulose carabamate (CC)	Wet-spinning	4	1100	0.50	0.54	[165]
10	Wool fibres	-	4	800	0.22	-	[165]
11	Wool fibres	-	4	800	0.16	-	[165]

2.6.1 Summary

Carbon fibres can be classified based on their properties. PAN and pitch are two types of commercial precursors for carbon fibre due to their good mechanical properties, however, they are petroleum based. Cellulose, the most abundant biopolymer, is a promising precursor for carbon fibre. The mechanism for the carbonisation of cellulose has been reviewed by several groups, since 1964 up until recently in 2012. Levoglucosan is the main component during the pyrolysis of cellulose which can decrease the carbon yield of cellulose-based carbon fibres. Therefore, a slow heating rate is used to prevent the excess formation of levoglucosan.

CHAPTER 3
METHODOLOGY

3.1 Materials

The materials used in this study were obtained from commercial sources. A summary of the main chemicals used in the current study and the properties of the materials, as reported by suppliers, are described in Table 3.1.

Table 3.1 A summary of chemicals used in this project.

No.	Materials	Description	Function	Suppliers
1	Cellulose acetate ($C_{76}H_{114}O_{49}$)	Molecular weight (M_w) of 30,000 g/mol, white powder with a density of 1.30 g/ml at 25 ºC.	As-received material	Sigma-Aldrich, UK
2	Acetone (C_3H_6O)	M_w of 58.08 g/mol, liquid anhydrous with purity $\geq$ 99.90%.	Solvent	Fisher Chemical, UK
3	Dimethylsulfoxide (DMSO)	M_w of 78.13 g/mol, liquid anhydrous with purity $\geq$ 99.90%, melting point (M_p) of 16.19 ºC and boiling point (b_p) of 189 ºC.	Solvent	Sigma-Aldrich, UK
4	Nano-crystalline cellulose (NCC)	White crystalline powders, M_w of 14,700-27,850 and a density of 1.50 g/cm^3.	As-received material	Celluforce, Canada

5	Cellulose	White powder with a density of 0.60 g/ml at 25 ºC.	As-received material	Sigma-Aldrich, UK
6	Pyridine (C_5H_5N)	M_w of 79.10 g/mol, liquid anhydrous with purity 99.80% and colourless, a density of 0.97 g/ml at 25 ºC, M_p of -42 ºC and b_p of 115 ºC.	Solvent and co-catalyst in the acetylation reaction	Sigma-Aldrich, UK
7	Acetic anhydride ($C_4H_6O_3$)	M_w of 102.09 g/mol and a density of 1.08 g/ml at 25 ºC.	As acetylating agent for the acetylation reaction	Acros Organic, UK
8	Polyacrylonitrile $(C_3H_3N)_n$	Powder form with mean particle size of 50 micrometres and containing copolymer (99.5 % Acrylonitrile).	Matrix of “carrier” polymer for spun-fibres	Good Fellow, UK
9	Potassium bromide (KBr)	M_w of 119 g/mol and M_p of 734 ºC.	Production of disks for FTIRS	Sigma-Aldrich, UK
10	Sodium hydroxide (NaOH)	M_w of 40 g/mol and pellet (anhydrous) with M_p of 318 ºC.	Solvent for deacetylate spun-fibre	Sigma-Aldrich, UK
11	Deionised water (DI)	pH = 7	Solvent	Department of Metallurgy and Materials, University of Birmingham

3.2 Procedures

3.2.1 Drying

Solid materials such as NCC, PAN, cellulose, cellulose acetate and KBr were dried before use. The NCC was dried in a vacuum oven for 5 hours at 80 ºC. After this period, the dried NCC was transferred to vial and capped. The sample was labelled as NCC-dried and stored in a desiccator. The same procedure was performed for PAN, cellulose, cellulose acetate and KBr.

3.2.2 Acetylation

3.2.2.1 Acetylation of nano-crystalline cellulose

Four acetylation procedures were investigated to introduce the acetyl groups on the NCC: (i) without dispersion; (ii) reduced the particle size via cryomilling; (iii) dispersion of pyridine using a sonicator; and (iv) using the material in a gel-form.

In the first procedure that was used for acetylation, one gram of NCC was added to a 250 ml three-necked round-bottom flask followed by 20 ml of anhydrous pyridine. Five ml of acetic anhydride was then added to the flask in a dropwise fashion. The acetylation on NCC was performed through the constant stirring of the reagents in a three-necked round-bottom flask at 80 ºC for 5, 10, 15 and 20 hours. After this period, the solution was cooled to room temperature. The product was then diluted with DI water and centrifuged at 4000 rpm for five minutes to separate the solid from the solution. The solution was centrifuged several times until the pH of the suspension was close to 7. The liquid was decanted and the solid recovered. Finally, the product was dried in a vacuum oven at 80 ºC for five hours. It was transferred to a vial and stored in a desiccator. These samples were coded as NCC-Ac 5h, NCC-Ac 10h, NCC-Ac 15h and NCC-Ac 20h. The as-received and NCC-Ac were analysed using FTIR spectroscopy, TGA, XRD and ESEM.

The second procedure that was used for acetylating the NCC was cryomilled before acetylation. Cryomilling of NCC was preformed using a Cryomill 6750 freezer/mill for five minutes. The next steps were the same as the first procedure described above. However, this process had a reaction time of 10 hours. This sample was then coded as NCC-Ac 10h-cy. The material was characterised using FTIR spectroscopy, TGA and ESEM.

The third procedure that was investigated for the acetylation of NCC involved the sonication of pyridine and the NCC mixture before acetylation. One gram of NCC was dispersed with 20 ml of pyridine in a 250 ml glass beaker using a sonicator (Ultrasonic processor UP 400St, Hielscher, UK). The sonicator was operated at 24 kHz for 10 minutes. A cooling system was used to maintain the temperature between 20 ºC and 30 ºC during sonication. After that, the suspension was transferred to a 250 ml three-necked flask. The acetylation was started by adding 10 ml of acetic anhydride to the suspension in dropwise fashion. The reaction was then carried out under constant stirring with a magnetic stirrer at 80 ºC for five hours. After this period, the suspension was cooled to room temperature and precipitated with DI water and acetone (1:1). The liquid was decanted and the solid was washed several times using DI water and acetone until achieving a pH close to 7 to remove by-products resulting from the reaction. The product was evaporated (Evaporator model MM70312) reduced pressure using a Vacuubrand CVC 3000 to evaporate DI water and acetone. Finally, the product was dried under vacuum at 80 ºC for five hours. The sample was coded as NCC-Ac dispersed. The NCC-Ac dispersed was characterised using FTIR spectroscopy, NMR, XRD, TGA and ESEM.

The fourth and final method that was used for acetylation involved using the NCC in a gel form. 1.5 g of NCC was weighted and transferred into a 250 ml glass beaker. 100 ml of DI water was added to produce 1.5% (w/v) of NCC. The suspension was sonicated at 24 kHz at 20 ºC - 30 ºC for 10 minutes. 30 ml of pyridine was added to the suspension and sonicated for 10 minutes at 20 ºC - 30 ºC. The suspension was transferred to a 250 ml three-necked bottom-flask. The acetylation was commenced by adding 15 ml of acetic anhydride in dropwise fashion. The reaction was carried out

under reflux in a nitrogen atmosphere for five hours at 80 ºC. After this period, the reaction was cooled to room temperature. Subsequent to this, the product was precipitated using DI water and acetone (1:1). The liquid was decanted and the solid was washed several times using DI water and acetone until the pH was close to 7. This was performed to remove by-products resulting from the reaction. The solid was recovered and the solution was decanted. The product was evaporated using a rotary evaporator as described previously. Finally, the solid was dried in a vacuum oven at 80 ºC for five hours. The product was coded as NCC-Ac gel-py1. The acetylated NCC was characterised using FTIR spectroscopy, NMR, XRD, TGA and ESEM. The conditions that were used in the acetylation process are summarised in Table 3.2. In addition, a schematic for the acetylation of NCC in a gel form is represented in Figure 3.1. A photograph of the acetylation procedure using for the NCC in a gel form using sonication is presented in Appendix 2.

Table 3.2 The parameter used for the acetylation of NCC in a gel-form.

No.	**Sample code**	**Sonication time (minutes)**		**Reaction time (hours)**	**Temperature (ºC)**	**Volume of acetic anhydride (ml)**
		DI water	**Pyridine**			
1.	NCC-Ac gel-py1	10	10	5	80	15
2.	NCC-Ac gel-py2	10	10	10	80	15
3.	NCC-Ac gel-py3	20	10	10	80	15
4.	NCC-Ac gel-py4	10	10	5	80	30
5.	NCC-Ac gel-py5	10	10	5	100	15
6.	NCC-Ac gel-py6	10	10	5	100	30

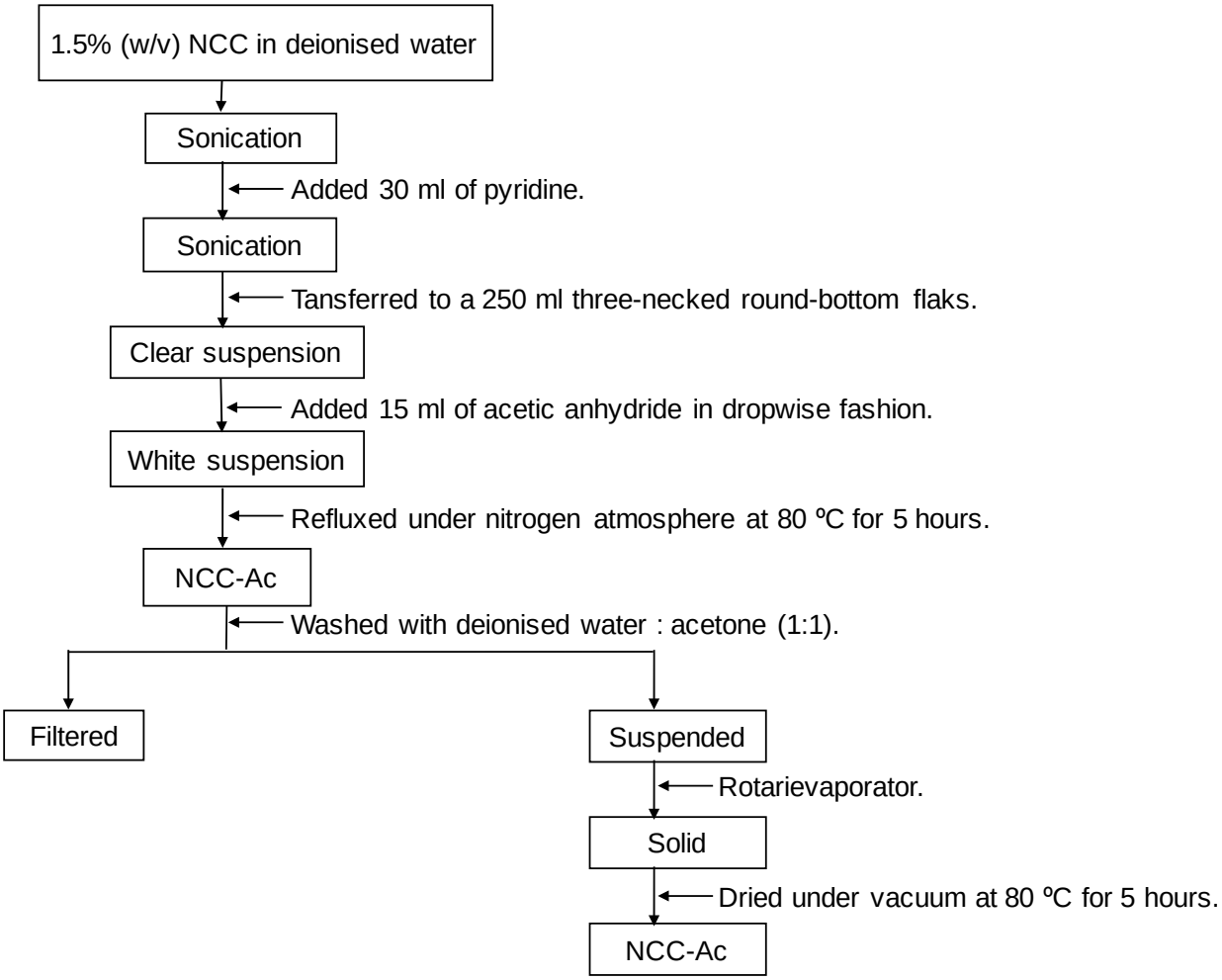

Figure 3.1 A flowchart for the acetylation of NCC.

The solubility of NCC and NCC-Ac was examined using DMSO as the solvent. A 6% (w/v) of NCC and NCC-Ac in DMSO was dispersed using sonication for 10 minutes. The viscosity of the solutions was characterised using a rheometer (Rheometry Discovery HR-1, TA Instrument) at shear rates in the range 1 - 10,000 s^{-1}.

3.2.2.2 Acetylation of cellulose

A gram of cellulose was weighted and transferred into a 250 ml glass beaker and 20 ml of pyridine was added. The cellulose and pyridine were dispersed using sonication as described previously. After sonicating the mixture for 10 minutes, the suspension was transferred to a 250 ml three-necked bottom-flask and the acetylation was started by adding 10 ml of acetic anhydride to the suspension in dropwise fashion. The reaction

was carried out with constant stirring at 80 ºC for five hours. The procedures described previously were used to produce and analyse the acetylated cellulose. In this instance, the product was coded as acetylated cellulose. The acetylated cellulose was characterised using FTIR spectroscopy, XRD, TGA and ESEM. The characterisation of acetylated cellulose was also compared with commercial cellulose acetate (M_w of 30,000 g/mol supplied by Sigma Aldrich).

3.2.3 Electro-spinning of cellulose acetate

3.2.3.1 Solution preparation

10 grams of cellulose acetate was weighted and transferred into a 250 ml glass beaker. 50 ml of acetone was added to the glass beaker to produce 20% (w/v) cellulose acetate solution. The reaction was performed through constant stirring under a nitrogen atmosphere at room temperature. After dissolving the cellulose acetate, it was transferred to a vial. The sample was coded as 20% (w/v) cellulose acetate in acetone and stored in a fridge at 10 - 15 ºC. This solution was used to electro-spin cellulose acetate at 15 ºC with an aluminium ground collector.

Another cellulose acetate solution was prepared by dissolving 10 grams of cellulose acetate in 50 ml mixture of acetone and DMSO with a ratio of 2:1 respectively. The solution preparation was carried out as the procedure described above. However, the second solution was stored at room temperature. This solution was used to electro-spin cellulose acetate at room temperature with a paper-base drum collector. The experimental set up was presented in Section 3.2.3.2.

3.2.3.2 Electro-spinning

The first set of condition that were used for electro-spinning were: (i) a voltage of 17 kV; (ii) polymer solution feed rate of 0.01 ml/hour; (iii) a needle tip-to-collector distance of 8.45 cm; (iv) and a rectangular (11 x 11 cm) aluminium foil ground collector. The electro-spinning was performed using a cooling system where the temperature of the

solution was maintained at approximately 15 ºC. The second set of parameter for electro-spinning process were: (i) a voltage of 17 kV; (ii) polymer solution feed rate of 0.01 ml/hour; (iii) a needle tip-to-collector distance of 8.45 cm; (iv) and a paper-base drum collector. The electro-spinning was performed at room temperature. The experimental set up for electro-spinning is illustrated in Figure 3.2. The morphology of spun-fibres was investigated using SEM.

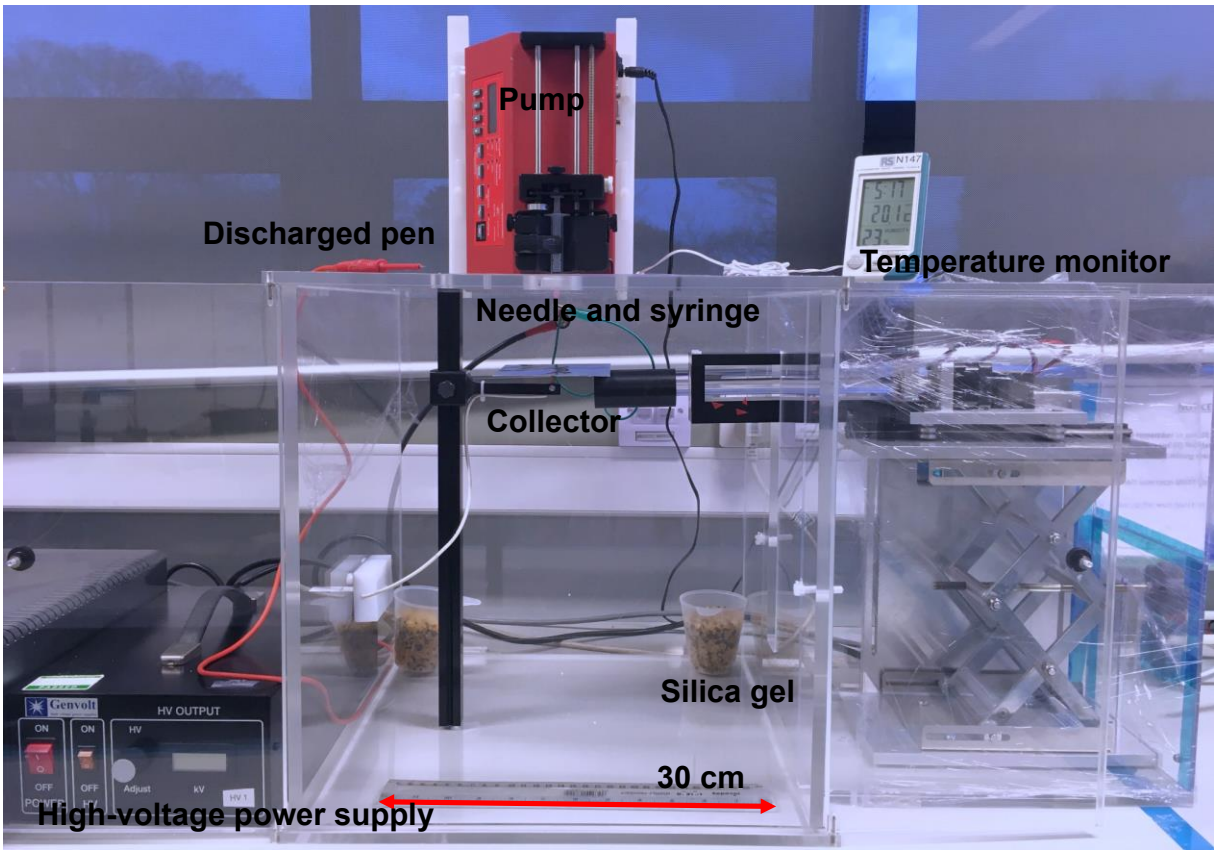

Figure 3.2 Photograph illustrating the electro-spinner set up.

3.2.4 Electro-spinning NCC with polyacrylonitrile

3.2.4.1 Solution preparation

A PAN solution with a concentration of 8% (w/w) in DMSO and NCC with a concentration of 4% (w/w) in DMSO were prepared. The PAN solution was prepared in a 250 ml three-necked bottom-flask through a constant stirring under a nitrogen atmosphere at room temperature. A similar procedure was used to prepared the NCC

gel. The polymer solution for electro-spinning was prepared by dispersing 9%, 17% and 21% of NCC suspension to the 8% (w/w) PAN solution in DMSO using ultrasonic bath (U Series Ultrawave, UK).

The conductivity of the solutions was characterised using a conductivity meter (Jenway 4510 Conductivity/TDS meter, UK). Before the conductivity measurement was performed, the equipment was calibrated using reference standard solution (HI7033, Hanna Instrument). The conductivity of the reference standard was 84 µm/cm at 25 ºC. A water bath was used to keep the temperature constant during the measurement.

3.2.4.2 Mechano-electro-spinning

A further experiment for electro-spinning was carried out using the mechano-electro-spinner (MES) designed by the University of Birmingham in collaboration with the CTM Ltd. A photograph of the MES equipment is presented in Figure 3.3. The conditions for electro-spinning using the MES were: (a) a voltage of 6,400 V; (b) feed rate of 0.5 mm/minute; and (c) transverse speed rate of 1,500 rpm and winding speed rate of 10,000 rpm.

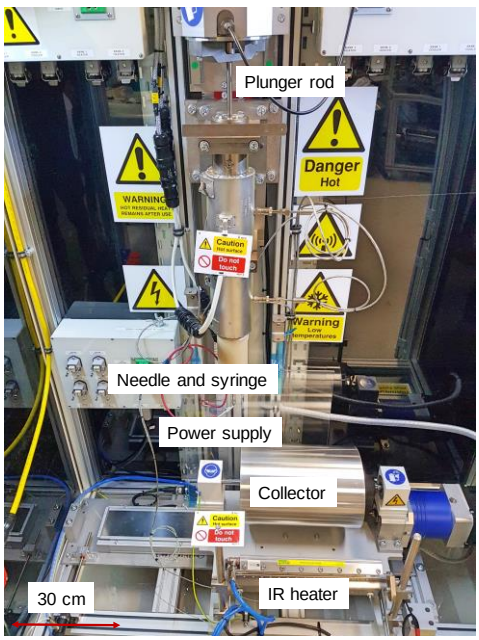

Figure 3.3 A photograph of the MES.

There are three types of electro-spinning in the MES equipment, namely:

- Liquid/solution electro-spinning
- Wet-spinning
- Melt-spinning

In this experiment, liquid/solution electro-spinning was used. The parameters used such as voltage, feed rate, transverse speed rate, winding speed rate, temperature and humidity were monitored by software monitor.

3.2.5 Wet-spinning

Wet-spinning of NCC and NCC-Ac was performed using a 6% (w/v) NCC and NCC-Ac solution in DMSO using acetone as the coagulation bath. A further experiment was carried out by introducing a 20% (w/v) cellulose acetate in DMSO to the NCC and NCC-Ac suspension. The concentration of NCC and NCC-Ac in cellulose acetate was 5%. The solutions were dispersed using sonication. The polymer solutions were spun with conditions as following: needle diameter of 0.25 mm, feed rate of 0.04 g/minute and winding speed of 0.44 m/minute. The morphology and cross-section of the fibre was analysed using ESEM. A photograph of the wet-spinning equipment is presented in Figure 3.4.

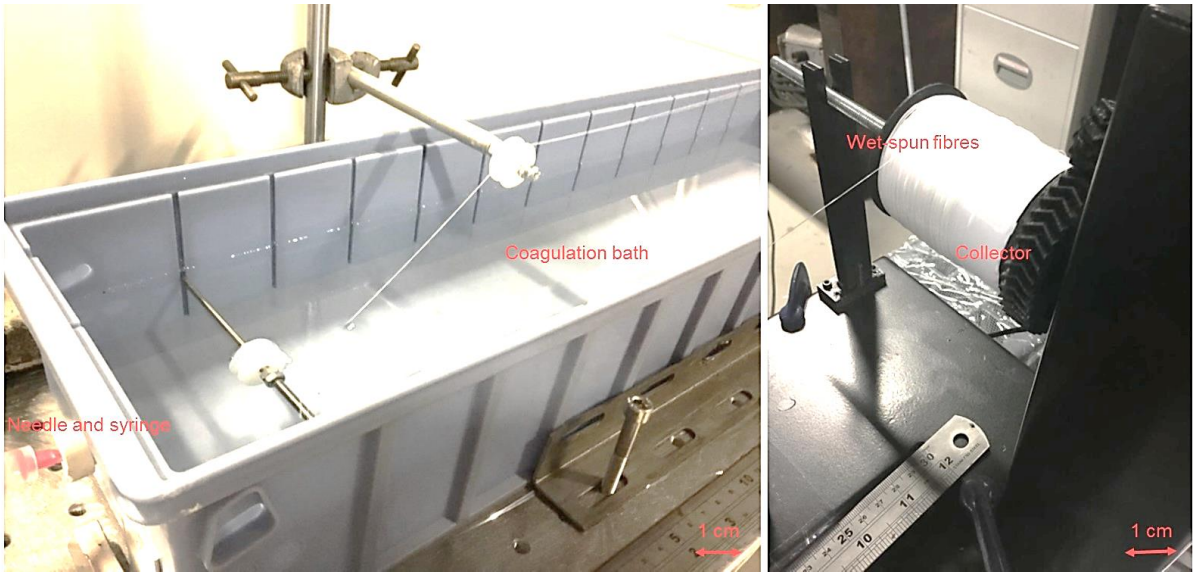

Figure 3.4 A photograph of the wet-spinning.

3.2.6 Deacetylation of NCC-Ac

A gram of NCC-Ac was immersed in 25 ml of 0.1 N NaOH for 24 hours at room temperature. The suspension was washed with DI water several times until the pH equalled 7. The solid was precipitated with DI water and allowed to form two stable phases. The solution was then decanted and the solid was recovered. The product was dried under vacuum at 80 ºC for 5 hours. The deacetylation on NCC-Ac was characterised using FTIR spectroscopy, XRD, TGA and ESEM.

The spun-fibres produced from the wet-spinning of NCC-Ac were also regenerated using 0.1 N NaOH for 24 hours at room temperature. After this period, the spun-fibres were washed with DI water until the pH was 7. The spun-fibres were dried at room temperature.

3.2.7 Carbonisation of wet-spun NCC fibres

Carbonisation of the wet-spun NCC fibres was performed using a tube furnace (Pyro Therm Furnaces) under a nitrogen atmosphere. The sample was placed in a graphite sample holder and placed inside the tube furnace. A heating rate of 0.5 $K.minute^{-1}$ was used for pre-carbonisation from 25 ºC to 400 ºC and the temperature was maintained for 1 hour at 400 ºC. The carbonisation was carried out from 400 ºC to 600 ºC at 1 $K.minute^{-1}$ and held isothermally for 1 hour at 600 ºC. The final heating sequence was from 600 ºC to 900 ºC at 1 $K.minute^{-1}$ and the isothermal for 1 hour at 900 ºC. The carbonised fibre was characterised using Raman spectroscopy and ESEM.

3.3 Characterisation

The characterisations of materials used and produced in this research project are described in the following sections.

3.3.1 Particle size analysis

Particle size distribution of the as-received of NCC before and after cryomilling was analysed using a dynamic light scattering instrument (Mastersizer 2000, Malvern Instrument, UK). A 2% (w/v) NCC solution was dispersed in distilled water and sonicated (U Series Ultrawave, UK) for six minutes. A few drops of the suspension were introduced to the dispersion unit the instrument using a pipette. The solution was agitated using a Hydro 2000MU at 1,200 rpm and data were acquired over five cycles.

3.3.2 Transmission electron microscope

A LoJeol 1200EX transmission electron microscope (TEM) was used to characterise the as-received NCC. A 0.01% (w/v) of NCC suspension in DI water was sonicated using an ultrasonic bath (U Series Ultrawave, UK) for 6 minutes. A drop of the suspension was deposited on a copper grid (200 mesh) using a pipette. The water was allowed to evaporate at room temperature. The solution on the grid was stained with a drop of 2% uranyl acetate and dried at room temperature. The excess of solution was removed using the tip of a filter paper. The sample was observed using an accelerating voltage of 80 kV. Particle size distribution was determined using ImageJ software analysis. The scale bar from TEM was used as the measurement scale. Brightness and contrast for the image was selected manually. Particle and counting analysis were carried out by drawing line over selected particles and clicked 'Analyse → Measure'. After that, several particles were chosen for the length and diameter measurements. Once the data were acquired and saved, the dimensions of the particles were imported to MS Excel for statically analysis.

3.3.3 Fourier transform infrared spectroscopy

An FTIR Spectrometer (Nicolet 8700, Thermo Scientific) was used to characterise the functional groups present in the materials used in this study. The samples for FTIR were prepared by grinding 200 mg of pre-dried potassium bromide (KBr) with 2 mg of NCC and NCC-Ac. The ground powder was transferred to a 13 mm compression mould

and compressed to 10 tons to make a flat circular disk. Similarly, a second (reference/background) disk of 200 mg of pre-dried KBr was made using the same procedure mentioned above. The reference disk was used to obtain the background FTIR spectrum. The instrument was operated in a transmission-mode in the range 400 - 4000 cm^{-1}, along with a resolution of 4 cm^{-1} and 100 scans.

3.3.4 Cross-polarisation magic-angle spinning ^{13}C-NMR spectroscopy

The chemical changes in the NCC before and after acetylation was also confirmed using a Solid-state NMR Bruker Avance III HD NMR Spectrometer operated by Durham solid-state NMR research group, University of Durham, United Kingdom. Three samples were collected for this characterisation namely, as-received NCC, NCC-Ac dispersed and NCC-Ac gel-py4. Solid-state ^{13}C NMR was operated at room temperature. The NMR measurement was operated at a frequency of 100 MHz for carbon. Dry and powdered NCC and NCC-Ac were packed into a 4 mm rotor. The solid-state ^{13}C NMR spectra were determined at a spinning speed of 10 kHz using a solid cross polarisation/magic angle spinning (CP/MAS) probe. The number of scan was measured for 1,800 and 7,200 for the as-received NCC and the NCC-Ac respectively.

3.3.5 X-Ray diffraction

The crystallinity of cellulose and NCC before and after acetylation was studied using X-Ray diffraction (Equinox 3000). The instrument was operated at 35 kV and 25 mA. The sample was placed on rotating with a diameter of 1.5 cm. X-Ray scanning was performed over 2 Theta ranging from 0 to 100º with a scan rate of 0.02º sec^{-1}. The scanning was operated for one hour. The index crystallinity of samples was calculated based on the Segal method [163]:

$$\%CrI = \frac{I_{002} - I_{am}}{I_{002}} \times 100\% \quad \text{..} [3.1]$$

where

I_{002} = the maximum intensity (in arbitrary units) of the 002 lattice diffraction.

I_{am} = the intensity of diffraction in the same units at 2 Theta = 18º.

3.3.6 Thermogravimetric analysis

The mass-loss characteristics of the materials used in this project was characterised using a thermogravimetric analyser (model TASC 414/4 NETZSCH). The specimen was heated from 25 ºC to 900 ºC at 10 K.minute^{-1} under an argon atmosphere.

3.3.7 Scanning electron microscope

A scanning electron microscope Jeol 6060 was used to analyse the morphology of the samples. The sample was placed on an adhesive-backed carbon tape and attached to the specimen holder. The sample was then sputter-coated (SC 500 emscope) with a thin layer of gold alloy to reduce the charging during analysis.

3.3.8 Environmental scanning electron microscope

A Philips XL-30 FEG Environmental SEM used to study the morphology of samples. Samples for ESEM were sputtered-coated with a thin layer of gold alloy using sputter coater (SC 500 emscope).

3.3.9 Raman spectroscopy

The structure of the carbonised material was investigated using Raman spectroscopy (Raman microscope enclosure, RE-04, Renishaw, UK). This spectrometer utilises a 488 nm laser to excite the molecular vibration. The samples were analysed without any sample treatment or preparation. The analysed region was visualised through a microscope with a magnification of 50x. The range of wavelengths collected was typically from 150 to 3200 cm^{-1} over a time period of at least 30 seconds and multiple accumulations for high sensitivity. For the measurement, it used the following parameters: (i) Spectral acquisition set up: select static, standard confocality, centre 520 cm^{-1}, laser and grafting as needed. (ii) Under acquisition: 1 s, 1 accumulation and 10% power.

CHAPTER 4
RESULTS AND DISCUSSION

4.1 Acetylation of NCC

In this study, sonication was used to improve the homogeneity and the dispersibility of NCC in DMSO. Generally, sonication converts the ultrasonic signal into a physical vibration through the formation, growth and subsequent collapse of bubbles. In the present study, two methods were used for the acetylation on NCC using ultrasound-based sonication. In the first case, the as-received NCC was dispersed in pyridine with sonication. In the second case, an aqueous gel of the NCC was sonicated, followed by the addition pyridine.

The techniques used in this study to characterise NCC before and after acetylation were:

(i) The morphology: TEM and ESEM.
(ii) Chemical properties: FTIR and NMR spectroscopy.
(iii) Physical properties: TGA, viscosity and conductivity.

NCC and NCC-Ac were spun using a carrier-polymer. PAN and cellulose acetate were used as the carrier-polymer for electro-spinning and wet-spinning respectively. Wet-spun fibres were carbonised to produce carbon fibre. The characterisation methods used for the fibres were:

(i) Electro-spinning: ESEM, FTIR, conductivity and viscosity.
(ii) Wet-spinning: ESEM.
(iii) Carbonisation: ESEM and Raman spectroscopy.

The results from these studies are discussed in the following sub-sections.

4.2 The morphology of NCC

4.2.1 Transmission electron microscope and image analysis

In this current study, the NCC was purchased from Celluforce, Canada. It was retailed as 'cellulose hydrogen sulphate sodium salt'. It was stated that the NCC was extracted using H_2SO_4 and the sulphur content of the as-received material was 0.86 - 0.89% with a sulphate content of 246 - 261 mmol/kg.

4.2.1.1 As-received and cryo-milled NCC

(i) As-received NCC

TEM micrographs of the as-received NCC dried at 80 ºC for 5 hours are presented in Figure 4.1 (a and b).

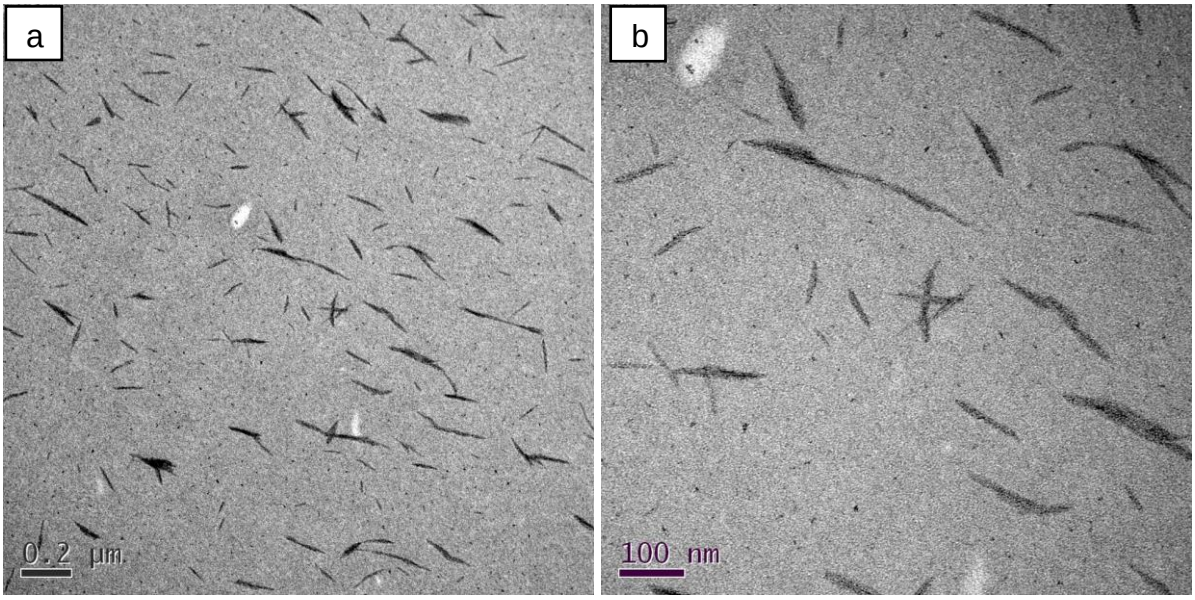

Figure 4.1 (a and b) TEM micrographs of as-received NCC.

The TEM micrographs in Figure 4.1 (a and b) illustrate the shape and dimensions of the as-received NCC material. The NCC resembles rod-like particles with a length and diameter distributions between 46 - 114 nm and 2.0 - 4.8 nm respectively. The data were obtained using image J software analysis, as described in Section 3.3.2, and

averaged by analysing 115 NCC particles. This is similar to the data provided by the supplier where the average length and diameter were 44 - 108 nm and 2.3 - 4.5 nm respectively. The length and diameter distributions for the as-received NCC are presented in Figure 4.2 (a and b).

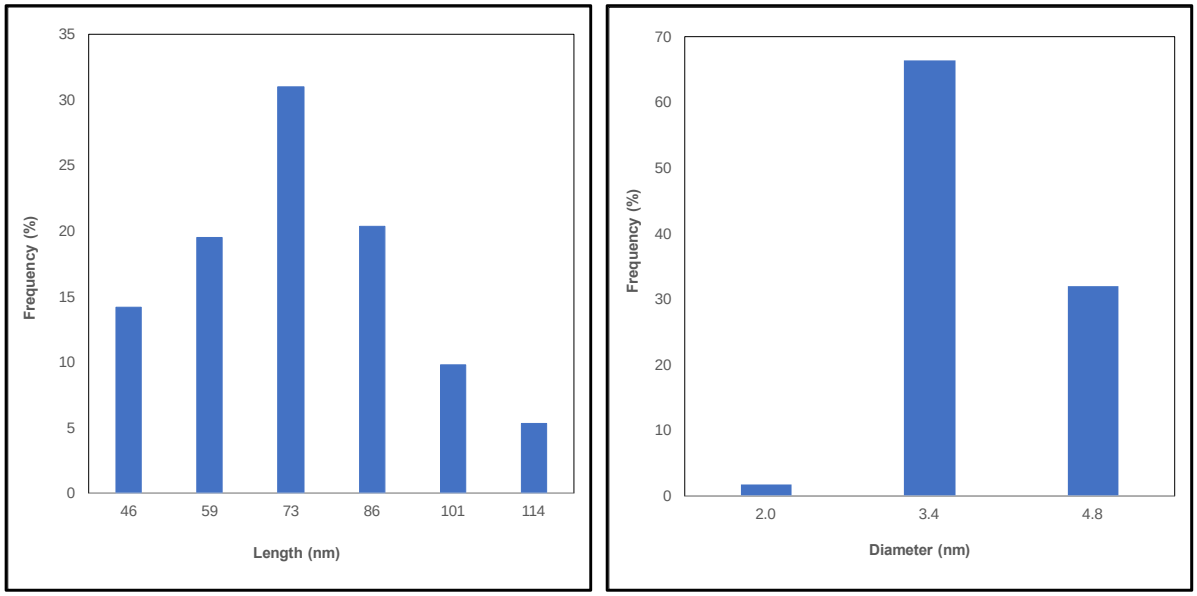

(a) (b)

Figure 4.2 (a) Length distribution of as-received NCC and (b) Diameter distribution of as-received NCC.

(ii) Cryo-milled NCC

The as-received NCC was dried at 80 ºC for 5 hours and cryo-milled. The typical TEM micrographs are shown in Figure 4.3 (a and b).

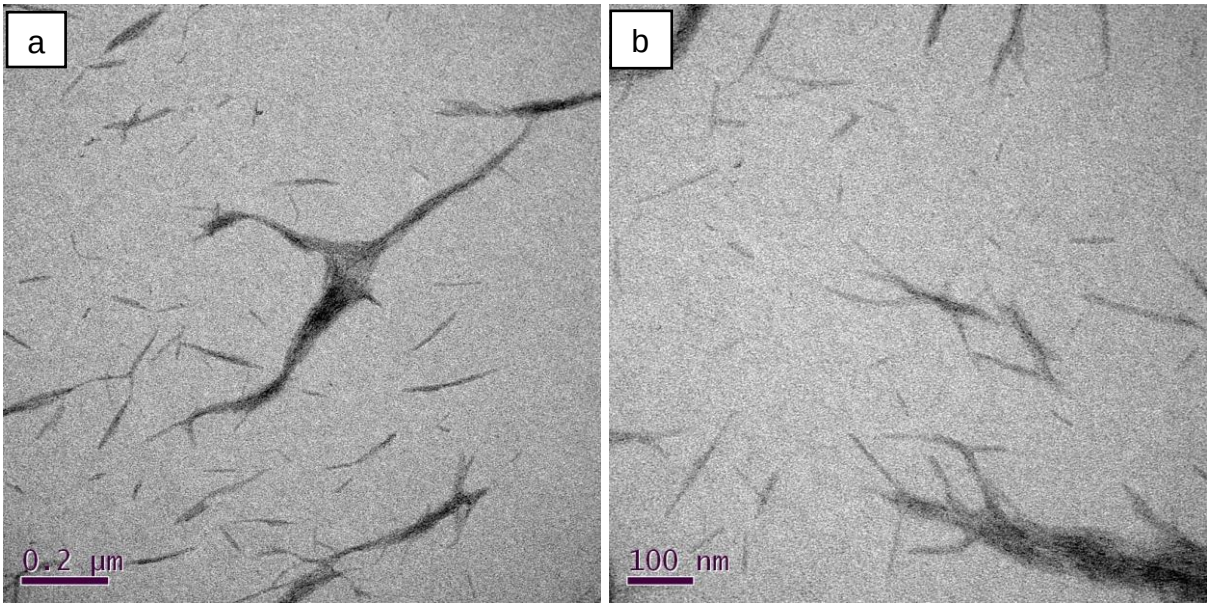

Figure 4.3 (a and b) TEM micrograph of NCC after cryo-milling.

Figure 4.3 demonstrates that the rod-like particles of NCC after cryo-milling agglomerate. In the cryo-milling process, the NCC was cooled to -196 ºC through the use of liquid nitrogen. With reference to Figure 2.5, NCC has surface charge that comes from sulphate groups during acid hydrolysis. It might be destroyed during the cryomilling process.

An atomic force (AFM) micrograph obtained from the supplier is shown in Figure 4.4. It was used to compare with that of TEM micrograph presented in this study.

Figure 4.4 AFM micrograph of NCC from supplier [167].

The AFM micrograph of the NCC shown in Figure 4.4 shows a rod-like profile as was observed with the TEM micrograph seen in this study. However, there is a slight different in the length and diameter of the NCC when compared to the data from the supplier. It might be caused by a variety of factors such as differences brightness and contrast used in the data acquisition. In addition, the sample preparation for TEM might have been different to the AFM sample preparation procedures. A summary of the lengths and diameters of the rod-like particles of NCC from several resources is summarised in Table 4.1.

Table 4.1 Diameter and length distribution reported for NCC extracted from H_2SO_4.

No.	**NCC type**	**Characterisation technique**	**Shape**	**Diameter (nm)**	**Length (nm)**
1	As-received	TEM	Needle	2.0 - 4.8	46 - 114
2	Cryo-milled NCC	TEM	Needle, agglomerates	N.A	N.A
3	As-received NCC*	AFM	Needle	2.3 - 4.5	44 - 108
4	NCC** [60]	TEM	Needle	3 - 20	200 - 600
5	NCC** [67]	TEM	Needle	4.5	300
6	NCC** [56]	TEM	Needle	2.77	122.66

*Data obtained from NCC supplier.
** Data obtained from references.

4.2.2 Environmental scanning electron microscope

The morphology of NCC was studied using ESEM. Typical micrographs of the as-received NCC and cryo-milled NCC dried at 80 ºC for 5 hours are shown in Figure 4.5.

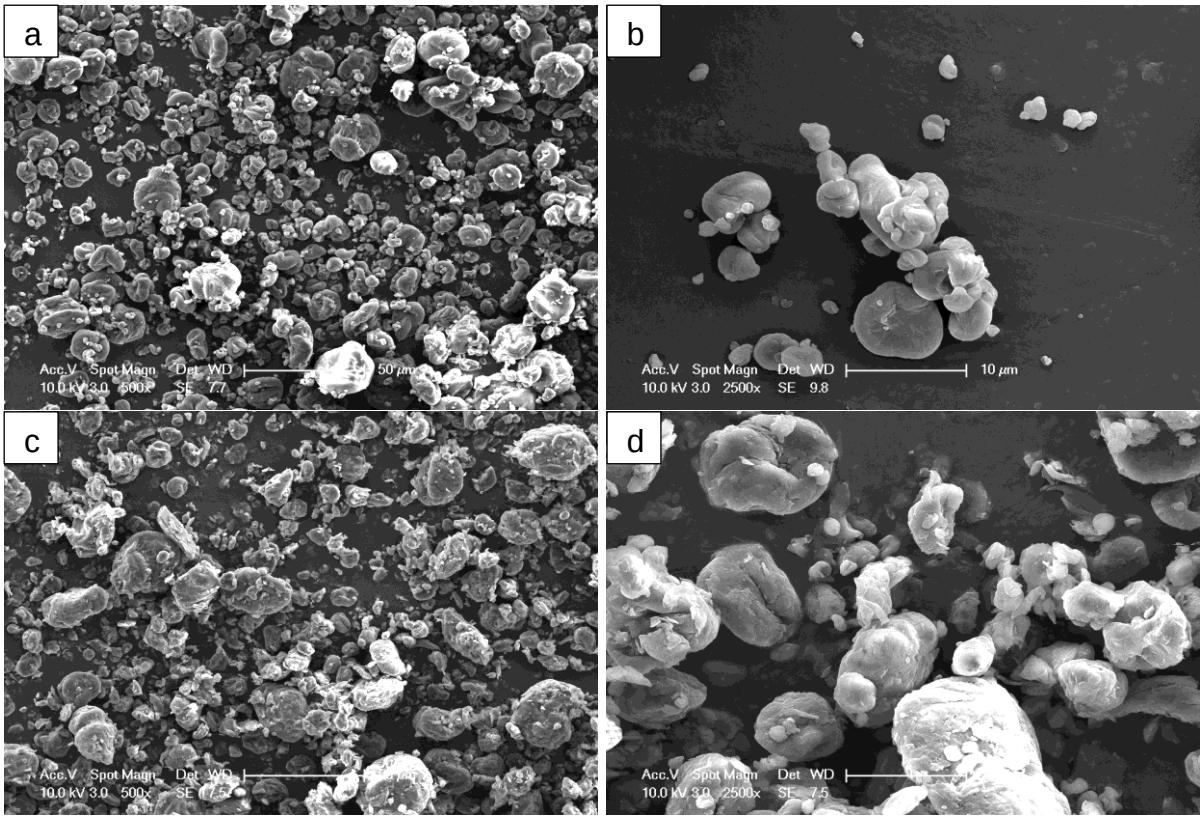

Figure 4.5 ESEM micrograph for (a-b) as-received NCC and (c-d) cryo-milled NCC.

From Figure 4.5, a smooth surface was observed for both as-received NCC and cryo-milled NCC. Similarly, the micrographs of acetylated NCC dried at 80 ºC for 5 hours are presented in Figure 4.6.

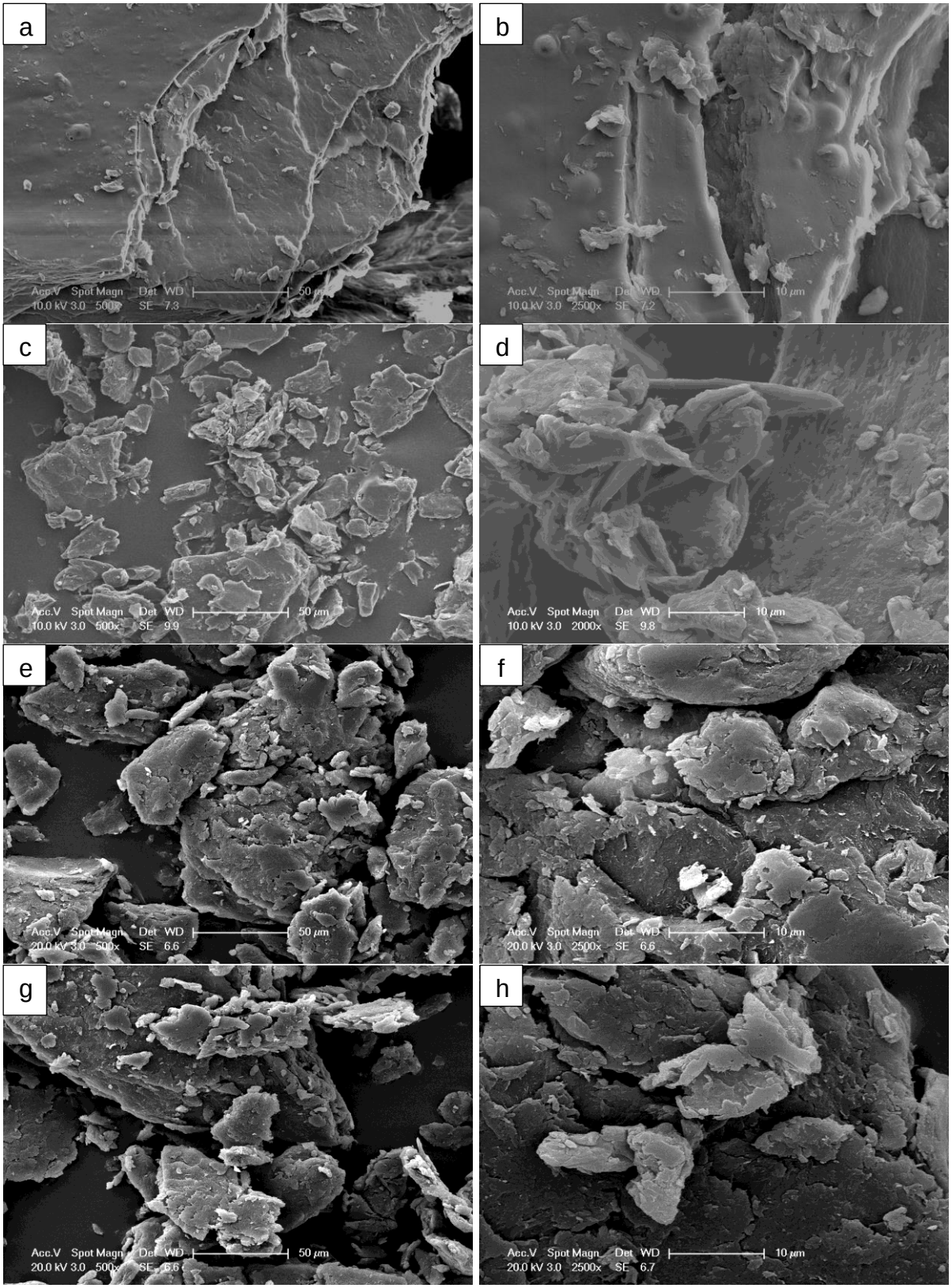

Figure 4.6 ESEM micrograph for (a-b) NCC-Ac 10h, (c-d) NCC-Ac 10h-cy, (e-f) NCC-Ac dispersed and (g-h) NCC-Ac gel-py.

The morphology of NCC after acetylation is seen to be rough and flake-like. During the acetylation, NCC formed a suspension in the solution. After drying, the suspension of NCC-Ac appeared in the form of iridescent films. This is due to the rod-like particle of NCC having a behaviour of a chiral nematic material at critical concentrations and it produces iridescent films upon dehydration [53].

4.3 Particle size analysis of as-received and cryo-milled NCC

The particle size distribution of as-received and cryo-milled NCC were in the range 1 - 140 µm and 1 - 60 µm respectively. The particle size distribution of NCC before and after cryo-milled is presented in Figure 4.7.

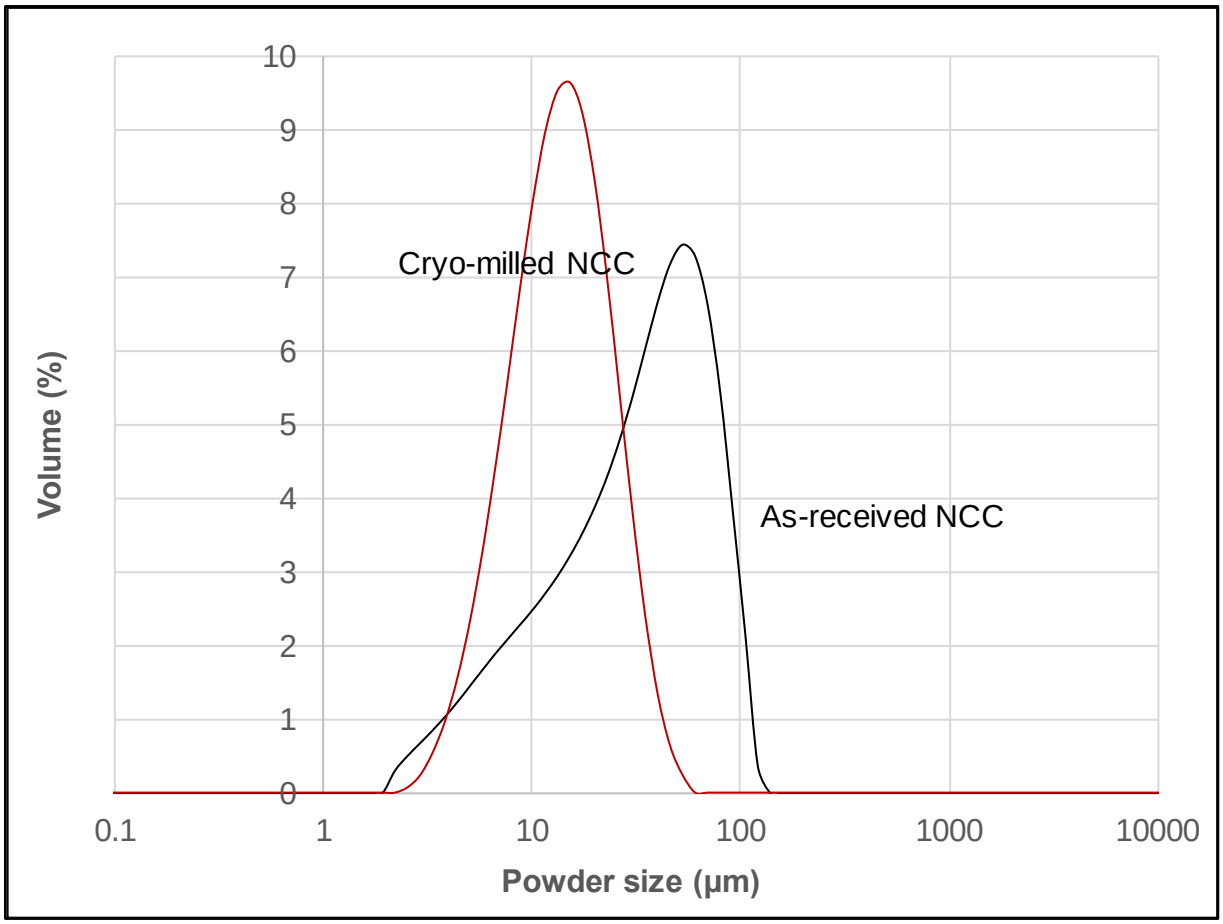

Figure 4.7 Particle size distribution of as-received NCC before and after cryo-milled.

The particle size distribution of cryo-milled NCC was half of that for the as-received material. During the cryo-milling process, the NCC was impacted by the mechanically

moving parts of the cryo-miller. As a result, it reduced the particle size of the material. The rod-like particles of NCC after cryo-milled was maintained as seen in Figure 4.3. In the cryo-milling process, it decreased the particle size of NCC without disturbing the rod-like particles of the NCC. However, the rod-like particles of the NCC seems to be agglomerate after the cryo-milling process.

4.4 FTIR spectroscopic analysis of NCC and NCC-Ac

FTIR spectral analysis of the NCC before and after acetylation was performed to identify the nature of the functional groups present. The FTIR spectra before and after acetylation as a function of reaction time is presented in Figure 4.8 with the peak assignment tabulated in Table 4.2.

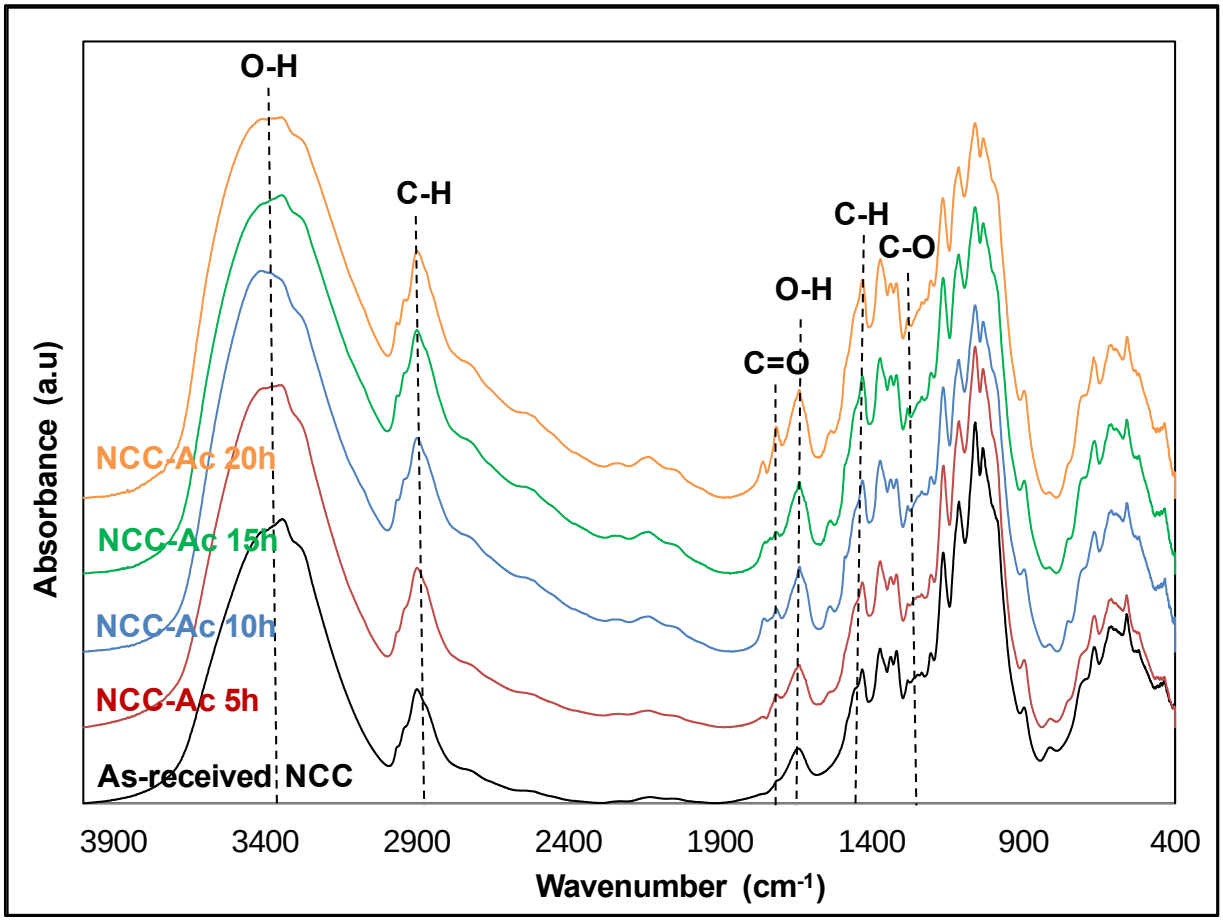

Figure 4.8 (a) FTIR spectra of NCC before and after acetylation for 0, 5, 10, 15 and 20 hours.

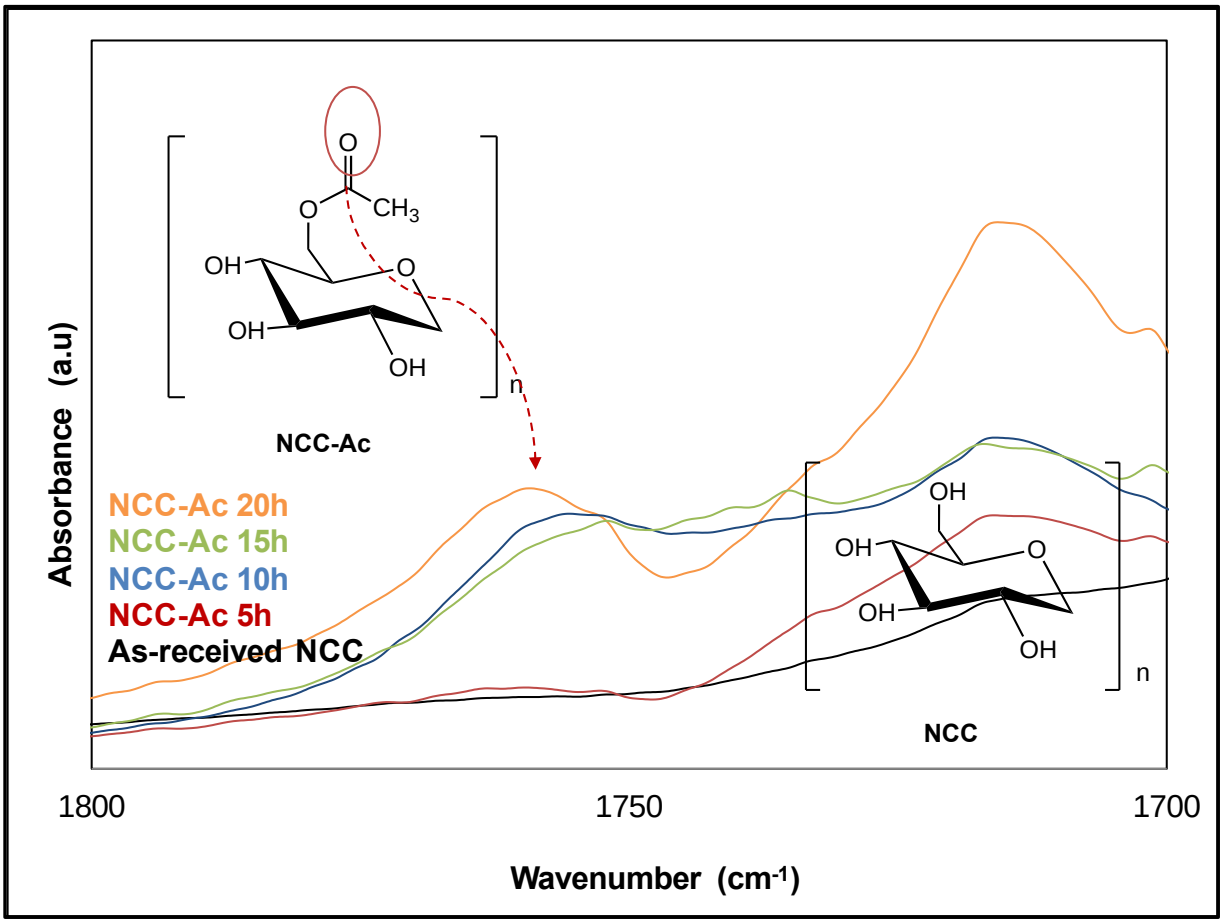

Figure 4.8 (b) Expanded view of Figure 4.8 (a) showing the FTIR spectra of NCC between 1600 - 1800 cm^{-1} before and after acetylation for 0, 5, 10, 15 and 20 hours.

With reference to Figure 4.8 (a), the absorbance band located at around 3350 cm^{-1} represents stretching due to hydrogen-bonded (O-H). The hydrogen bonding in NCC is associated with the structure of cellulose-I [168]. The absorption intensity of the O-H group after acetylation decreases because the hydroxyl groups in NCC are partially substituted by acetyl groups [169]. The absorption at 2900 cm^{-1} represents C-H stretching in cellulose. After acetylation, a new low-intensity peak appears around 1740 cm^{-1} which is attributed to the carbonyl (C=O) stretching vibration introduced with the acetate groups on the surface [29,96]. The peak is seen to increase slightly with increasing reaction time (see Figure 4.8 (b)). Moreover, the absorbance band at approximately 1640 cm^{-1} represents O-H bending and is said to be associated with absorbed water in cellulose [169]. Evidence for nature the acetylation reaction is given by the presence of three functional groups present at approximately 1730 cm^{-1}

(carbonyl C=O stretching of ester), 1371 cm^{-1} (C-H in –O(C=O)-CH_3) and 1232 cm^{-1} C-O stretching of acetyl group [170]. FTIR spectra for cryo-milled NCC before and after acetylation and NCC-Ac sonicated is presented in Figures 4.9 and 4.10 respectively.

Table 4.2 FTIR spectral assignments for unmodified and modified NCC.

No.	Wavenumber (cm^{-1})	Functional group	Reference
1	3443 - 3495	O-H stretching (cellulose-II)	[168]
2	3278 - 3345	O-H stretching (cellulose-I)	[168]
3	3400 - 3000	O-H stretching (acid, methanol)	[52]
4	2890	H–C–H stretching (alkyl, aliphatic)	[52,171,172]
5	1720 - 1740	C=O stretching (carbonyl)	[29,96]
6	1640	Fibre–OH (absorbed water)	[173]
7	1429	HCH and OCH bending vibration (methylene group)	[171]
8	1371	CH deformation vibration (CH_3 or OH in plane bending)	[171,174]
9	1270 - 1232	C–O–C, ether bond (aryl-alkyl ether C-O stretching of acetyl group)	[171]
10	1170 - 1082	C–O–C antisymmetric bridge stretching (pyranose ring skeletal)	[171]
11	1108	OH (C-OH)	[171]
12	1071 - 1067	(C-O) stretching	[174]
13	1041 - 1054	C-O symmetric stretching (C-O of primary alcohol)	[172]
14	896 - 915	COC, CCO, and CCH deformation and stretching vibration (β glucosidic linkages between the sugar units)	[172]
15	700	CH_2 vibrations	[175]

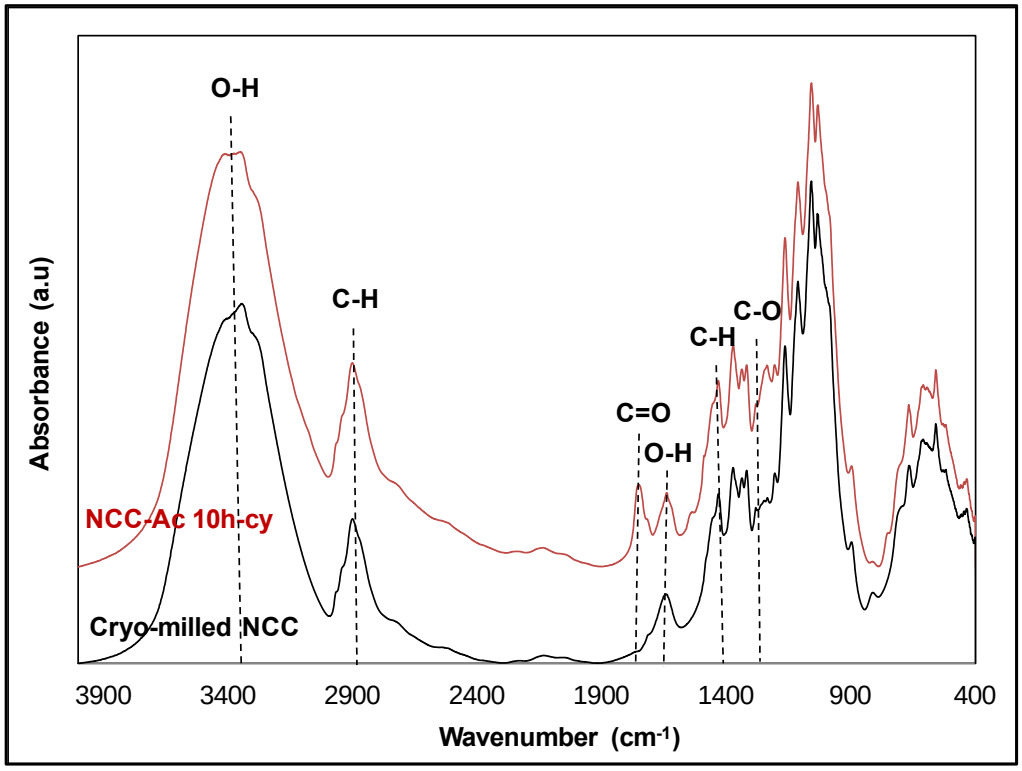

Figure 4.9 FTIR spectra of cryo-milled NCC before and after acetylation.

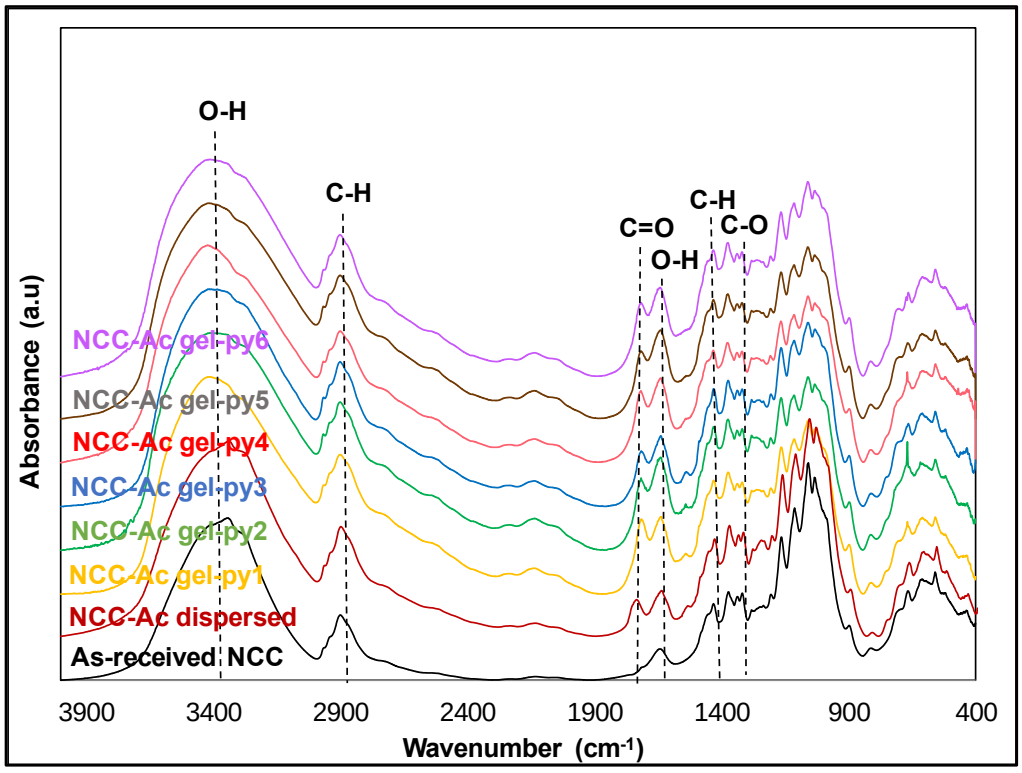

Figure 4.10 FTIR spectra for acetylated NCC using sonication and in an aqueous gel-form. The sample codes were summarised in the Section 3 (Table 3.2).

With reference to Figures 4.9 and 4.10, the carbonyl C=O stretching absorbance band for the NCC-Ac is seen at around 1730 cm^{-1}. Similarly, the absence of a peak at 1700 cm^{-1} and between 1760 and 1840 cm^{-1} confirms there is no unreacted acetic anhydride and by-products of acetic acid in the samples [176]. It is also seen that the peak for the acetyl group in the NCC-Ac in the gel-form was higher than that for the dispersed NCC-Ac. However, the material that was responsible these peaks had almost identical processing parameters including increasing reaction time, sonication time, temperature, concentration of acetic anhydride and increasing temperature and concentration of acetic anhydride. To confirm this observation, normalisation was applied using the software package Omnic™ (Thermo Scientific). An illustration of the normalisation is illustrated in Figure 4.11 and the peak assignments are tabulated in Table 4.2.

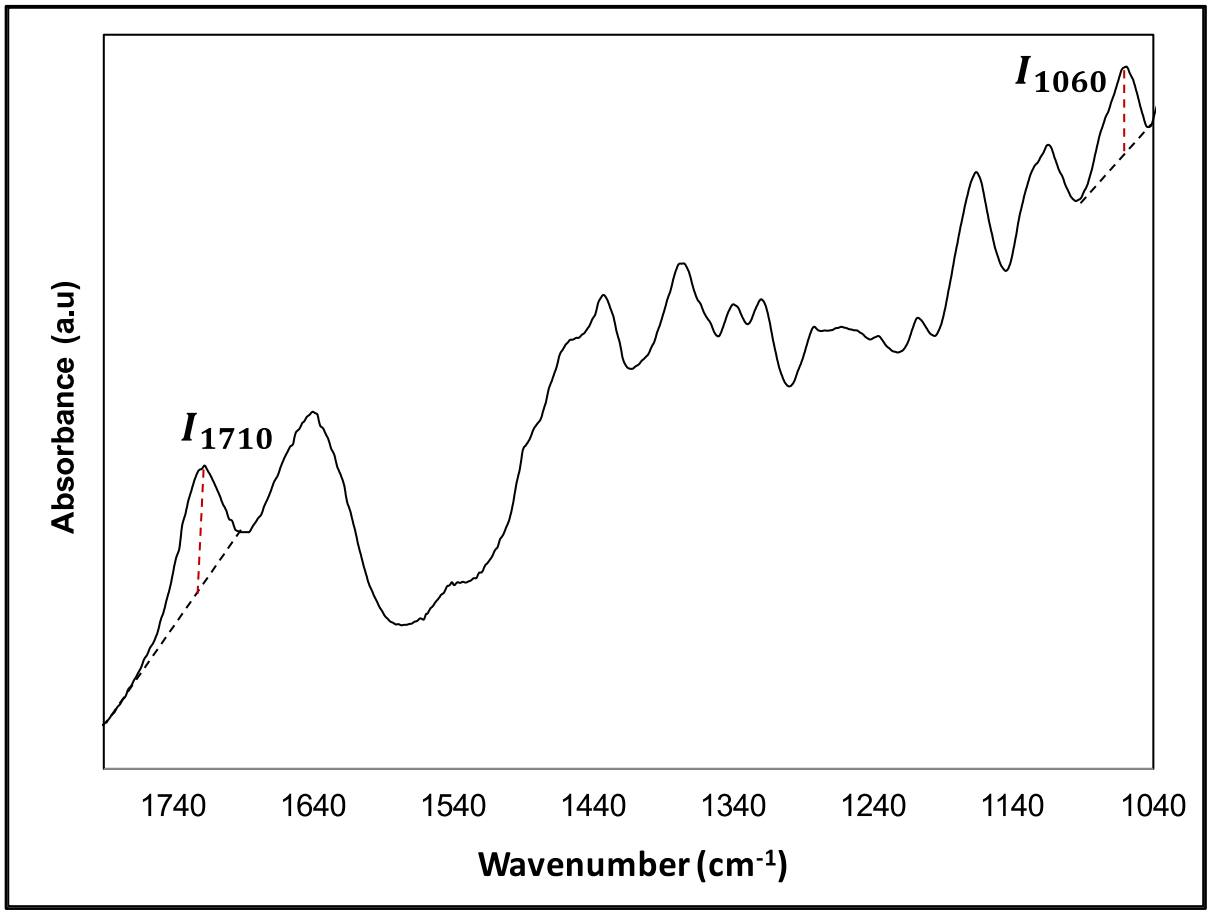

Figure 4.11 An illustration of the method that was used for defining the baseline and corresponding peak in the FTIR spectrum at 1710 cm^{-1} and 1060 cm^{-1}. The peak at 1060 cm^{-1} was used to normalise the peak at 1710 cm^{-1}.

With reference to Figure 4.11, the normalisation was carried out by dividing the peak height of 1710 cm^{-1} with that at 1060 cm^{-1}. The extrapolation was carried out between the troughs at 1790 cm^{-1} and 1690 cm^{-1} and, between the troughs, at 1090 cm^{-1} and 1040 cm^{-1}. The absorbance at 1060 cm^{-1} that corresponds to C-O stretching was used as an internal standard. Cetin *et al*., [25] calculated the peak ratio I_{1710}/I_{1060} as a function of reaction time between NCC and vinyl acetate. Fahma *et al*., [27] also used this normalisation procedure as a function of reaction time between NCC and acetic anhydride as did Frisoni *et al*., [177].

Table 4.3 A summary for the peak ratio of I_{1710}/I_{1060} for NCC-Ac.

No.	**Samples**	$\boldsymbol{I_{1710}}$	$\boldsymbol{I_{1690}}$	$\boldsymbol{I_{1710}/I_{1060}}$
1	NCC-Ac 5h	0.02	0.17	0.11
2	NCC-Ac 10h	0.04	0.14	0.28
3	NCC-Ac 15h	0.04	0.12	0.33
4	NCC-Ac 20	0.07	0.12	0.58
5	NCC-Ac 10h-cy	0.12	0.18	0.66
6	NCC-Ac dispersed	0.1	0.16	0.62
7	NCC-Ac gel-py1	0.14	0.1	1.45
8	NCC-Ac gel-py2	0.13	0.1	1.30
9	NCC-Ac gel-py3	0.11	0.08	1.37
10	NCC-Ac gel-py4	0.14	0.08	1.75
11	NCC-Ac gel-py5	0.11	0.08	1.37
12	NCC-Ac gel-py6	0.13	0.1	1.30

Several experimental procedures were used to introduce the acetyl group to the NCC. However, the results showed that the acetylation was not able to penetrate the crystalline core. Based on the cellulose structure, the conformation inside and outside the crystal are different. In the surface of cellulose, it has a *tg* (*trans-gauche*) hydroxymetyl conformation with intramolecular hydrogen bonding between $O_3…O_5$ and $O_2…O_6$ hydroxyl groups. It is connected by weak C-H…O hydrogen bonds, hence, the acetyl group is able to penetrate this area. Whilst inside, the crystal has a *gg*

(*gauche-gauche*) hydroxymethyl conformation with the position of O_6 on the top of chair conformation. It prevents the formation of $O_2H…O_6$ intramolecular hydrogen bonds. Similarly, this conformation has a dihedral angle of 60° between the adjacent substituent making it the most stable conformation [178]. The illustration of *tg* and *gg* hydroxymethyl cellulose conformation is presented in Figure 4.12.

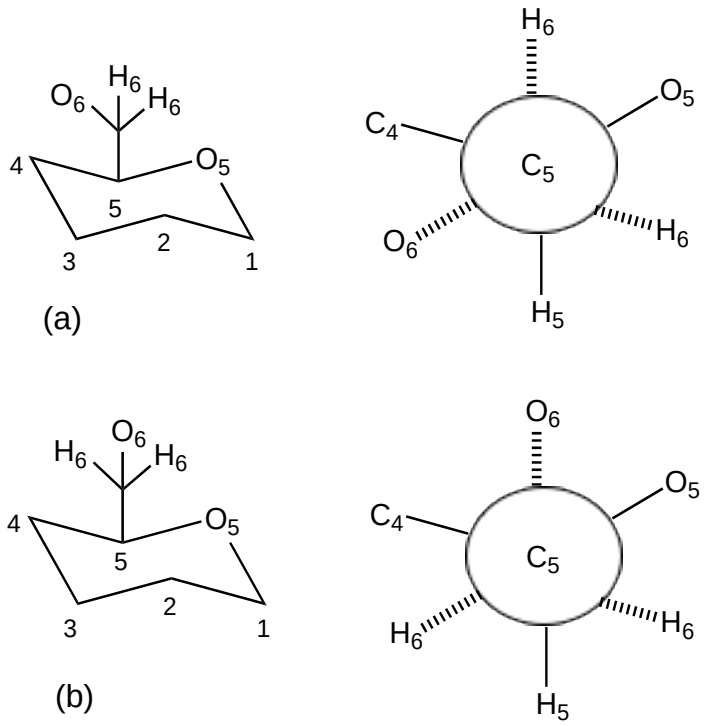

Figure 4.12 Hydroxymethyl cellulose conformation; (a) *tg* (*trans-gauche*) conformation, and (b) *gg* (*gauche-gauche*) conformation [178].

In addition, Burk and Brummit [97] stated that a high degree of substitution for acetylated cellulose cannot be prepared as there is a steric hindrance around the oxygen bridges within the crystalline structure. A cellulose monomer in the boat conformation is shown in Figure 4.13 which demonstrates the steric repulsion.

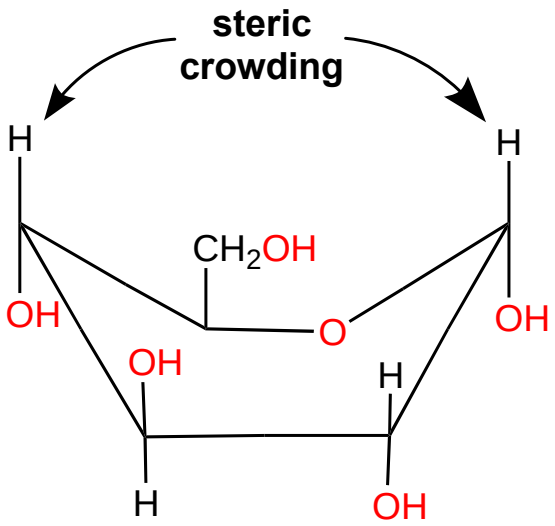

Figure 4.13 Steric hindrance of cellulose [97].

The results of the FTIR spectroscopic investigation shows that the acetylation of NCC has been successful. Several parameters were modified to introduce acetyl groups to the NCC. For example increasing the reaction time, reducing particle size of the as-received NCC by cryo-milling and performing the acetylation in the gel-state. It was found that increasing the reaction time for the acetylation does not give a significant increase in the carbonyl group as it produces for more acetic acid as a by-product. The presence of acetic acid can delay the reaction, thus decreasing the rate of acetylation. With reference to Table 4.3, increasing the dispersion of the reagents and the concentration of acetic anhydride, introduced a more intense absorbance of the carbonyl peak.

4.5 CP/MAS ^{13}C-NMR analysis of NCC and NCC-Ac

Further characterisation using CP/MAS ^{13}C solid-state NMR, was carried out to investigate the structure of NCC before and after acetylation. The CP/MAS ^{13}C NMR spectrum of as-received NCC is shown in Figure 4.14.

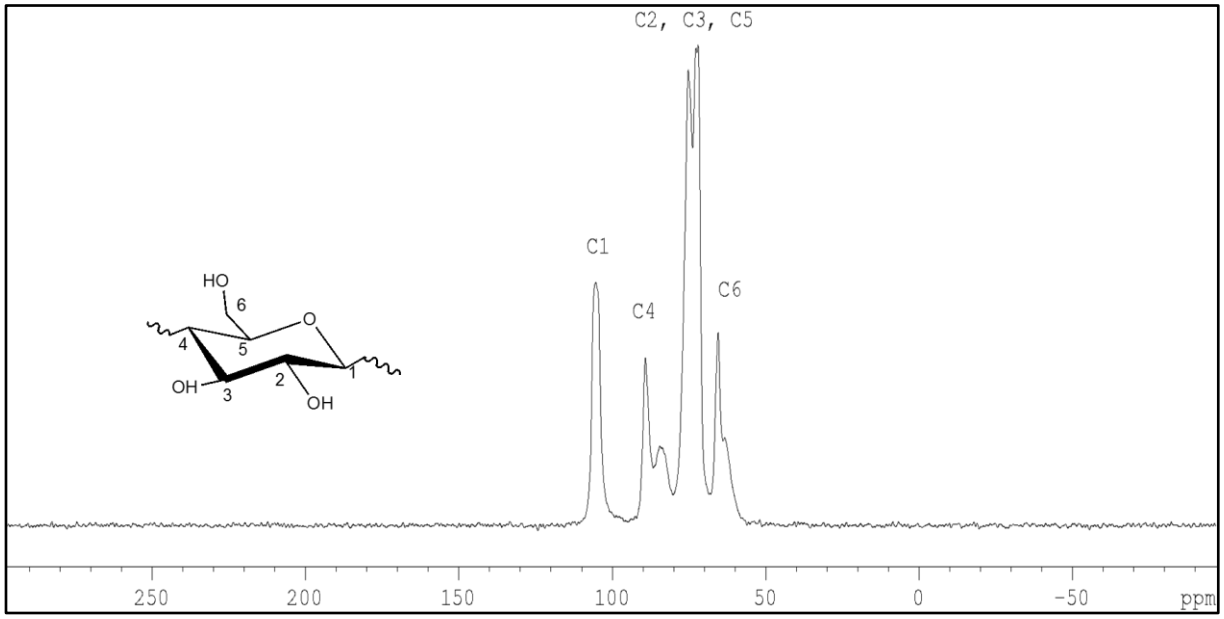

Figure 4.14 ^{13}C solid-state NMR spectrum of as-received NCC at room temperature. The data acquisition parameters were 1800 scans using a frequency of 100 MHz with respect to ^{13}C and a spinning speed of 10 kHz.

With reference to Figure 4.14 and the structure of NCC along with the coding of the position of the carbons, the appearance of each peak is elaborated as follow. The peak at 105 ppm is assigned to C_1. The resonance line at 89 ppm is assigned to C_4 for the crystalline region and 84 ppm for the amorphous sections. The crystalline region of C_6 and the disordered component are assigned to the chemical shifts at 65 and 63 ppm respectively. Similarly, the carbon atoms at positions C_2, C_3 and C_5 are assigned to the peaks at 75 and 72 ppm [29].

In addition, two samples of acetylated NCC were characterised using solid-state ^{13}C NMR, these samples were coded as NCC-Ac dispersed and NCC-Ac gel-py4 (see Table 3.2 for a description of the codes). The selection of the samples was based on the ratio of I_{1710}/I_{1060} data from the FTIR spectral investigation presented in Table 4.3. NCC-Ac gel-py4 had the highest I_{1710}/I_{1060} ratio and NCC-Ac dispersed was used to compare the results between the acetylated NCC in the gel-form and that of the dispersed material that was sonication. The NMR spectra for the sample is presented in Figure 4.15.

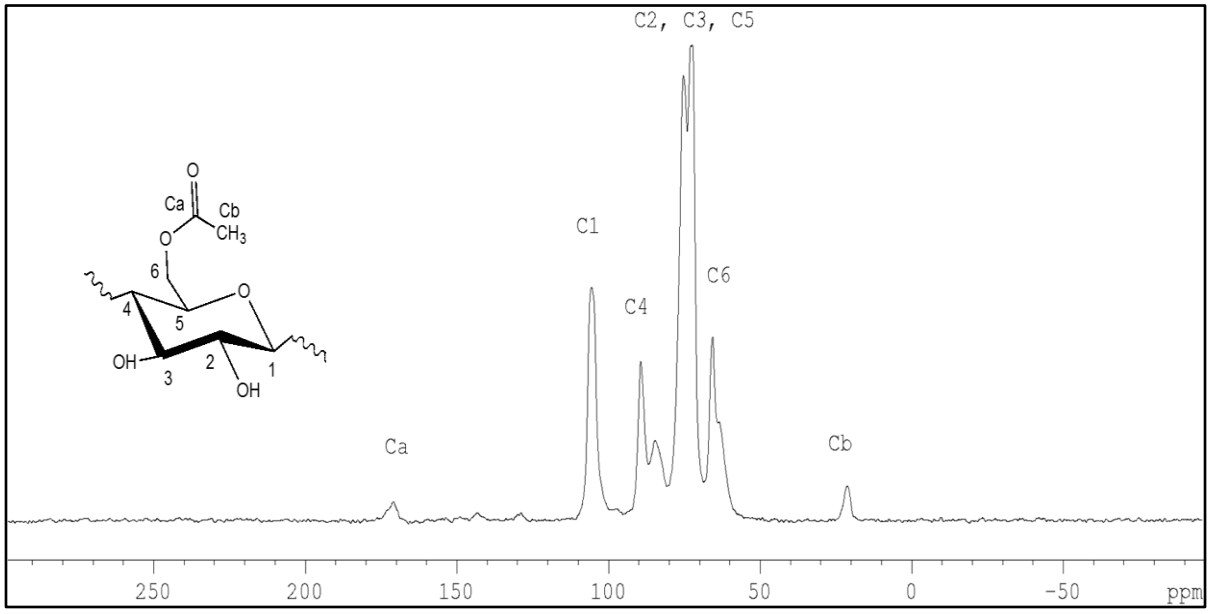

Figure 4.15 (a) ^{13}C solid-state NMR spectrum of NCC-Ac dispersed at room temperature. The data acquisition parameters were 7200 scans using a frequency of 100 MHz with respect to ^{13}C and a spinning speed of 10 kHz.

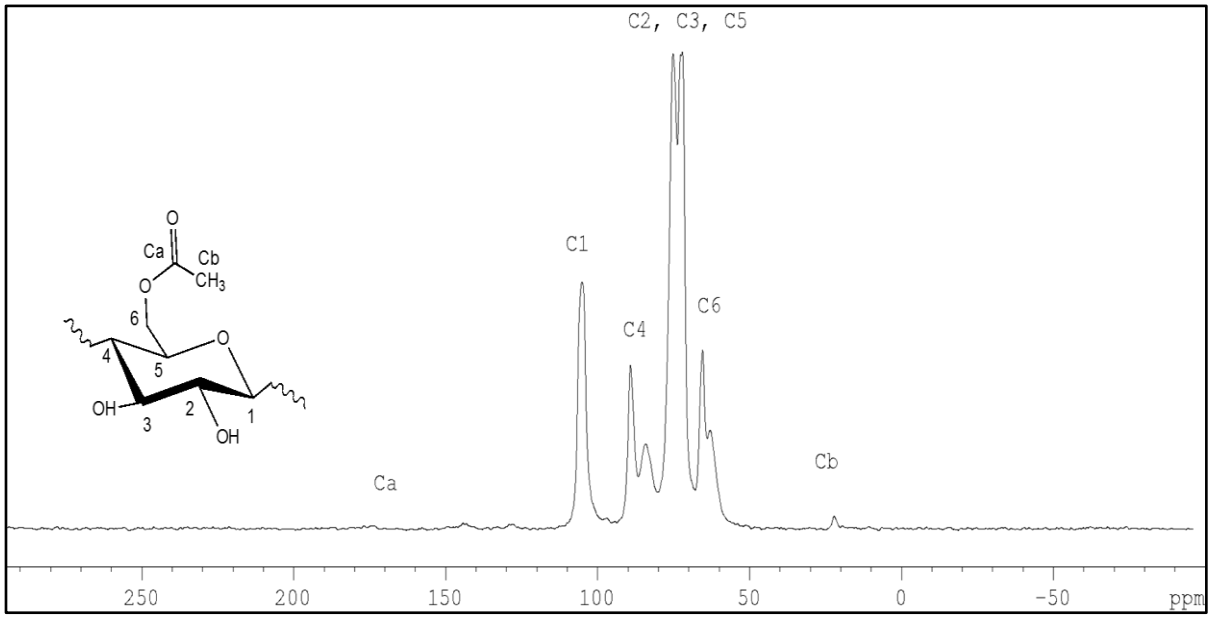

Figure 4.15 (b) ^{13}C solid-state NMR spectrum of NCC-Ac gel-py4 at room temperature. The data acquisition parameters were 7200 scans using a frequency of 100 MHz with respect to ^{13}C and a spinning speed of 10 kHz.

Figure 4.15 shows the solid-state CP/MAS ^{13}C-NMR spectrum for NCC-Ac dispersed (spectrum a) and NCC-Ac gel-py4 (spectrum b). From Figures 4.15, it can be seen that

there are two new chemical shifts after acetylation: at 170 ppm belonging to the acetyl group (C=O); and 21 ppm for the aliphatic functional group (CH_3) [29]. The presence of these peaks confirms the acetylation of NCC. Similarly, the intensity of C_6 and C_4 (amorphous) decreased, whilst the intensity of C_6 and C_4 (crystalline) was maintained after acetylation. The intensity of the carbonyl peak in the aliphatic compound of NCC-Ac dispersed was higher than that in the NCC-Ac gel-py. This is inconsistent with FTIR spectral results. Based on the cellulose structure, it is seen that the C_6 is substituted first, as it possessed the more reactive primary OH group. The second OH substitution in the acetylation reaction occurs at the C_3 and C_2 positions.

In addition, the NMR spectra were used to determine the degree of substitution (DS) for NCC after acetylation based on Equation 4.1 [179]. This equation was used by Berlioz *et.al.,* [180] where they divided the sum of the intensities of C_1 to C_6 with the peak intensity of the carbonyl (C=O) group. The method for the integration of the peak is presented in Appendix 6. The degree of substitution is defined as:

$$DS = \frac{6\ x\ I_{CO}}{I_C} \qquad \text{Equation 4.1}$$

where

I_{CO} = the peak corresponding to the carbonyl of the ester bond.

I_C = the sum of all the carbons of the cellulose.

6 = the number of carbon atoms in one anhydroglucose unit of cellulose.

Table 4.4 Degree of substitution for NCC-Ac dispersed and NCC-Ac gel-py4.

No.	Samples	Equation 4.1	Degree of substitution
1	NCC-Ac dispersed	$\frac{6\ x\ 1}{80.7}$	0.07
2	NCC-Ac gel-py4	$\frac{6\ x\ 1}{513.3}$	0.01

The NMR results show that surface acetylation on NCC has occurred successfully. NCC-Ac dispersed has a degree of substitution (DS) of 0.07 whilst NCC-Ac gel-py 4

has a DS of 0.01. The carbonyl groups, as well as the aliphatic peak, are higher for NCC-Ac dispersed than NCC-Ac gel-py. This may be on account of water reacting with acetic anhydride to reduce its concentration. Another explanation is that the hydroxyl groups of NCC are strongly bonding with water and therefore inhibit the reaction occurring with another reagent such as acetic anhydride.

4.6 XRD analysis of NCC and NCC-Ac

In order to investigate the effect of acetylation on the crystalline structure of NCC, XRD analysis was performed. The XRD pattern of NCC before and after acetylation is presented in Figure 4.16.

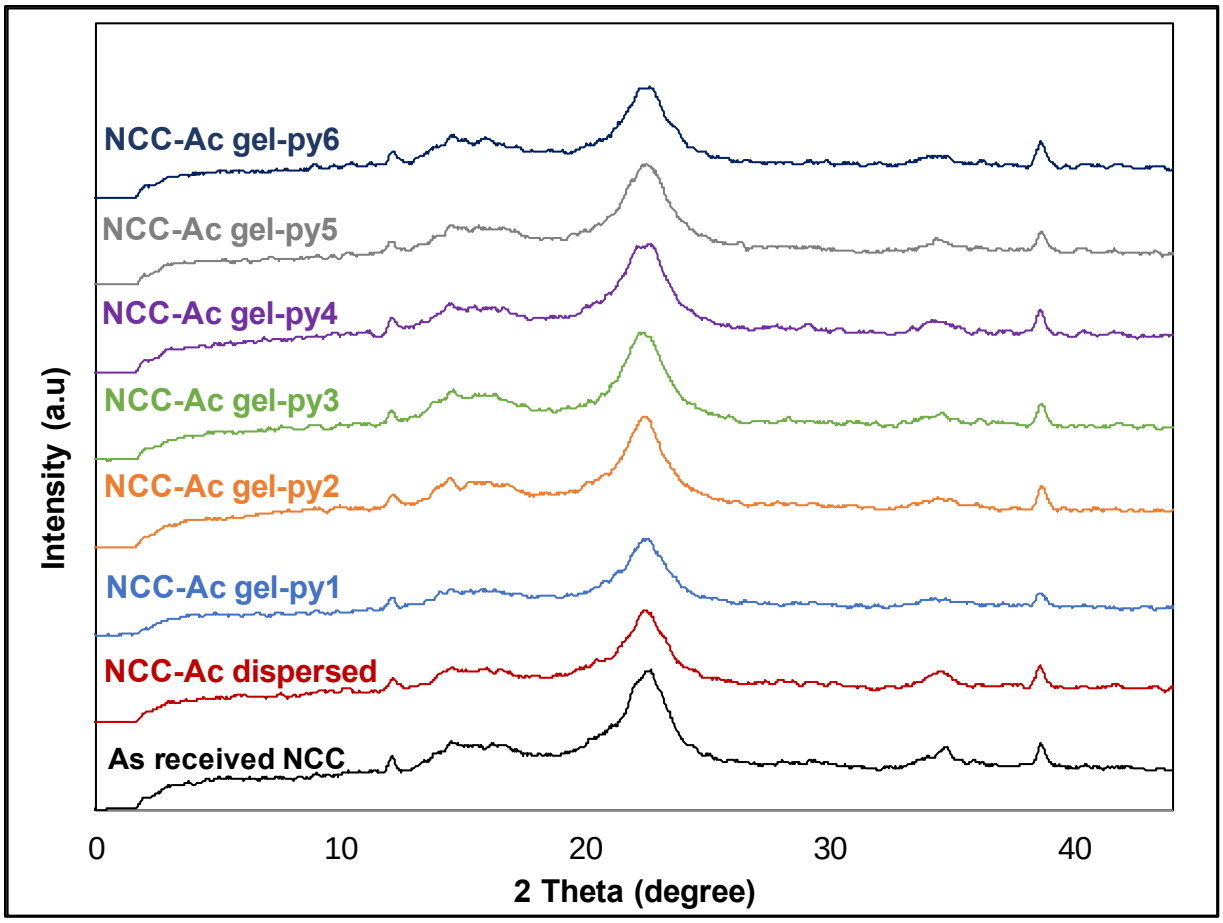

Figure 4.16 XRD pattern of NCC before and after acetylation.

With reference to Figure 4.16, NCC was presented as cellulose-I which had 2 Theta angles at around 14.5, 16.3, 23.5 and 34.5º assigned to the typical reflection planes of

101, $10\bar{1}$, 002 and 040 respectively [28,180]. The structure of NCC as cellulose-I was the same as the OH stretching from the FTIR spectra. The results also show that the crystalline structure of NCC was preserved after chemical modification. Using Equation [3.1], the crystallinity of the as-received NCC was calculated to be 72% whilst NCC-Ac was 68%. Introducing an acetyl group on NCC disrupts the intra- and inter-molecular hydrogen bonds which in turn disrupts the crystal structure of NCC [28]. Decreasing the crystallinity of NCC after acetylation was also reported by other authors as summarised in Table 4.5.

Table 4.5 The crystallinity of NCC before and after acetylation.

No	**Samples**	**Acetylating agent**	**Crystallinity (%)**	
			Before acetylation	**After acetylation**
1.	NCC	Acetic anhydride	72	68
2.	NCC* [181]	Acetic anhydride	81	74
3.	NCC* [182]	Fatty acid methyl ester	77	75
4.	NCC* [23]	Fatty acid and trifluoroacetic anhydride	86	76
5.	NCC* [96]	Acetic anhydride	77	68

*Data obtained from references.

4.7 Thermogravimetric analysis of NCC and NCC-Ac

The TGA traces for NCC before and after acetylation are represented in Figure 4.17, 4.18, 4.19 and 4.20. In the Figure 4.17, the TGA traces for the as-received and acetylated NCC as a function of processing time show three distinct regions. The first stage is from room temperature to 100 ºC. In this region, the dehydration of the sample is assumed to be the prominent feature [183]. The weight lost in this region is approximately 2% and 1% for unmodified and modified NCC respectively.

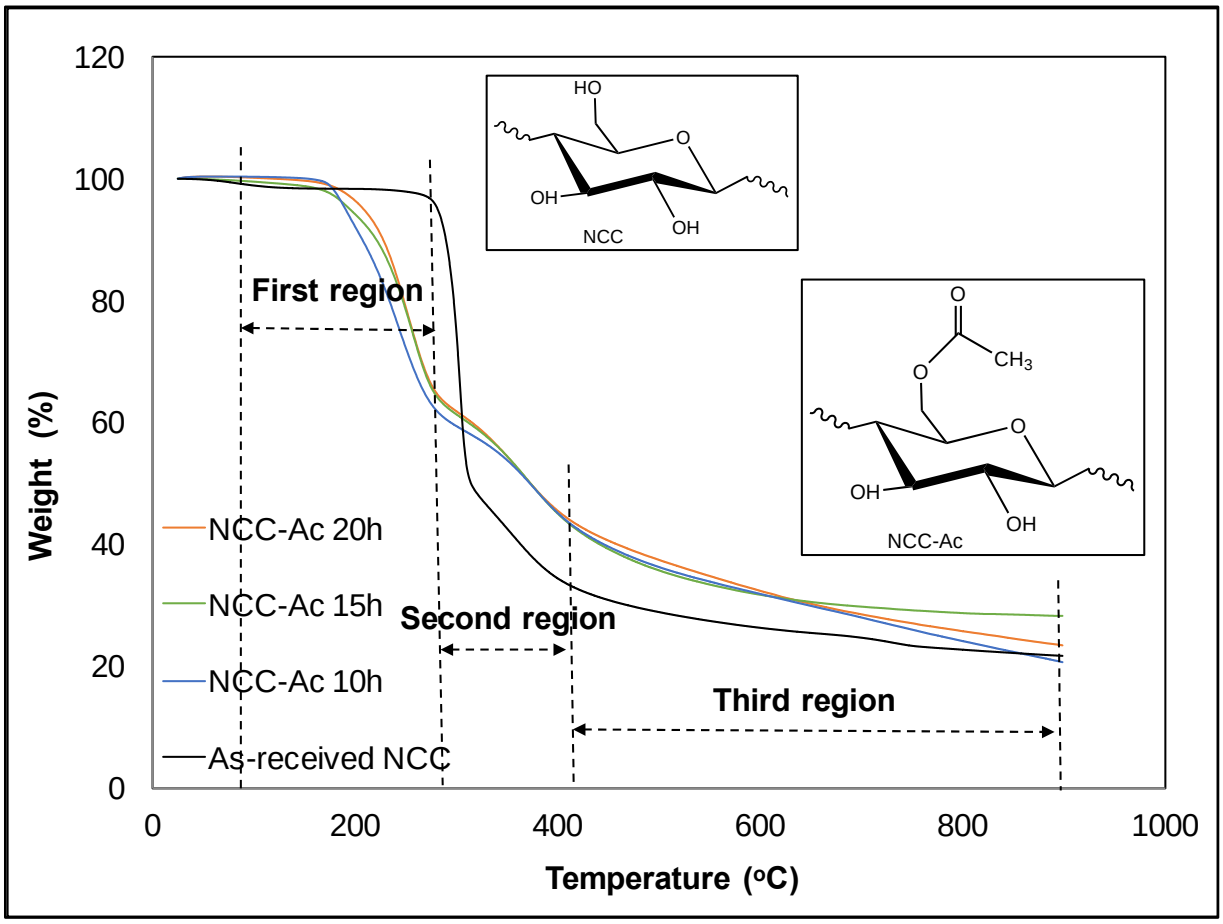

Figure 4.17 TGA traces of NCC before and after acetylation for 0, 10, 15 and 20 hours with a heating rate of 10 K.minute^{-1} in argon.

The second step region in the TGA trace is seen to be between 270 ºC to 400 ºC for the as-received material. In this region, the NCC started to decompose to the monomer of D-glucopyranose [184] . At 400 ºC, the NCC lost around 65% of its original mass. However, the degradation of NCC after acetylation shifted to a lower temperature, specially between 170 ºC to 400 ºC. The yield of the acetylated NCC at 400 ºC is about 58%. The decrease in the onset thermal degradation temperature for NCC after acetylation can be rationalised through degree of the crystallinity.

In the XRD-section (sub-section 4.6), the degree of crystallinity of NCC decreases after acetylation by approximately 13%. The crystallinity in NCC is formed by the interactions of hydrogen bonds in the cellulose structure [185]. The thermal decomposition also includes the breakage of the crystal structure of NCC. As a result, thermal

decomposition takes place more readily in NCC with a lower degree of crystallinity [175].

The final mass-loss in the TGA trace was observed to commence around 400 ^{o}C for both as-received and NCC-Ac. This region is attributed to the completing decomposition. The residue for NCC after acetylation was slightly higher than the as-received material.

The TGA traces for the as-received NCC and cryo-milled NCC are represented in Figure 4.18 and the TGA traces for NCC-Ac 10h-cy is presented in Figure 4.19. Similarly, the TGA traces for acetylated NCC using sonication is shown in Figure 4.20. A summary for TGA results is presented in Table 4.4.

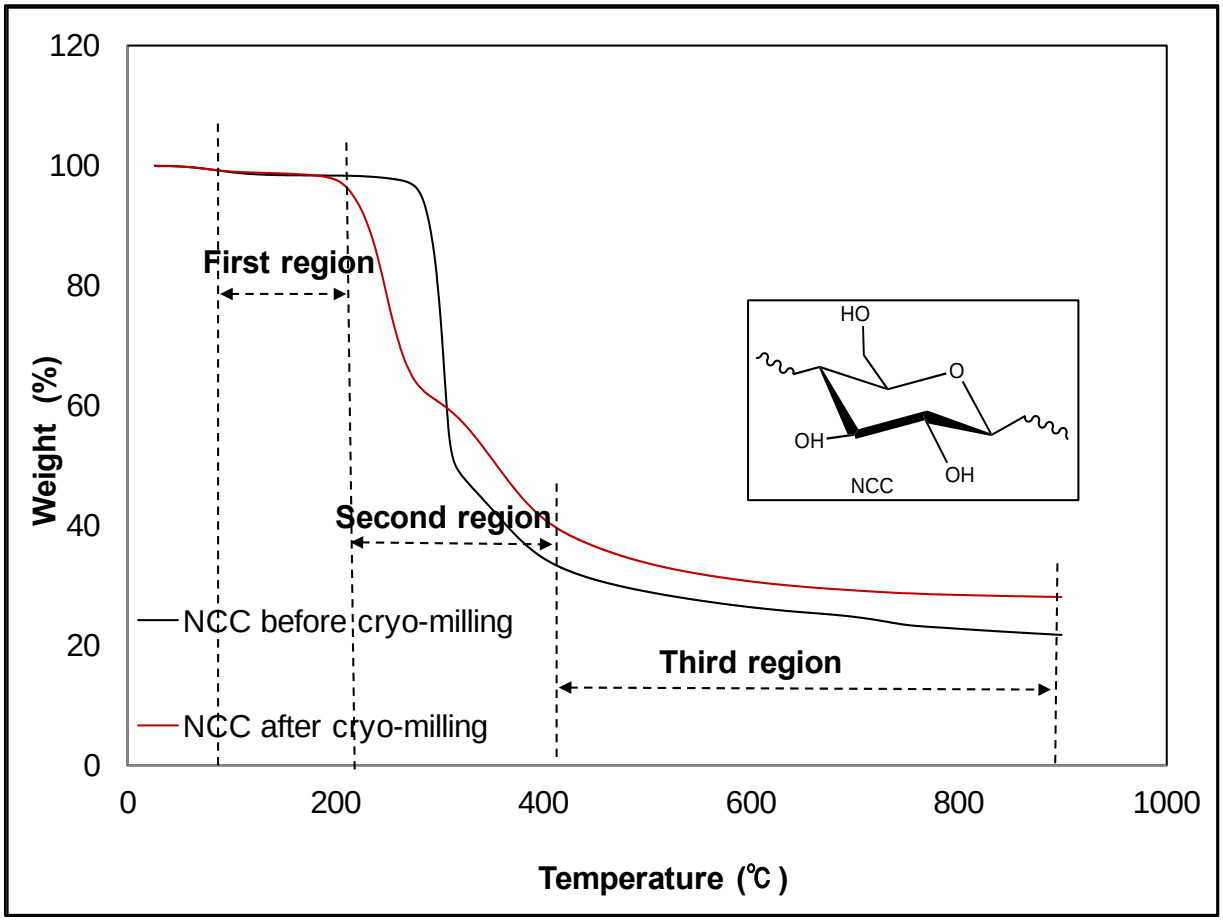

Figure 4.18 TGA traces of NCC before and after cryo-milling with a heating rate of 10 K.minute^{-1} in argon.

With reference to Figure 4.18, the TGA traces of the NCC after cryo-milling showed a decrease in the thermal decomposition. Cryo-milled NCC started to degrade at 200 ^{o}C. This is probably due to decreasing the surface charge on NCC by the cryo-milling. This is supported from the TEM micrograph as the nano-particle of NCC can be seen to agglomerate after cryo-milling. The dispersibility of NCC in DI water also decreased after cryo-milling. From the investigation, it was found that the as-received NCC is highly dispersed in DI water, in comparison to the cryo-milled NCC which precipitated in the solution. The percent residue of cryo-milled NCC which precipitated in the solution. The percent residue of cryo-milled NCC increased by approximately 7% compared to the NCC before cryo-milling.

The TGA traces for NCC-Ac 10h-cy is represented in Figure 4.19. The first stage is from room temperature to 100 ^{o}C due to the evaporation of moisture. The weight lost in this area is 1%, the same trend as the cryo-milled NCC before acetylation. The thermal decomposition of cryo-milled NCC before and after acetylation is seen to be between 200 ^{o}C to 400 ^{o}C. The weight loss in this region is 56% for cryo-milled NCC and 55% for NCC-Ac 10h-cy. The final step is from 400 ^{o}C to 900 ^{o}C with present residue of 28% for both materials.

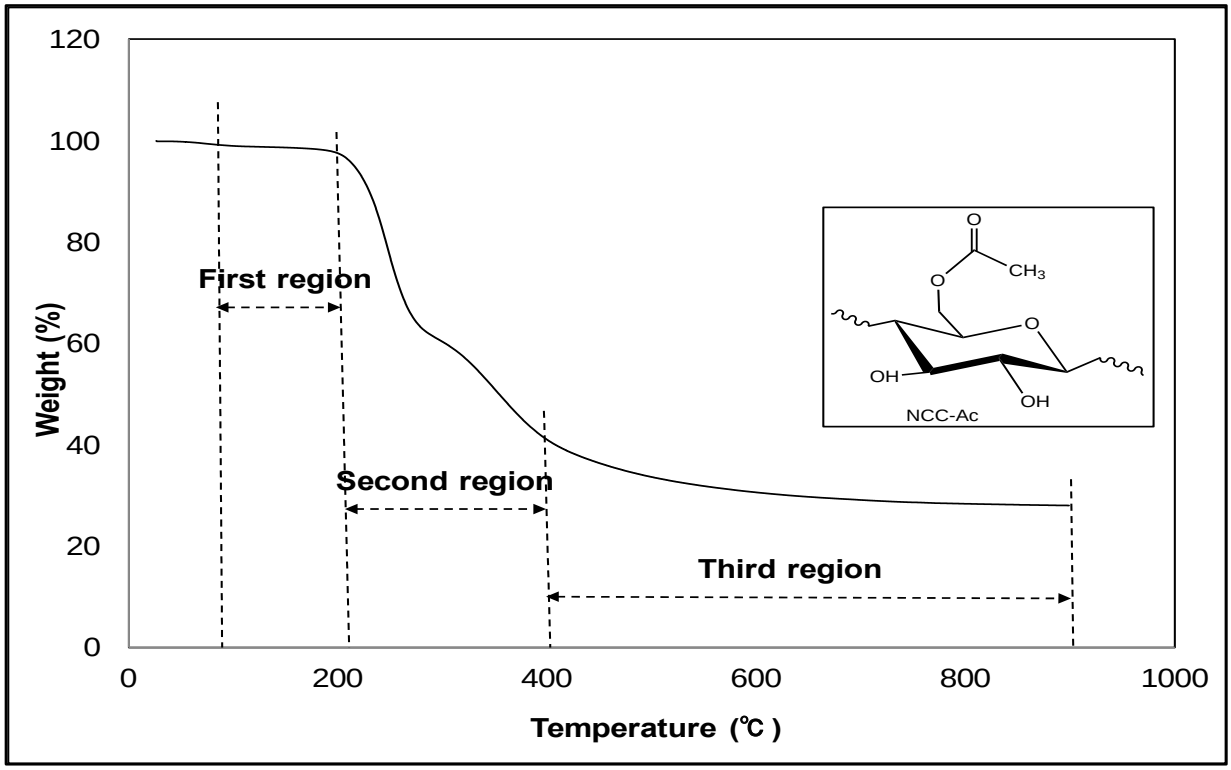

Figure 4.19 TGA trace for NCC-Ac 10h-cy with a heating rate of 10 K.minute^{-1} in argon.

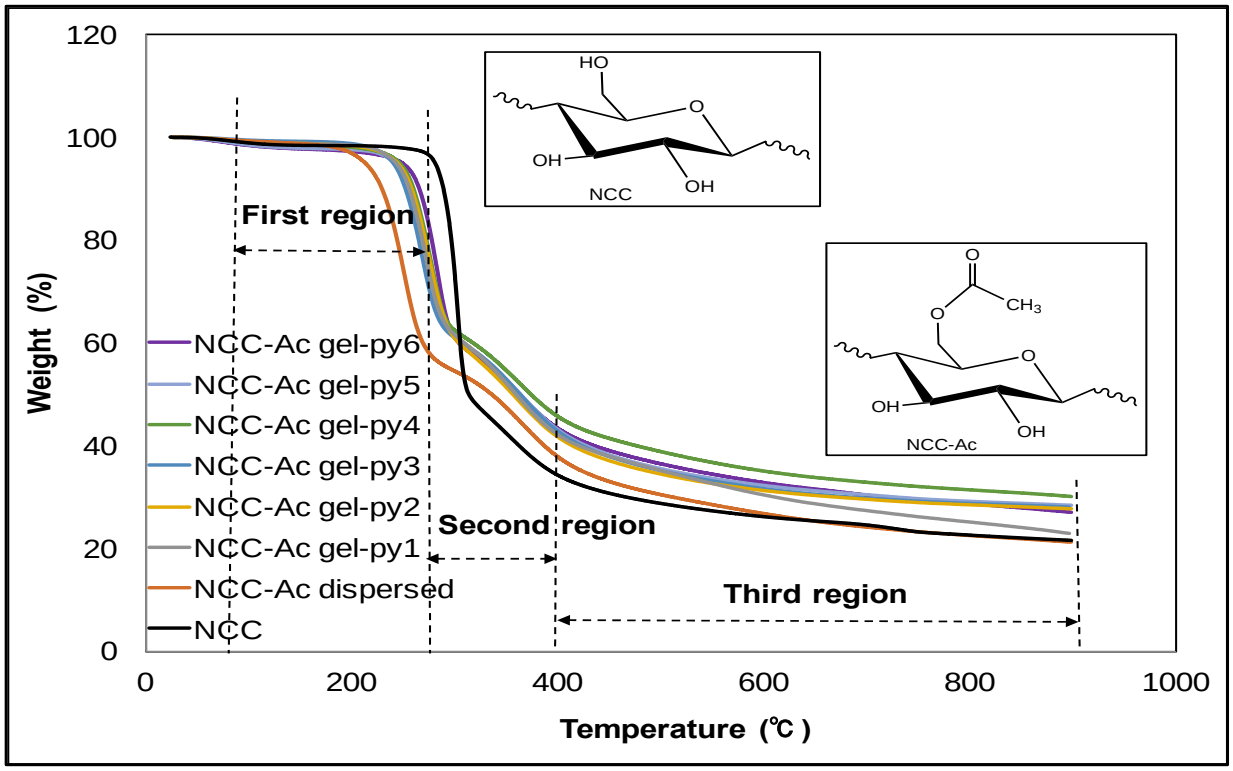

Figure 4.20 TGA traces for NCC and NCC-Ac dispersed and gel-form with a heating rate of 10 K.minute^{-1} in argon.

A summary for thermal behavior of NCC before and after acetylation is summarised in Table 4.6.

Table 4.6 A summary of the thermal behaviour for NCC before and after acetylation with increasing reaction time, reducing particle size, and in aqueous gel-form.

No.	**Samples**	**Process**	**TGA experiment (heating rate of 10K.minute^{-1} in argon) : RT - 900 ºC**								
			First region			**Second region**			**Third region**		
			T_1, ºC	**T_2, ºC**	**Yield at T_2, w%**	**T_1, ºC**	**T_2, ºC**	**Yield at T_2, w%**	**T_1, ºC**	**T_2, ºC**	**Yield at T_2, w%**
In-house results											
1	As-received NCC	-	80	270	97.15	270	400	34.37	400	900	21.57
2	Cryo-milled NCC	-	80	200	97.60	200	400	41.12	400	900	28.04
3	NCC-Ac 10h	10 hours reaction time	80	170	99.47	170	400	45.16	400	900	20.60
4	NCC-Ac 15h	15 hours reaction time	80	170	98.03	170	400	45.18	400	900	28.23
5	NCC-Ac 20h	20 hours reaction time	80	170	98.96	170	400	45.41	400	900	23.28
6	NCC-Ac 10h-cy	Cryomilled NCC with 10 hours reaction time	80	200	98.49	200	400	41.12	400	900	28.04

7	NCC-Ac dispersed	Dispersion of pyridine using a sonicator	80	180	98.12	180	400	37.63	400	900	21.05
8	NCC-Ac gel-py1	Gel-form with 5 hours reaction time	80	200	98.39	200	400	41.88	400	900	22.98
9	NCC-Ac gel-py2	Gel-form with 10 hours reaction time	80	200	98.24	200	400	41.53	400	900	27.56
10	NCC-Ac gel-py3	Gel-form with increasing sonication time	80	200	98.66	200	400	42.35	400	900	27.87
11	NCC-Ac gel-py4	Gel-form with increasing the concentration of acetic anhydride	80	200	98.02	200	400	45.69	400	900	30.10
12	NCC-Ac gel-py5	Gel-form with increase the temperature at 100 ^{o}C	80	200	97.52	200	400	43.11	400	900	28.41
13	NCC-Ac gel-py6	Gel-form with increasing the concentration of acetic anhydride and temperature at 100 ^{o}C	80	200	97.18	200	400	43.22	400	900	26.83

References data											
14	NCC-Ac [181]	Acetylation using acetic anhydride and pyridine at 100 ºC for 4 hours.	80	240	N.A	240	330	N.A	330	500	N.A
15	NCC-Ac [186]	Modification in supercritical carbon dioxide at 50 ºC for 4 hours	80	225	N.A	225	400	N.A	400	500	N.A
16	NCC-Ac [187]	Acetylation using acetyl chloride and pyridine at 50 ºC for 5 hours	80	250	N.A	250	380	N.A	380	500	N.A

The boiling points of the materials used for acetylation are 115 ºC (pyridine) and 139 ºC (acetic anhydride). Before the TGA experiments, the samples were dried at 80 ºC for 5 hours under vacuum. From the TGA experiment, the onset temperature for dried - acetylated NCC in the second region is about 190 ºC, or much higher than the boiling temperatures of pyridine and acetic anhydride. It indicates that the acetyl groups are bonded covalently with C_6 of the structures. The acetylation on the NCC was successful.

4.8 The viscosity of NCC and NCC-Ac

The viscosities of NCC and NCC-Ac in DMSO were measured using a Rheometry Discovery HR-1 rheometer from TA Instrument, see Section 3.2.2. The viscosity data are presented in Figure 4.21.

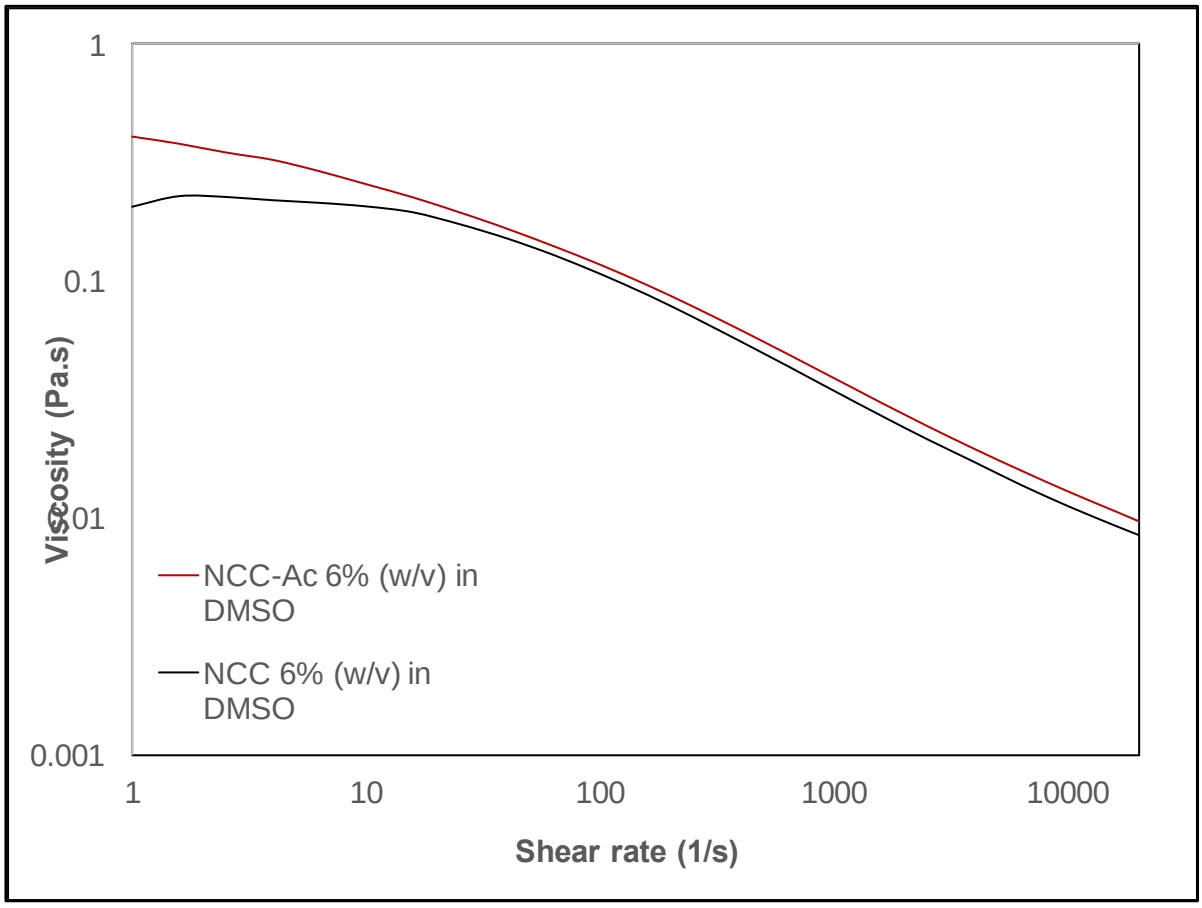

Figure 4.21 The viscosity of NCC before and after acetylation; the solvent used was DMSO.

NCC-Ac was slightly more viscous than NCC at a shear rate of 1 s^{-1}. The viscosity of NCC-Ac was 0.40 Pa.s whilst that of NCC was 0.20 Pa.s. A plateau was observed for the suspension of NCC where its viscosity remained unchanged from the shear rate of 1 s^{-1} to 10 s^{-1}. The same behaviour was not observed for the NCC-Ac suspension. The viscosity of the two solutions decreased significantly with increasing the shear rate from 10 s^{-1} to 1000 s^{-1}. It was 0.20 Pa.s to 0.01 Pa.s and 0.25 Pa.s to 0.01 Pa.s for NCC and NCC-Ac respectively.

The solubility of NCC before and after acetylation was also reported by Taib. *et al.,* [188] which increased the solubility of NCC-Ac in some organic solvents. The data is summarised in Table 4.7.

Table 4.7 The solubility of NCC and NCC-Ac in organic solvents, (-) sign indicated insoluble whereas (+) sign indicated soluble [188].

Solubility							
	DI water	**N-hexane**	**Chloroform**	**DMSO**	**Acetone**	**Toluene**	**DMF**
NCC	+	-	-	-	-	-	-
NCC-Ac	+	-	+	+	+	-	+

In addition, the complex viscosity of NCC-Ac increased as the increasing of degree of substitution values of NCC [189]. This is due to the hydrophobicity of NCC-Ac being improved by the acetyl groups [189].

4.9 Acetylation of cellulose

Acetylation of cellulose was carried out to investigate the effect of highly crystalline material on the acetylation process. Cellulose was dispersed in pyridine using sonication and acetylated using acetic anhydride as described in Section 3.2.2.2. The purification and drying method for acetylated cellulose was the same as that used for the acetylation of NCC. The characterisation of the acetylated cellulose was carried

out using ESEM, FTIR spectroscopy, XRD and TGA. The solubility of cellulose was examined in acetone. The properties of acetylated cellulose produced in this study was compared with that of commercial cellulose acetate.

4.9.1 Environmental scanning electron microscope of cellulose and acetylated cellulose

The morphology of as-received cellulose, acetylated cellulose and commercial cellulose acetate was studied using an ESEM. Typical micrographs of the as-received cellulose, acetylated cellulose and commercial cellulose acetate dried at 80 ºC for 5 hours in a vacuum oven are presented in Figure 4.22.

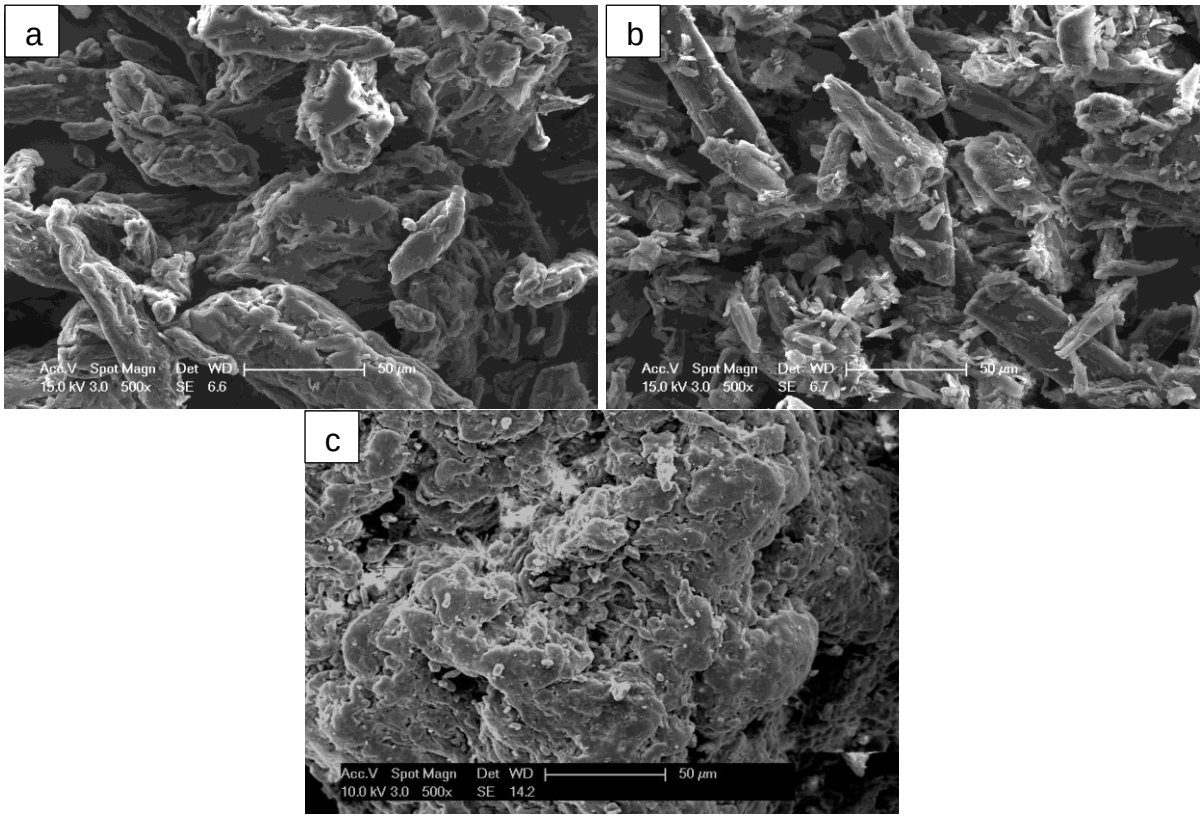

Figure 4.22 ESEM micrographs for (a) as-received cellulose, (b) acetylated cellulose and (c) commercial cellulose acetate.

The morphology of the as-received cellulose is seen to be smooth and compact. After acetylation, it takes a flakier form. In addition, the dimensions of the cellulose particles decrease after acetylation. This may have been due to the fact that after drying, the

acetylated cellulose was cryo-milled. However, the surface of commercial cellulose acetate is smooth and has a powdery form. This is due to the manufacturing process of commercial cellulose acetate not being the same as the procedure used to produce acetylated cellulose in this study.

4.9.2 FTIR spectroscopic analysis of cellulose and acetylated cellulose

Cellulose was acetylated with the same condition as NCC (dispersing pyridine to cellulose using sonication with a reaction time for 5 hours at 80 ºC as described in Section 3.2.2.2). The FTIR spectra for cellulose before and after acetylation is presented in Figure 4.23. As mentioned previously, the three main ester components indicating the success of the acetylation were 1730 cm^{-1} carbonyl C=O stretching of ester, 1371 cm^{-1} C-H in –O(C=O)-CH_3 and 1232 cm^{-1} C-O stretching of acetyl group. The intensity of the three peaks increases after acetylation and becomes more intense peaks than those for acetylated NCC. This suggests that acetylation introduces a greater proportion of acetyl groups to the cellulose structure than NCC. Based on the XRD pattern of NCC and cellulose in Figure 4.16 and 4.24 respectively, cellulose structure is more amorphous and therefore allowing for a greater penetration of the acetyl groups. However, compared with commercial cellulose acetate, the acetyl groups of acetylated cellulose in this study is still lower. From the FTIR spectral assignments analysis (see Table 4.2), the O-H stretching of cellulose and acetylated cellulose manufactured in this project were considered as cellulose-I, whilst the O-H stretching of commercial cellulose acetate were cellulose-II.

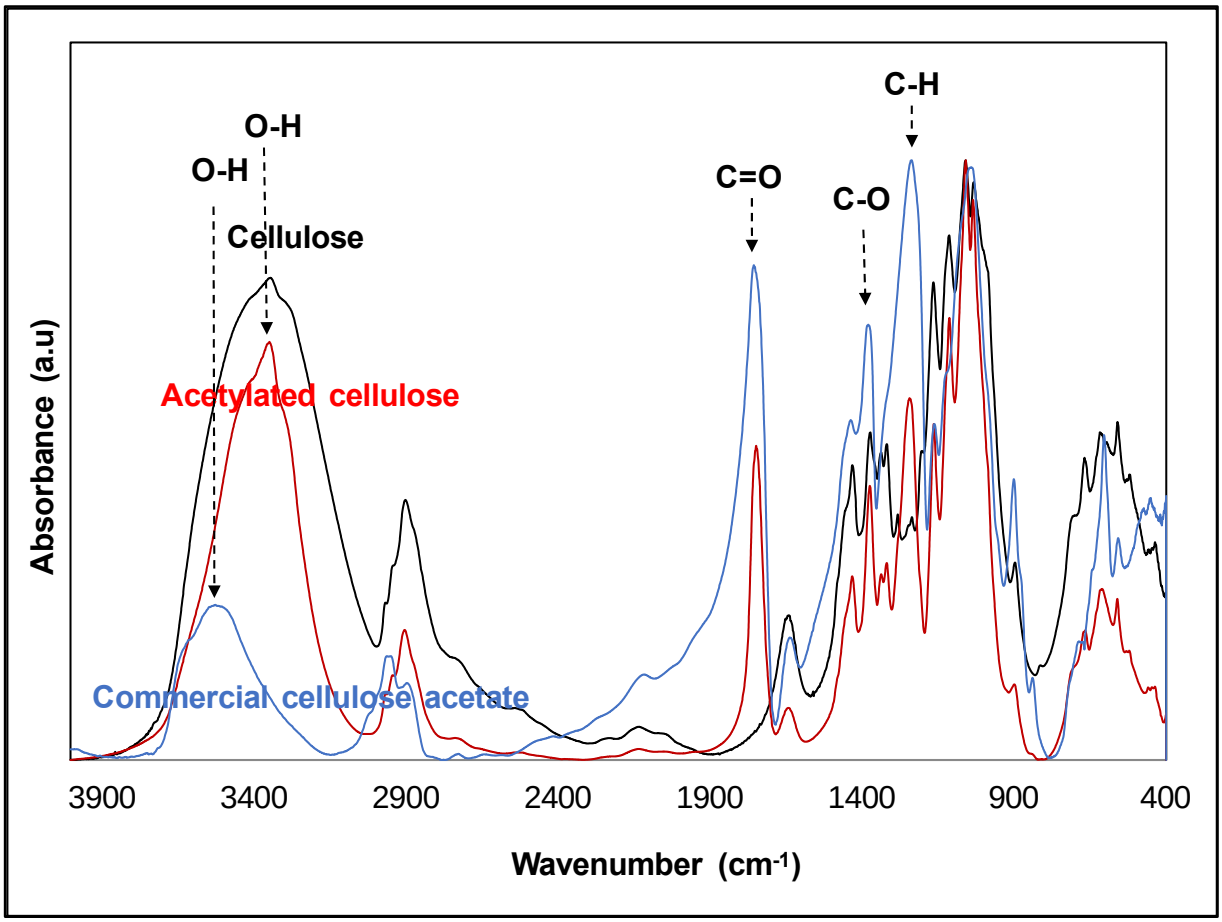

Figure 4.23 FTIR spectra of cellulose before and after acetylation and commercial cellulose acetate.

4.9.3 XRD analysis of cellulose and acetylated cellulose

The crystallinity of cellulose before and after acetylation was studied and it was compared with that of commercial cellulose acetate. The XRD patterns for the three polymers are presented in Figure 4.24. The cellulose used in this study was cellulose-I which had a diffraction index at 14.5, 16.3, 23.5 and 34.5^{o}. The crystallinity of cellulose after acetylation was maintained even though the crystallinity index of cellulose before and after acetylation decreased from 65% to 58%. However, the XRD pattern of commercial cellulose acetate was diffused. This indicated that commercial cellulose acetate is fully substituted and resulted in the damage of the crystallinity of native cellulose.

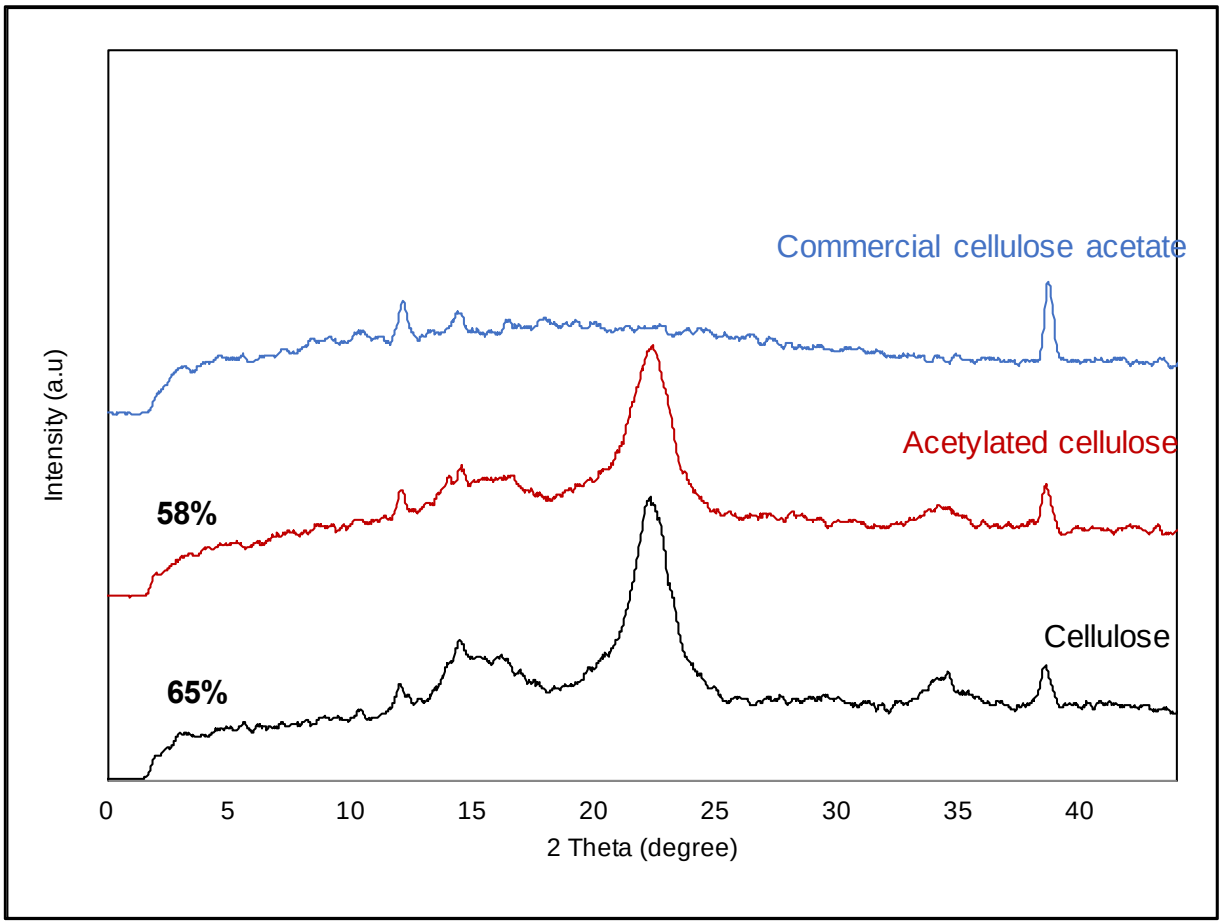

Figure 4.24 XRD pattern of cellulose before and after acetylation.

4.9.4 Thermogravimetric analysis of cellulose and acetylated cellulose

The thermal behaviour of cellulose before and after acetylation was observed using TGA analysis. With reference to Figure 4.25, cellulose started to decompose at 300 °C. Acetylated cellulose also started to degrade at the same temperature. However, the percentage of cellulose residue after acetylation was lower. Cellulose had a residue of 9.80% whilst acetylated cellulose had a residue of 4.07%. In addition, the thermal degradation of commercial cellulose acetate was higher by approximately 10 °C than acetylated cellulose and had a residue of 12.30%. The trend for the thermal decomposition of cellulose and acetylated cellulose was the same as that reported in the literature [185]. The thermal stability of commercial cellulose acetate was better than acetylated cellulose produced in this study due to the raw material used being different. Cellulose acetate produced in this project came from commercial cellulose

which was extracted from cotton. A summary for the thermogravimetric of cellulose and acetylated cellulose is summarised in Table 4.8.

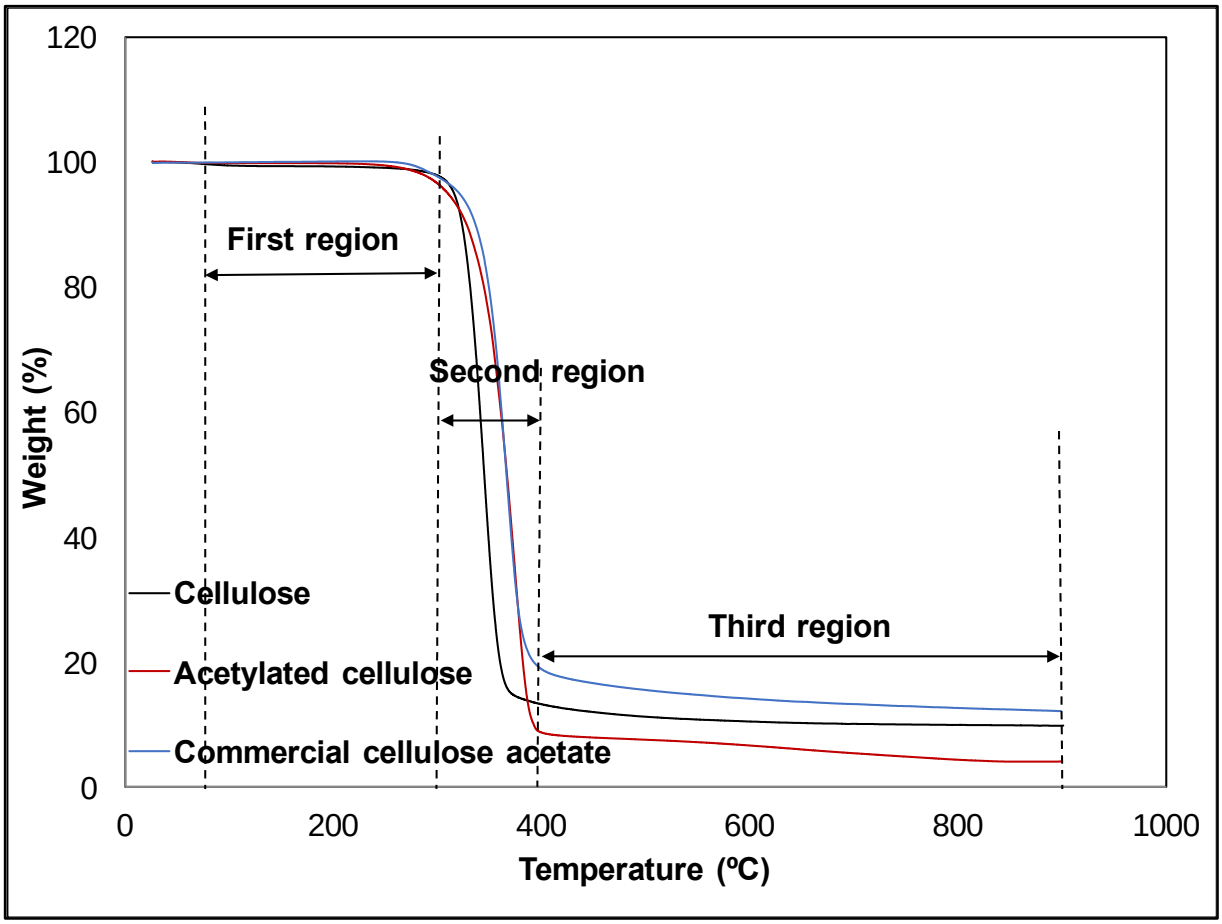

Figure 4.25 TGA traces for cellulose, acetylated cellulose, and commercial cellulose acetate with a heating rate pf 10K.minute^{-1} in argon.

Table 4.8 A summary of thermal behaviour for cellulose before and after acetylation and commercial cellulose acetate.

No.	Samples	TGA experiment (heating rate of 10K.minute^{-1} in argon) : RT - 900 ºC								
		First region			Second region			Third region		
		T_1, ºC	T_2, ºC	Yield at T_2, w%	T_1, ºC	T_2, ºC	Yield at T_2, w%	T_1, ºC	T_2, ºC	Yield at T_2, w%
1.	Cellulose	80	300	97.78	300	360	20.56	360	900	9.80
2.	Acetylated cellulose	80	300	96.45	300	390	10.90	390	900	4.07
3.	Commercial cellulose acetate	80	300	97.74	300	390	20.74	390	900	12.29

4.10 Deacetylation of NNC-Ac

Deacetylation of NCC-Ac was carried out using 0.1 N NaOH for 24 hours at room temperature. The deacetylated NCC-Ac was filtered under vacuum. The deacetylated NCC-Ac was then rinsed repeatedly using DI water until the pH reached 7. Deacetylation of NCC-Ac was performed to convert NCC-Ac to NCC. This procedure was necessary prior to carbonisation of NCC fibre to prevent the fibre from melting during the carbonisation process. The mechanism of deacetylation of NCC-Ac is illustrated in Figure 4.26.

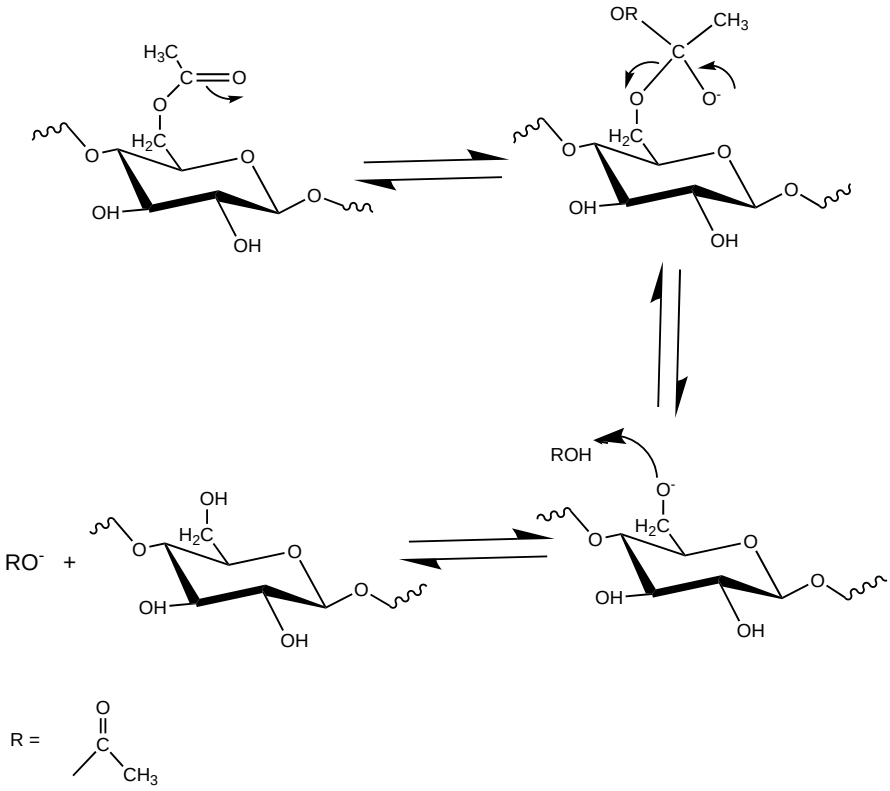

Figure 4.26 Deacetylation of NCC-Ac [190].

4.10.1 Environmental scanning electron microscope of deacetylated NCC-Ac

The morphology of deacetylated NCC-Ac was studied using an ESEM. Typical micrographs of the deacetylated NCC-Ac dried at 80 ºC for 5 hours in a vacuum oven are shown in Figure 4.27 (a and b).

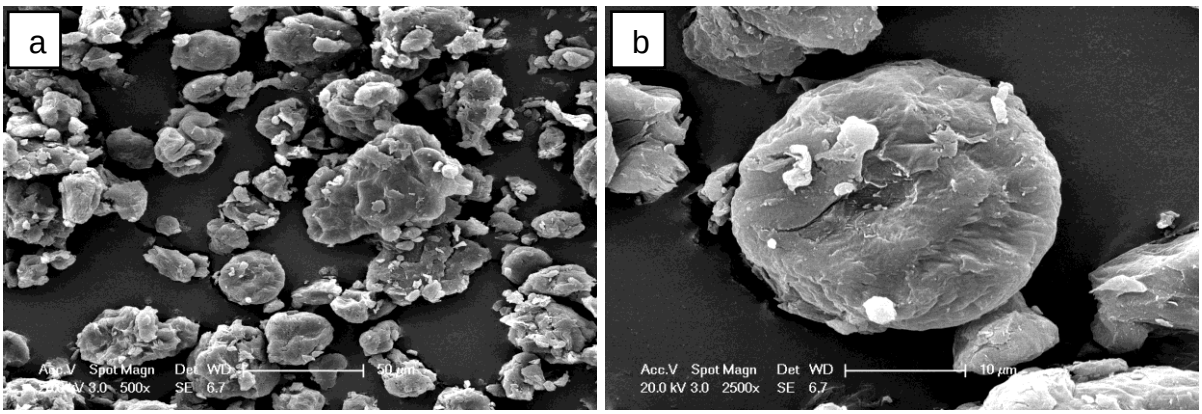

Figure 4.27 (a and b) ESEM micrographs of deacetylated NCC-Ac.

From the Figure 4.27 (a and b), it can be seen that the surface morphology of NCC-Ac after deacetylation is converted to a powder form. This might be due to OH^- ion from NaOH diffused into the surface of NC-Ac to substitute the acetyl groups [191]. Similarly, immersing NCC in NaOH solution regenerates NCC-Ac.

4.10.2 FTIR spectroscopic analysis of deacetylated NCC-Ac

To confirm the chemical structure of NCC-Ac before and after deacetylation, FTIR spectroscopic analysis was carried out. The FTIR spectra for NCC-Ac before and after deacetylation is shown in Figure 4.28.

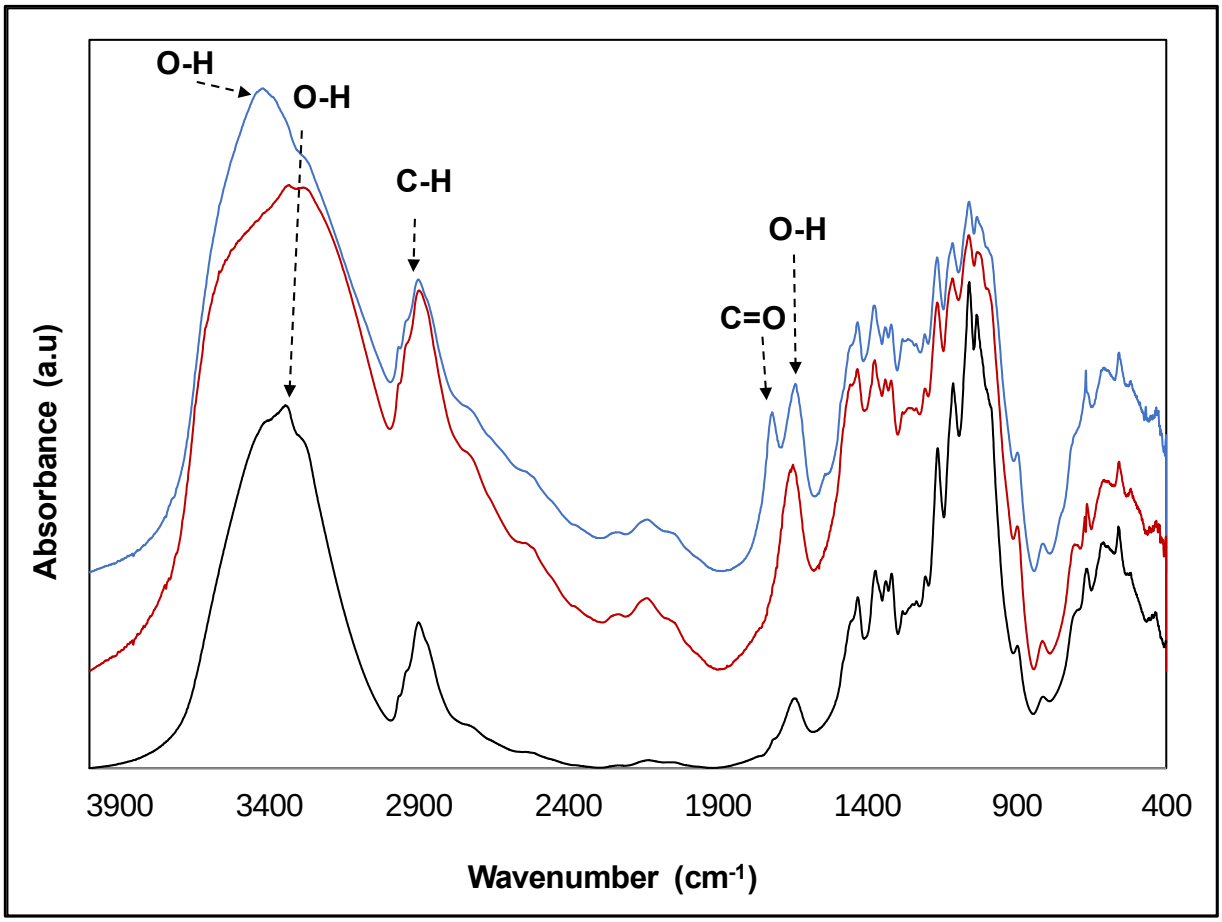

Figure 4.28 FTIR spectra of NCC, NCC-Ac and deacetylated NCC-Ac.

With reference to Figure 4.28, the absorbance band located at around 3350 cm^{-1} can be attributed to the hydrogen-bonded (O-H) stretching of NCC and NCC-Ac reflexing to cellulose-I. However, this absorbance band can be seen to shift to 3420 cm^{-1} for

deacetylated NCC. Similarly, the carbonyl (C=O) group of NCC-Ac at 1720 cm^{-1} disappears after deacetylation. This indicates that deacetylation was successfully.

4.10.3 XRD analysis of deacetylated NCC-Ac

The XRD for NCC, NCC-Ac and deacetylated NCC-Ac are shown in Figure 4.29. It demonstrates that the crystallinity of NCC was unchanged after chemical modification. The crystalline form of cellulose-I is maintained in the material. However, the crystalline index of the as-received NCC decreased after modification. The as-received NCC had an index crystallinity of 75%, but after acetylation and deacetylation it decreased to 68% and 62% respectively. Decreasing the crystallinity of cellulose acetate deacetylation was also reported by Ahmed *et al.,* [192].

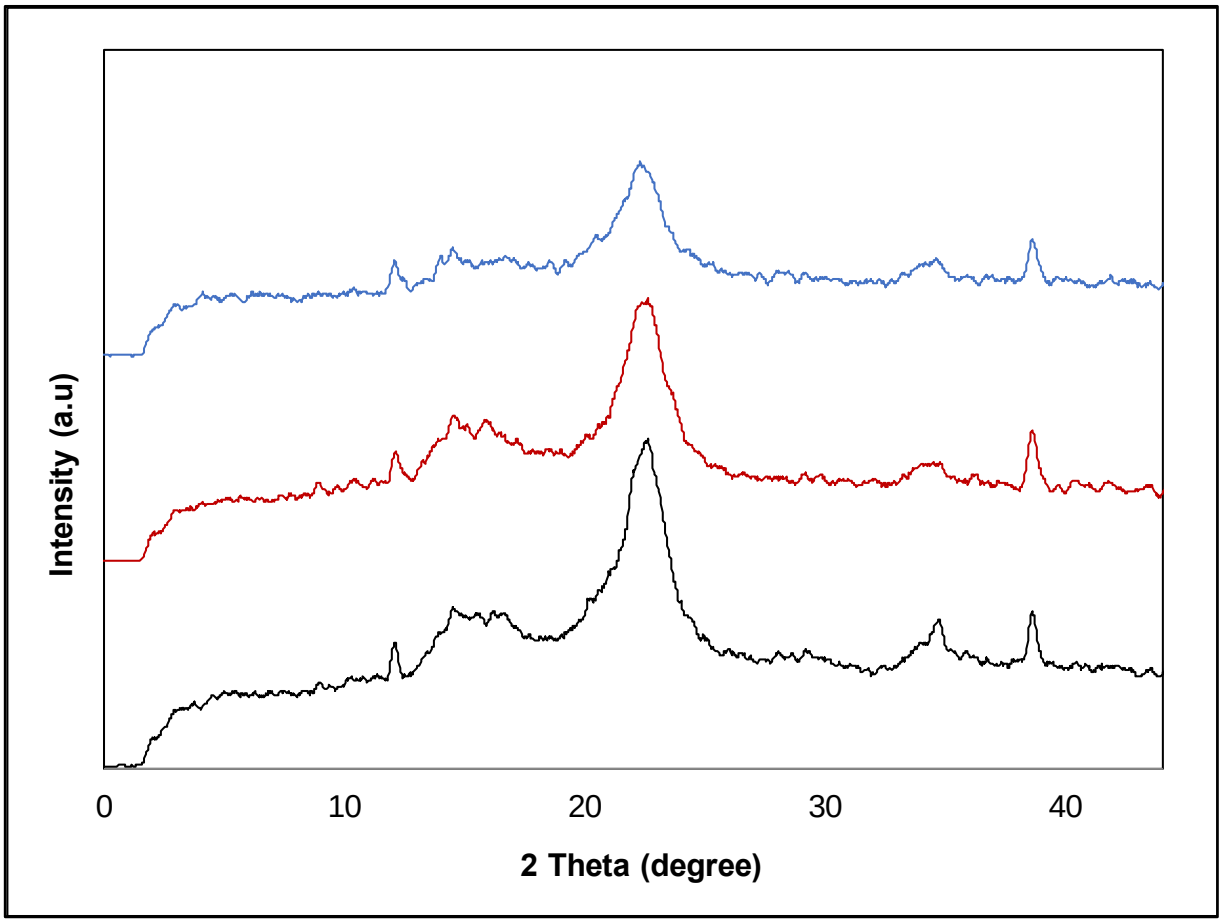

Figure 4.29 XRD pattern of NCC, NCC-Ac before and after deacetylation.

4.10.4 Thermogravimetric analysis of deacetylated NCC-Ac

The TGA traces for NCC, NCC-Ac and deacetylated NCC-Ac are represented in Figure 4.30.

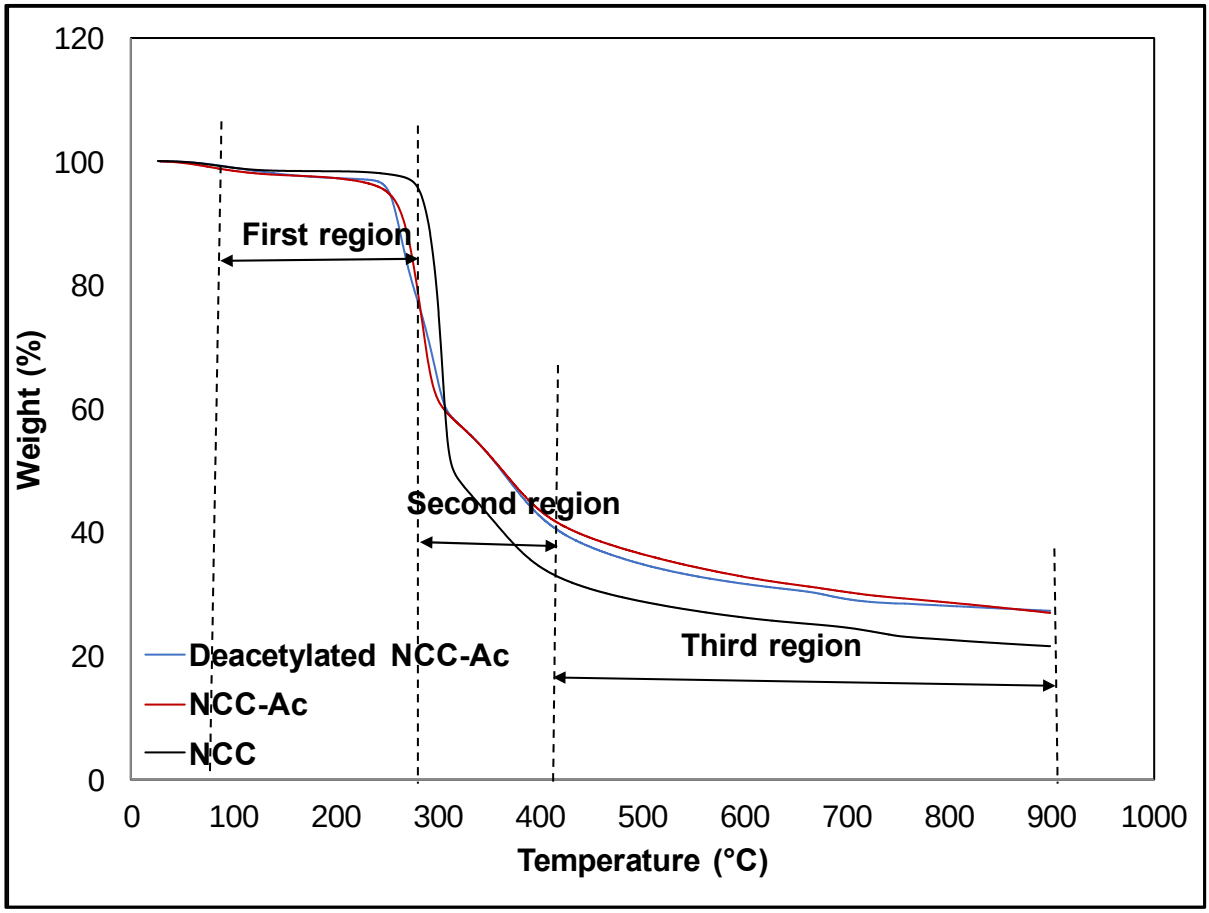

Figure 4.30 TGA traces of NCC, NCC-Ac and deacetylated NCC-Ac with a heating rate of 10 K.minute^{-1} in argon.

In the Figure 4.30, the TGA traces for the as-received and modified NCC show three distinct regions. The first region is from room temperature to 100 ºC showing dehydration of the samples. The weight lost in this area is around 1%. The second step region in the TGA trace is between 270 ºC and 400 ºC for the as-received material with a loss of around 65% of its original mass. NCC-Ac and deacetylated NCC-Ac start to decompose at lower temperature which are from 160 ºC to 400 ºC with approximately 58% mass loss. As stated previously, the thermal decomposition occurs more readily in NCC with lower degree of crystallinity. The final temperature is at 900 ºC having a

residue of 21.57%, 26.83% and 27.27% for the as-received NCC, NCC-Ac and deacetylated NCC respectively.

4.11 Electro-spinning

4.11.1 Electro-spinning conductivity of cellulose acetate

Commercial cellulose acetate with a molecular weight (M_w) of 30,000 was used as the precursor to produce nano-fibre via electro-spinning. A 20% (w/v) of cellulose acetate in acetone was spun at 15 ^oC using a cooling system to avoid rapid evaporation of acetone and to prevent clogging at the tip of the needle. Acetone has a boiling point at 58 ^oC and evaporates at room temperature. Before electro-spinning, the conductivity of the polymer solution and the temperature of the cooling system were measured. The conductivity of the cellulose acetate solution was 3.45 μS/cm at 15 ^oC and it almost doubled at 22 ^oC. The cooling system testing was able to maintain the temperature of the cellulose acetate solution at 15 ^oC for approximately 2 minutes. The data for the conductivity and the cooling system measurements are presented in Figure 4.31.

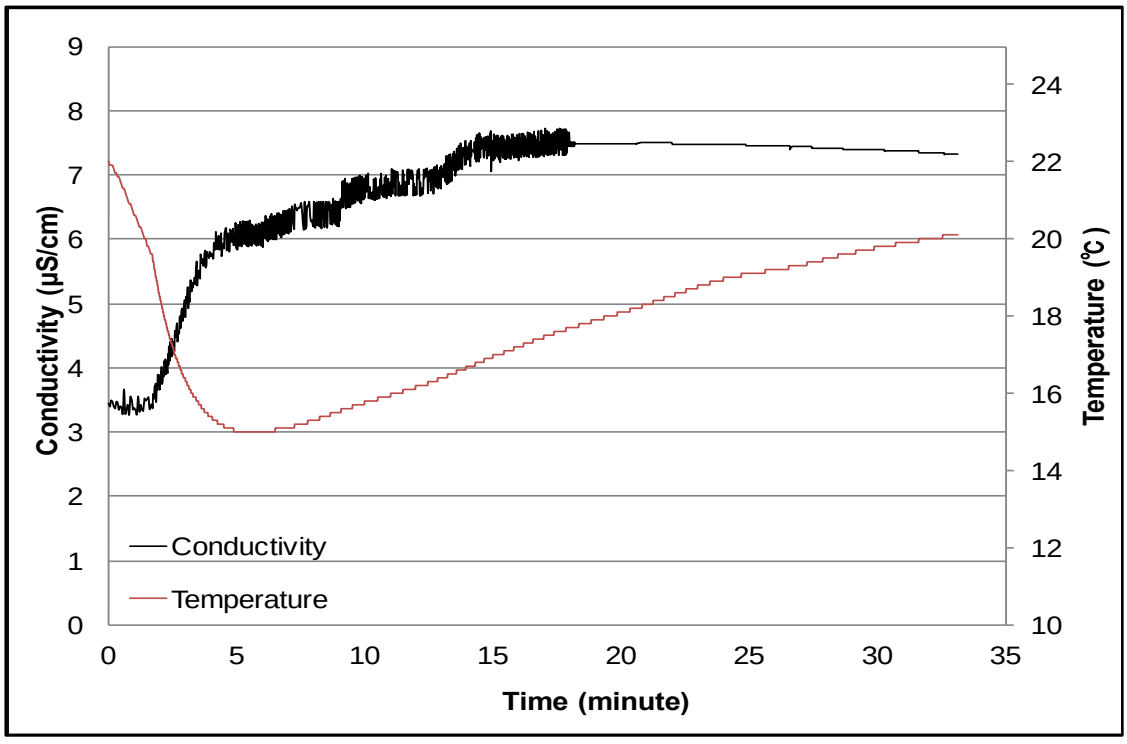

Figure 4.31 The conductivity and the temperature for CA 20% (w/v) in acetone.

The electro-spun fibres using cellulose acetate 20% (w/v) in acetone were collected using a flat aluminium collector. The orientation of fibres was random. In addition, bead-fibres were produced due to the conductivity being low. Higher conductivity in polymer solution is able to stretch the solution resulting fine fibres. The SEM micrographs for the cellulose acetate spun-fibres are shown in Figure 4.32 (a-d).

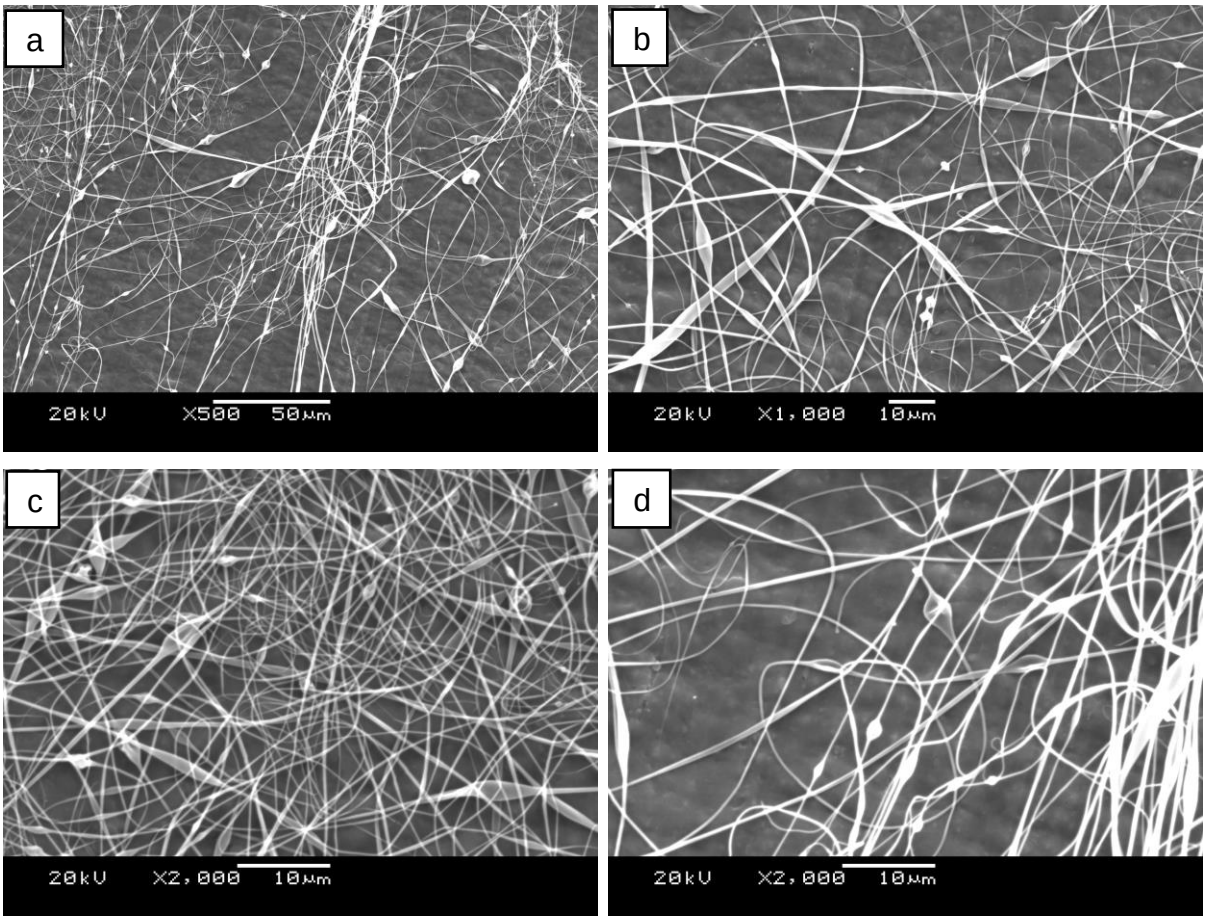

Figure 4.32 (a-d) SEM micrographs cellulose acetate spun-fibre 20% (w/v) in acetone.

Owing to the low conductivity of the cellulose acetate solution and the rapid evaporation of acetone, a binary solvent was used to increase both properties. As mentioned in Chapter 2, cellulose acetate dissolves in a solvent with Hildebrand solubility parameters (δ) ranging from 9.5 and 12.5 (cal/cm^3) [124]. Dimethylsulfoxide (DMSO) has a (δ) of 10.2 [193] and has a boiling point of 189 ^{o}C. Hence, DMSO is a suitable mixed solvent to dissolve cellulose acetate and to increase the evaporation rate of solution.

Similarly, the conductivity of cellulose acetate 20% (w/v) in acetone:DMSO (2:1) increased to 8.25 µS/cm at 25 ^{o}C and the viscosity was 8.99 (Pa-s). From the ESEM result (see Figure 4.33), bead-free and smooth fibres were obtained. Furthermore, the electro-spinning process was continuous due to the conductivity being high enough and the evaporation of the cellulose acetate solution being controllable. The conditions governing the conductivity of the cellulose acetate solution, that were needed for producing bead-free and continuous electro-spinning fibres were consistent with the results reported by the previous researcher [124].

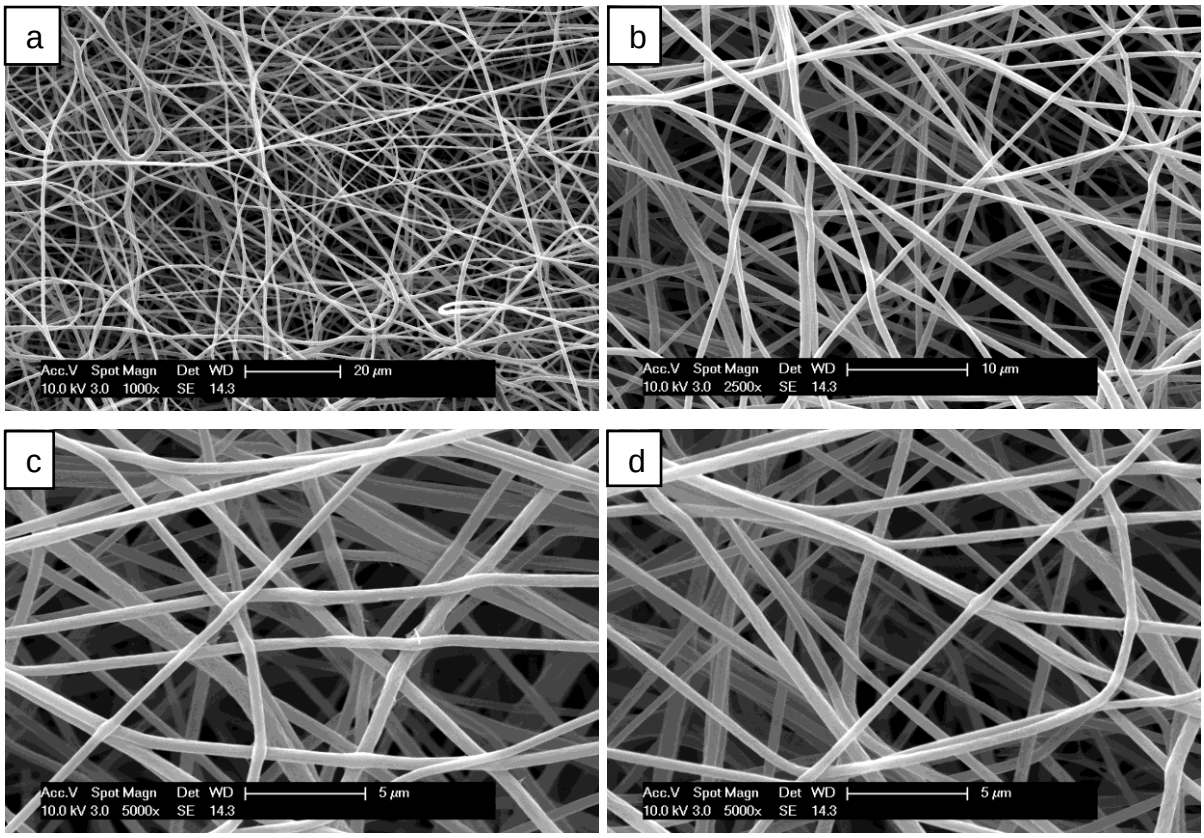

Figure 4.33 (a-d) ESEM micrograph of spun-fibres cellulose acetate 20% (w/v) in acetone:DMSO (2:1).

4.12 Mechano-electro-spinning of NCC with polyacrylonitrile (PAN)

NCC was electro-spun using PAN as the ‘carrier’ polymer. The solution was prepared under reflux in a nitrogen atmosphere at room temperature. 8% PAN in DMSO and 4% NCC in DMSO were mixed using sonication to prepare spun-polymer solution with a concentration of NCC in PAN solution corresponding to 9%, 17% and 21%.

The conductivity and viscosity of PAN solution was measured prior to electro-spinning. The addition of NCC into PAN solution increased the conductivity but decreased the viscosity of the polymer solution. Initially, the conductivity of PAN solution was 15.41 µS/cm and increased to 17.73 µS/cm, 19.63 µS/cm and 21.59 µS/cm after introducing 9%, 17% and 21% of NCC to the solution respectively. The data for the conductivity of PAN solution in DMSO is represented in Figure 4.34.

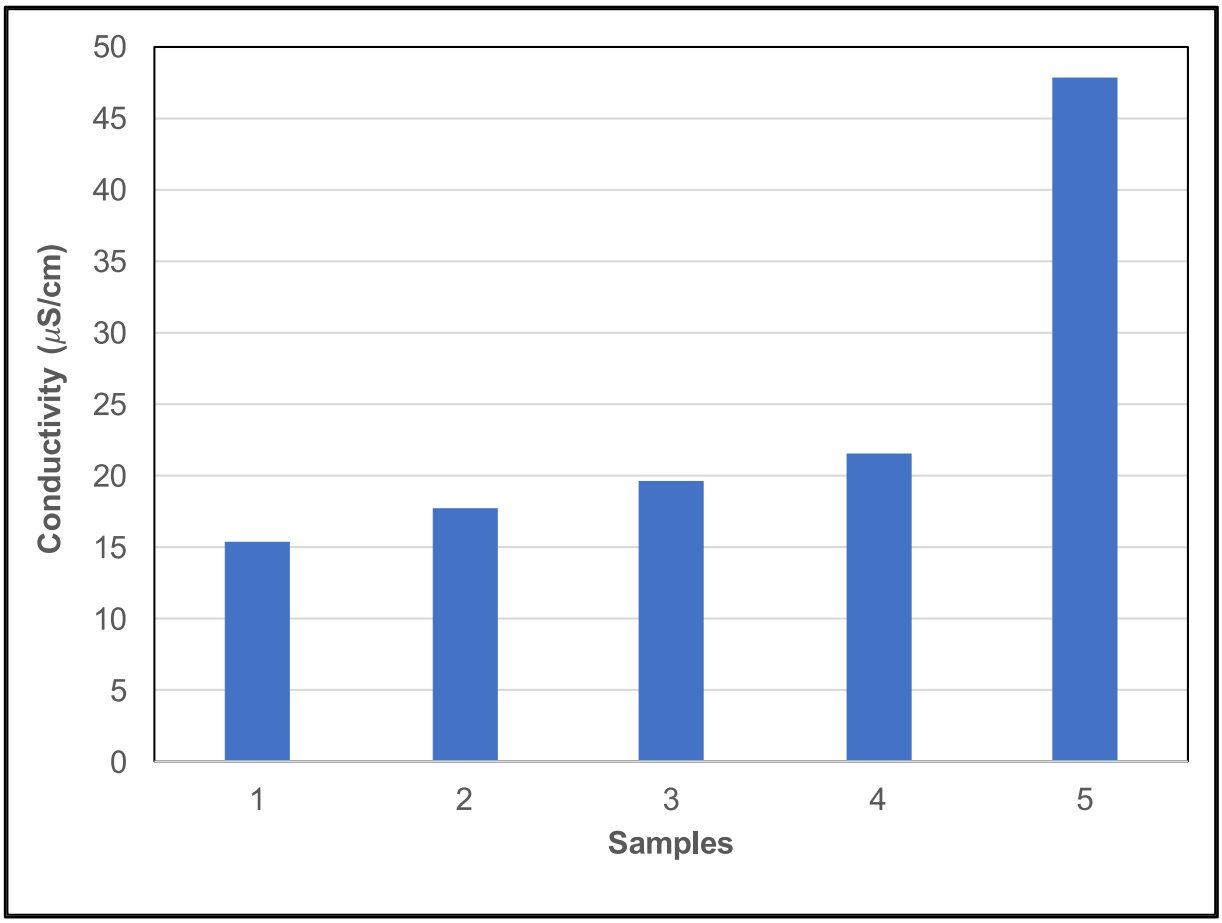

Figure 4.34 The conductivity of: (1) PAN 8% (w/w) in DMSO, (2) 9% NCC in PAN solution, (3) 17% NCC in PAN solution, (4) 21% NCC in PAN solution and (5) NCC 4% (w/w) in DMSO.

In addition, the viscosity of PAN solution was 13 Pa-s and decreased to 6.5 Pa-s and 4 Pa-s after the addition of 9% and 17% NCC respectively. The viscosity of PAN solution containing 21% of NCC was almost the same as the viscosity of 4% (w/w) NCC in DMSO which was 1 Pa.s. The viscosity of PAN solution is presented in Figure 4.35.

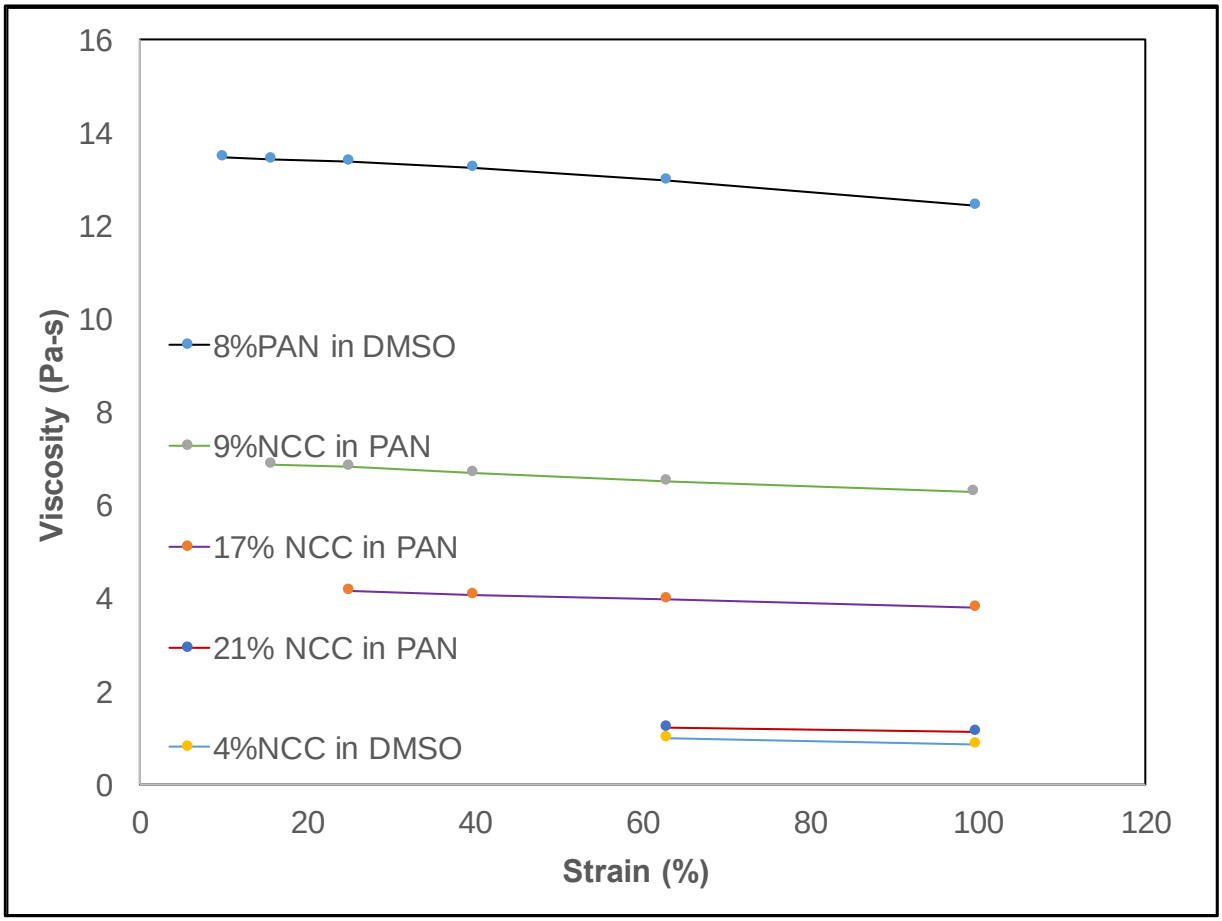

Figure 4.35 The viscosity of: (1) PAN 8% (w/w) in DMSO, (2) 9% NCC in PAN solution, (3) 17% NCC in PAN solution, (4) 21% NCC in PAN solution and (5) NCC 4% (w/w) in DMSO.

The conductivity and viscosity of the polymer solution influences the fibre morphology of spun-fibres. The diameter of spun-fibres of PAN decreased from approximately 500 µm to around 200 µm with the addition of NCC due to the conductivity of polymer solution increasing. This result is in agreement with a previous study [194]. However, some researchers reported that a higher conductivity leads to an increase in the surface tension of the spinning jet. This would result in a decrease in the viscosity of the polymer solution and therefore the spinning would be more fluent and there would be an increase in the mass flow. Hence, a large diameter of spun-fibres would be produced [195,196]. Similarly, too high a concentration of NCC produced bead-fibres due to poor compatibility of NCC with PAN polymer solution. The morphology of PAN spun-fibres is presented in Figure 4.36.

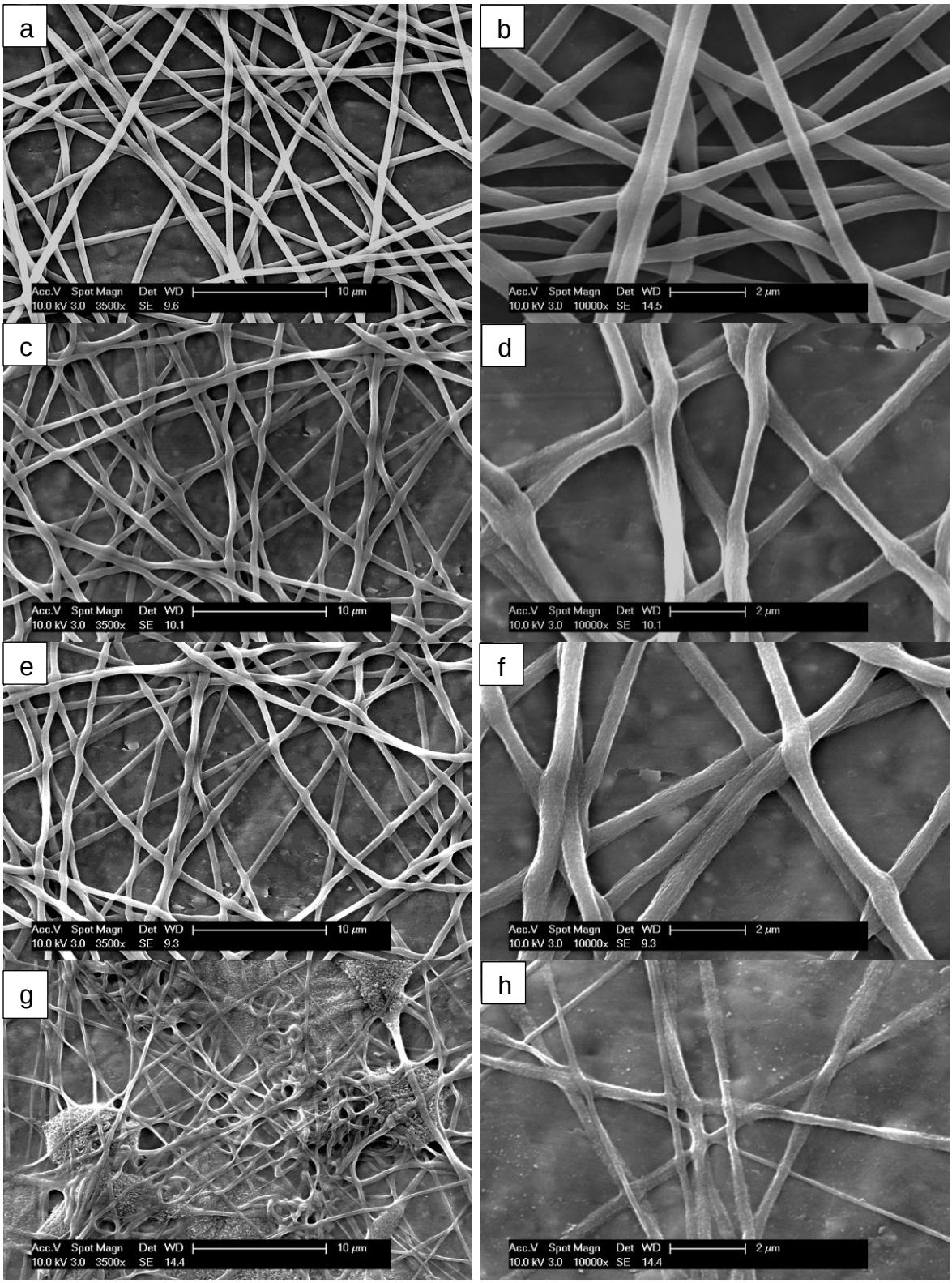

Figure 4.36 ESEM micrograph; (a-b) PAN 8% (w/w) in DMSO, (c-d) 9% NCC in PAN solution, (e-f)) 17% NCC in PAN solution and (g-h) 21% NCC in PAN solution.

To identify the chemical changes in PAN spun-fibres before and after the addition of NCC, an FTIR spectral analysis was carried out. The spun-fibres were removed from the aluminium collector by immersing them in hot water and then drying them under vacuum at 80 ^{o}C. The FTIR spectra for PAN spun-fibre reinforced with NCC is presented in Figure 4.37.

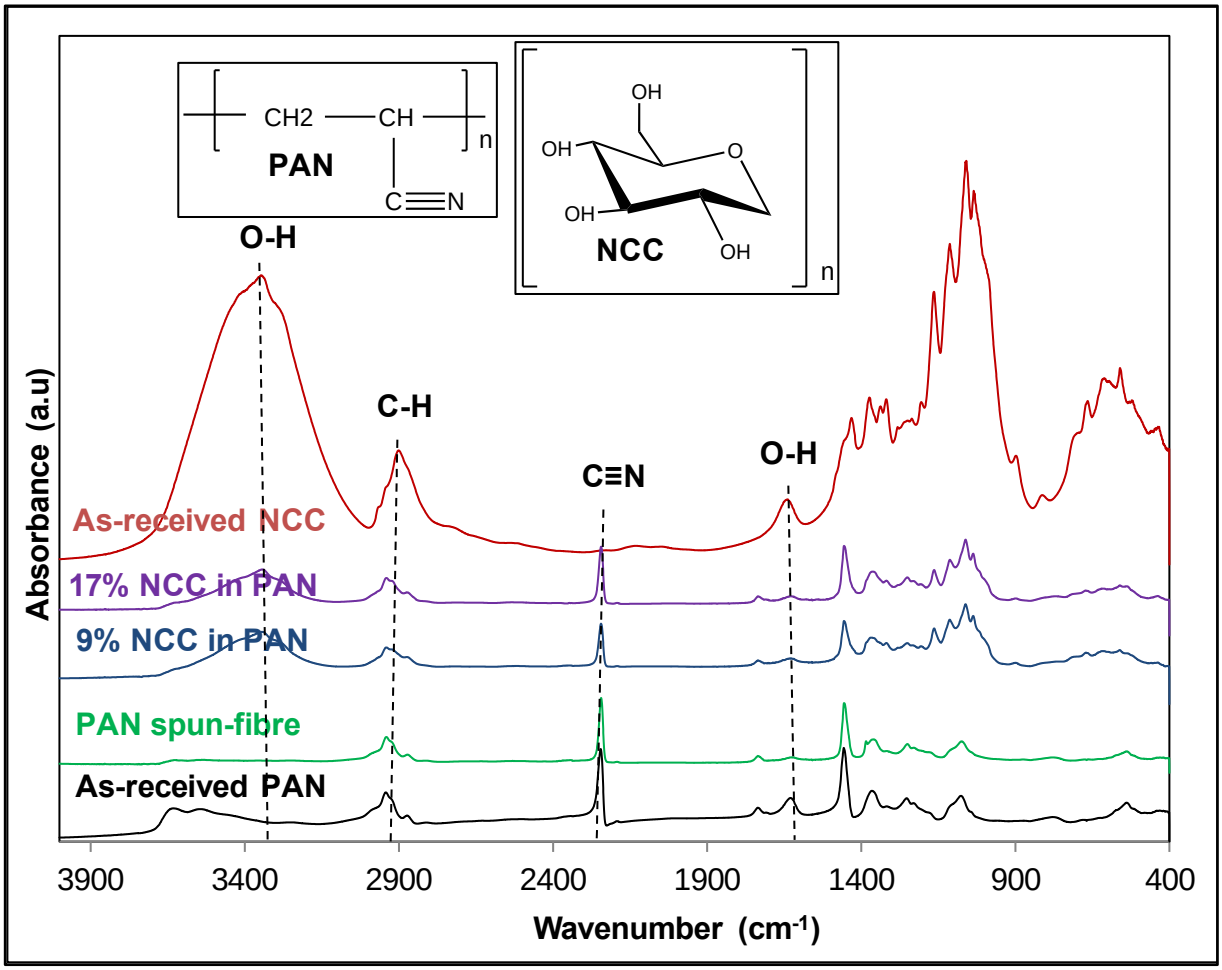

Figure 4.37 FTIR spectra of as received NCC, as received PAN, PAN spun-fibre reinforced with 0%, 9% and 17% NCC.

With reference to Figure 4.37, the absorbance band at around 3350 cm^{-1} indicates hydrogen-bond (O-H) bonding stretching from NCC. This absorbance appears for fibres containing 9% and 17% NCC in PAN fibre where the absorbance O-H for as-received PAN is at around 3600 cm^{-1}. The absorbance band at 2240 cm^{-1} assigned to

the C≡N structure appears for the PAN-NCC spun-fibres [197]. In addition, O-H groups at around 1610 cm^{-1} for both as-received PAN and NCC disappears for the spun-fibres.

In summary, the presence of NCC in the polymer solution is said to increase the conductivity of the solution due to the introduction of anionic charge from NCC [80,81,83]. This is reported to give a significant improvement in the properties of electro-spun fibre composites: (i) producing thinner fibre [87], (ii) improving the tensile strength and Young's modulus of the spun-fibres [89], (iii) increasing the tensile failure strain of spun-fibres [91], (iv) increasing the thermal stability of the electro-spun fibres [82] and (v) improving the crystallinity of the spun-fibres [83]. However, the inclusion of NCC leads to the formation of "bead fibres" and the morphology of fibres containing NCC is rougher than those without NCC [79]. This is reported to be due to the poor dispersion and compatibility of NCC with the polymer solution [79]. It is also known that fibres cannot be electro-spun if the concentration of NCC is too high. This causes the viscosity of polymer solution to drop when NCC reaches critical concentration [93].

4.13 Pyrolysis of wet-spun NCC spun-fibres produced via wet-spinning

Final objective for this study is to produce carbonised fibres from NCC and NCC-Ac. NCC with a concentration of 6% (w/v) in DMSO was prepared by dispersing the polymer using sonication. The temperature used was between 20 and 30 ºC during the sonication period. The same technique was also used to prepare 6% (w/v) NCC-Ac in DMSO. NCC has a critical concentration at 3% in a solution, hence 6% (w/v) NCC and NCC-Ac in DMSO produced suspension in a gel-form.

4.13.1 SEM of wet-spun NCC and NCC-Ac

4.13.1.1 Wet-spun fibres

The morphologies and cross-section areas of wet-spun NCC and NCC-Ac are represented in Figure 4.38.

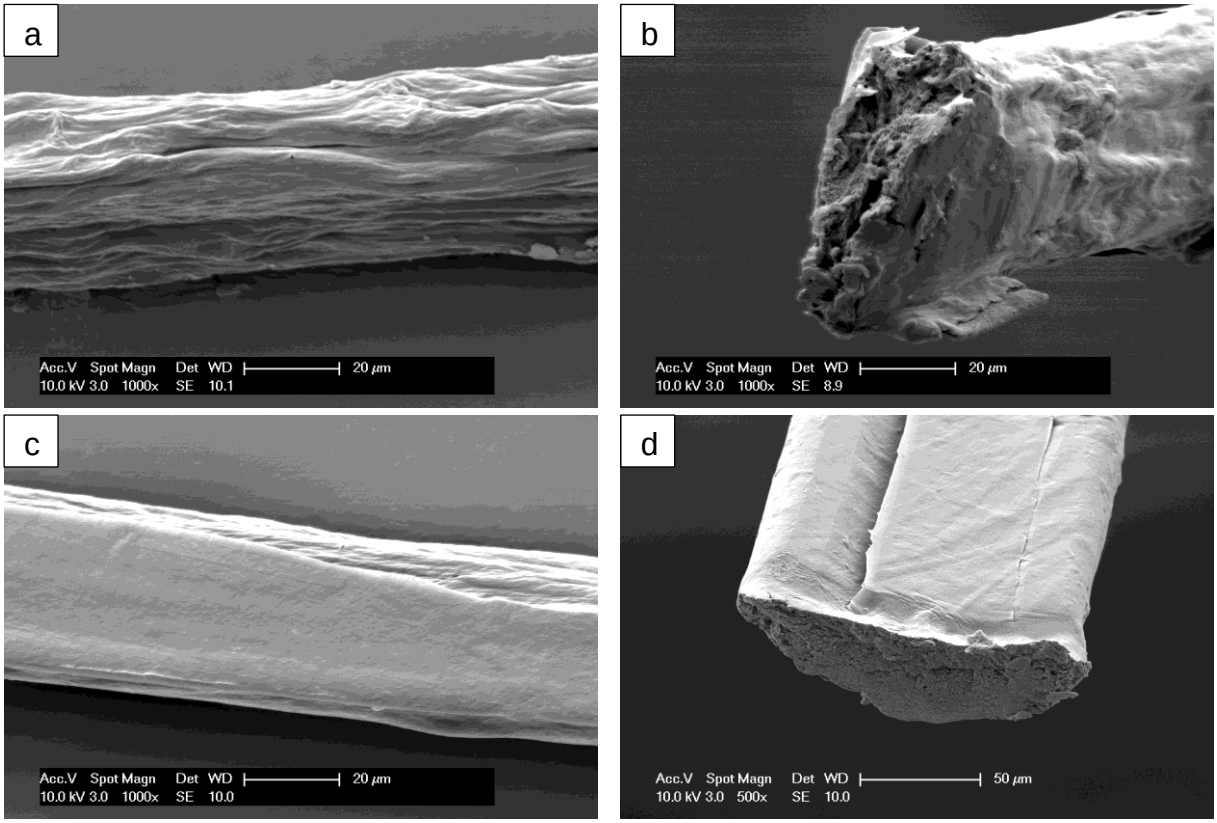

Figure 4.38 ESEM micrographs and cross-section areas of (a-b) wet-spun NCC and (c-d) wet-spun NCC-Ac.

With reference to Figure 4.38, it can be seen that the morphology of wet-spun NCC-Ac is smoother than NCC. The same appearance is also seen for the cross-section areas. This is due to the acetylation on NCC increasing the homogenity of NCC in DMSO as shown in the Figure 4.21 which increases the viscosity of NCC in DMSO.

Further research has been carried out by Inam Khan and Bongkot Hararak in the Sensors and Composites Group and they have demonstrated that it is possible to generate fibres with a circular cross-section and reduced porosity. A 20% (w/v) cellulose acetate in DMSO was prepared under reflux and was used as the ’carrier’ polymer. The solution of cellulose acetate was mixed with the NCC gel using ultra-sonication. The concentration of NCC in the cellulose acetate solution was 5%. The same solution concentration was prepared for NCC-Ac. The micrographs and cross-section areas for wet-spun cellulose acetate reinforced NCC and NCC-Ac are presented in Figure 4.39.

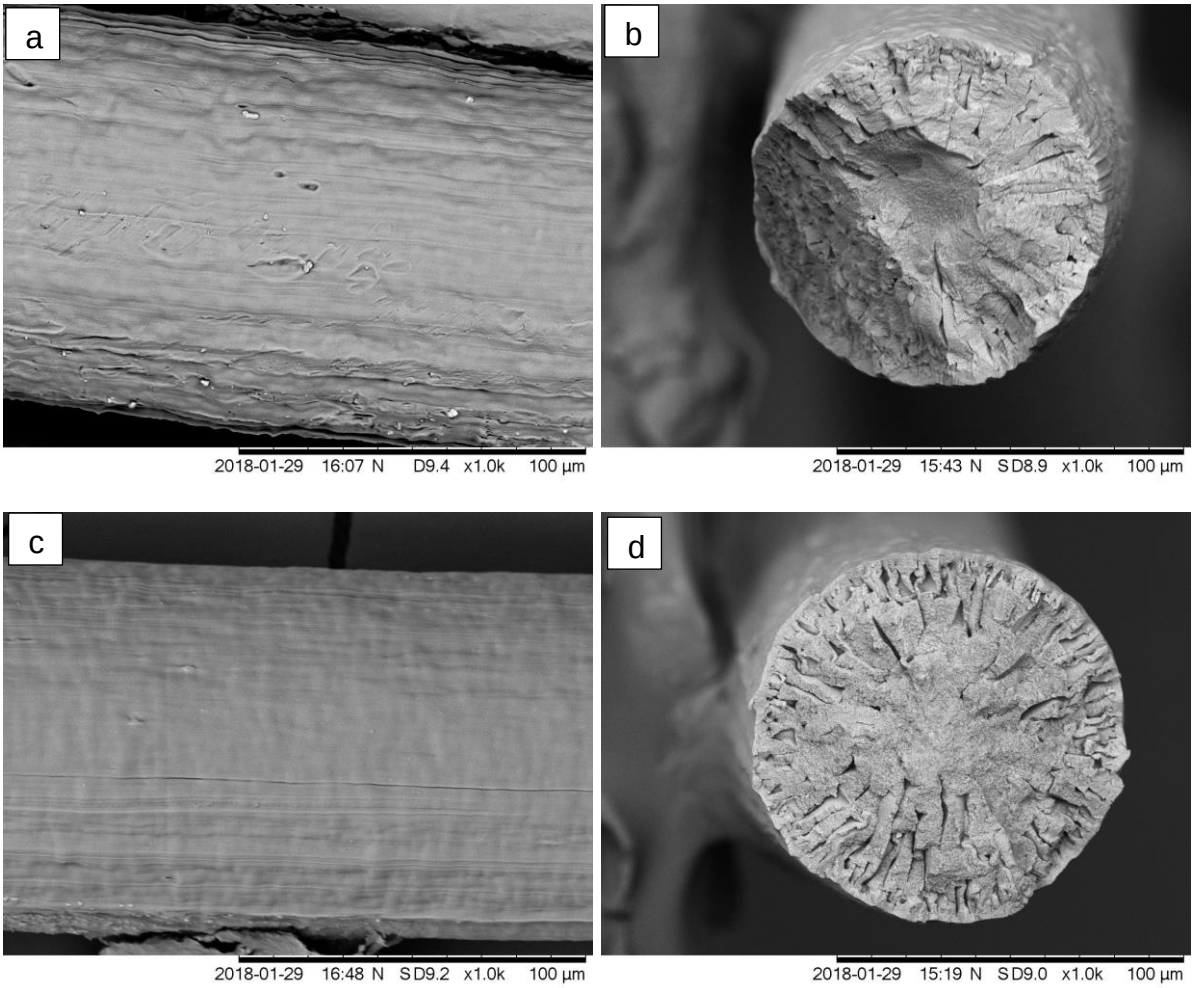

Figure 4.39 SEM micrographs and cross-sections area of (a-b) wet-spun cellulose acetate reinforced 5% NCC and (c-d) wet-spun cellulose acetate reinforced 5% NCC-Ac. Data generated by I Khan and B Hararak.

With reference to Figure 4.39, longitudinal lines are observed on the surface which might come from inner bone of the needle. The cross-section area also shows pore on the fibre. Similarly, the wet-spun cellulose acetate reinforced NCC is seen to contain grooves and there are some particles on the surface of the fibres. This is due to NCC having poor compatibility with the polymer solution as explained in Sub-section 4.12. On the other hand, the morphology of cellulose acetate reinforced NCC-Ac is smoother and has fewer particles on it. The acetylation on NCC increases its compatibility with the polymer matrix. Pores on the fibres are also observed from the cross-section area of the fibres.

4.13.1.2 NCC-derived carbonised fibres

Before pyrolysis, NCC-Ac was deacetylated by immersing the fibres in 0.1N NaOH for 24 hours at room temperature. After that, the fibres were rinsed using DI water and dried at room temperature. The longitudinal and cross-sectional views of NCC and deacetylated NCC-Ac based carbonised fibre heated at 900 ºC with a heating rate of 1 K.minute^{-1} are shown in Figure 4.40.

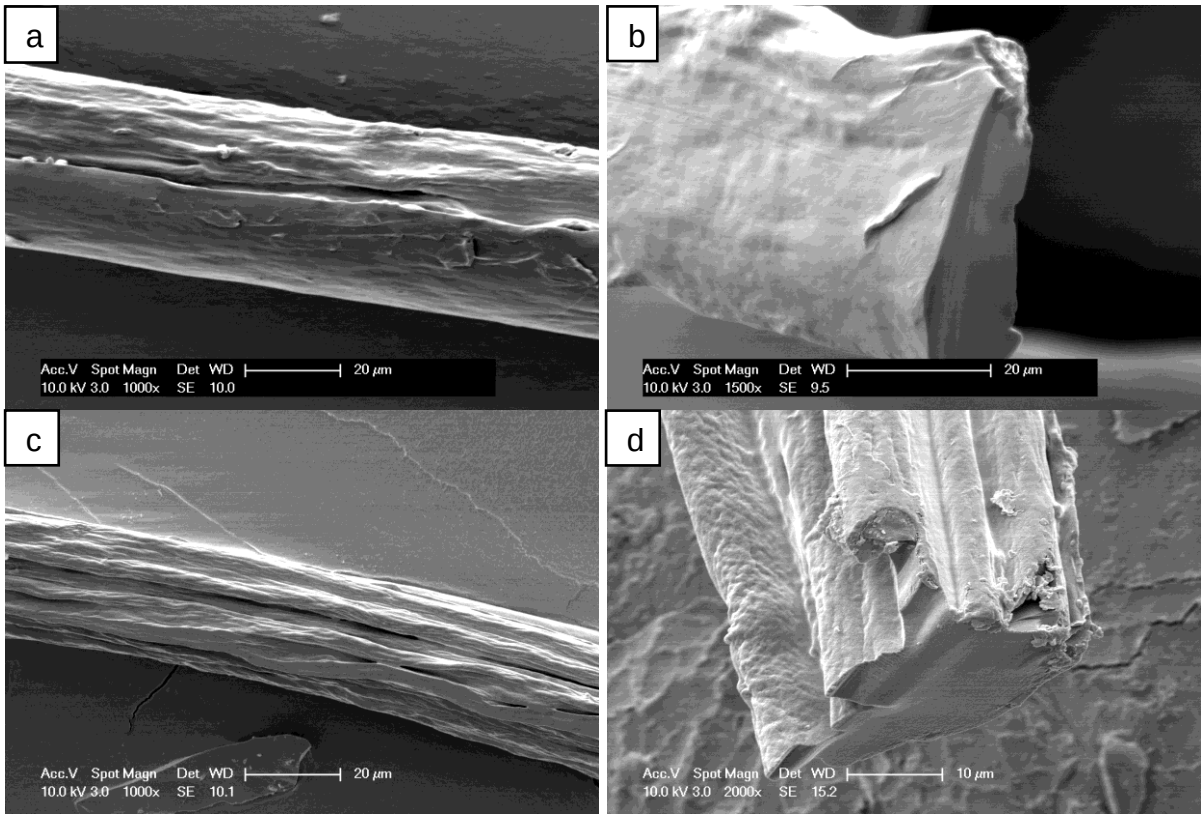

Figure 4.40 ESEM longitudinal and cross-sectional views of (a-b) NCC-carbon fibre and (c-d) deacetylated NCC-Ac-carbon fibre.

With reference to Figure 4.40, the cross-section areas of the carbonised fibres are found to be compact and void-free. This is probably due to NCC being loss mass during the pyrolysis by releasing levoglucosan. This process also decreased the diameter of NCC carbonised fibre by approximately 20 µm. Some reasons might be some gases such as H_2O, CO and CO_2 being released during the pyrolysis.

4.13.2 Raman spectroscopy of carbonised NCC wet-spun fibre

In this study, a laser with a wavelength 488 nm (an Ar^+ laser) was used as the excitation light source. A laser at this wavelength has a penetration depth 100 nm [198].

In Raman spectroscopy, the crystalline structure of carbon has four spectral regions which indicates either the amorphous or the crystalline carbon material as summarised in Table 4.9.

Table 4.9 The major Raman lines of carbon fibres [199].

No.	Line	Location (cm^{-1})	Present in	Attributes to
1	D	1350 - 1370	Poorly graphitised fibres.	Breathing mode of A_{1g} symmetry of aromatic ring sp^2, introduced by small crystal size and structural disorder.
2	G	1575 - 1582	Single graphite crystal and all carbon fibres.	Stretching motion of sp^2 hybridised C atoms, the vibrational mode E_{2g}.
3	D’	~1620	Non-graphitised fibres.	Disorder and small crystallite size.
4	G’	2690 - 2730	Crystalline graphite and graphitised fibres.	Second-order overtone of a different in-plane vibrational D.

According to Tuinstra-Koenig equation, the ratio of I_D/I_G, can be used to determine the graphite crystalline size of carbon material (200). The Raman spectra for NCC-derived carbon fibre is represented in Figure 4.40.

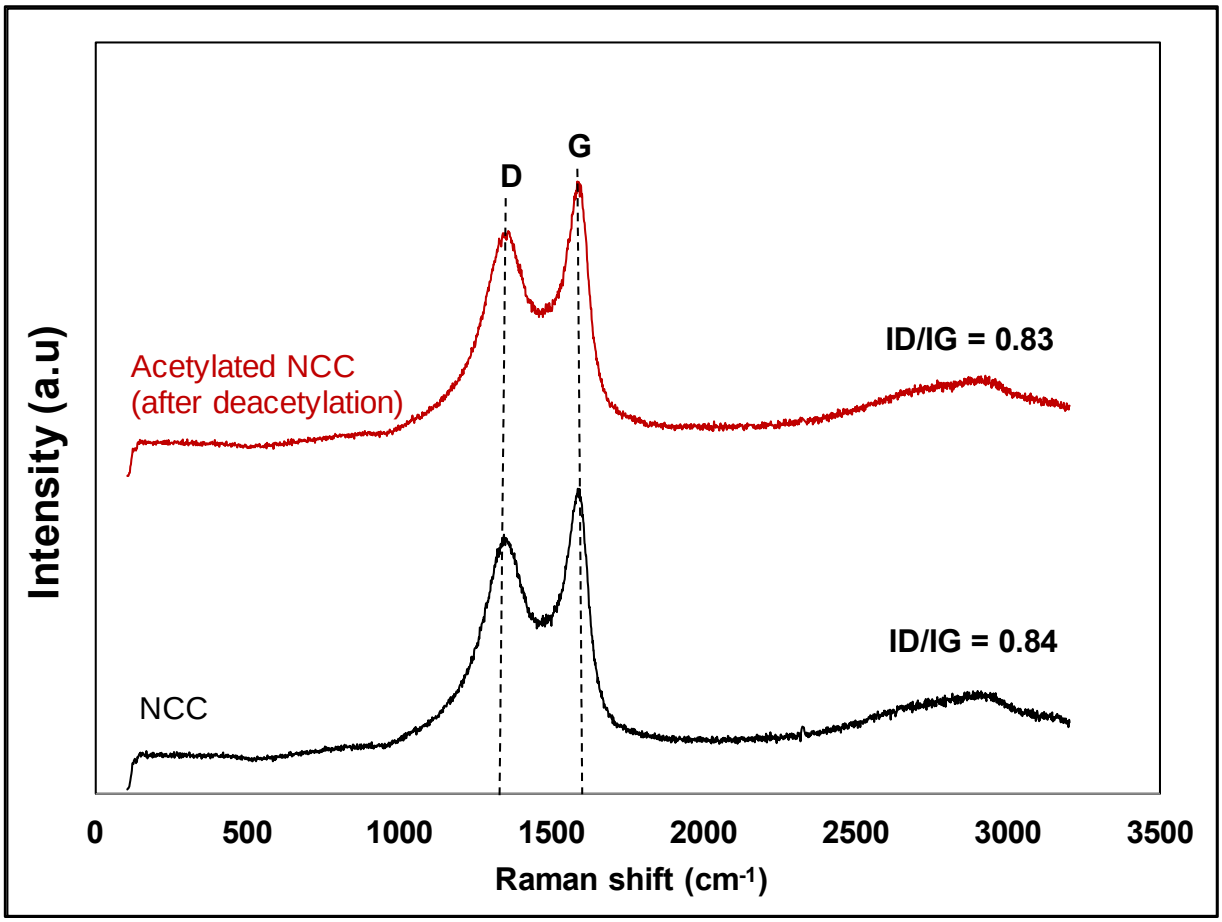

Figure 4.41 Raman spectra of NCC and NCC-Ac-derived carbonised fibre.

From Figure 4.41, it can be seen that there are two peaks at 1580 cm^{-1} for G band and at 1358 cm^{-1} for D band. It indicates the presence of carbon material in the sample. The ratio I_D/I_G is 0.84 for NCC carbonised fibre and 0.83 for deacetylated NCC-Ac carbonised fibre. The chemical modification of NCC through acetylation and deacetylation did not result in a significant impact on the Raman spectrum. Furthermore, the carbonisation process for both wet-spun fibres was successful.

CHAPTER 5
CONCLUSIONS AND FUTURE RESEACRH

5.1 Conclusions

5.1.1 Acetylation of NCC

The surface acetylation on NCC has been carried out successfully using acetic anhydride and pyridine as the acetylating agent and the catalyst, respectively. Several methods were investigated such as increasing reaction time of acetylation, reducing particle size of NCC using cryo-milling and processing in an aqueous gel-form. The key findings are summarised in the following sub-sections.

5.1.1.1 Morphology

The rod-like particle of NCC was characterised using a TEM where the diameter lengths of the NCC were found to be between 2.0 - 4.8 nm and 46 - 114 nm respectively.

In addition, the morphology of the as-received NCC before and after acetylation (dried at 80 ºC for 5 hours) was investigated using an ESEM. It shows that the morphology of NCC changes from smooth to rough and flake-like after acetylation. This is due to the rod-like of NCC having chiral nematic behaviour when at critical concentration, after drying, the solid material forms iridescent films.

5.1.1.2 FTIR spectroscopy

The presence of carbonyl (C=O) groups indicated that the acetylation reaction was successful and this was determined using an FTIR spectroscopy. The results showed a new peak 1730 cm^{-1} (carbonyl C=O stretching of ester). In addition, the two peaks at

1371 cm^{-1} (C-H in O(C=O)-CH_3) and 1232 cm^{-1} (C-O stretching of acetyl group) showed a slight increase in intensity after acetylation. Evidence for the acetylation of NCC is provided by the presence of the three functional groups.

The product of acetylated NCC was purified successfully using a mixing solution of DI water and acetone (1:1). The absence of peaks at 1700 cm^{-1} and between 1760 and 1840 cm^{-1}, confirmed that the unreacted acetic anhydride and by-products of acetic acid had been removed.

5.1.1.3 CP/MAS ^{13}C-NMR spectroscopy

The presence of new chemical shifts in the NMR spectra after acetylation at 170 ppm belonging to the acetyl group (C=O) and 20 ppm for the aliphatic compound (CH_3) indicates that the acetylation reaction was successful. Using CP/MAS ^{13}C-NMR, the degree of substitution of acetylated NCC was determined to be between 0.01 and 0.07.

5.1.1.4 XRD

The crystalline structure of NCC as cellulose-I is maintained after acetylation. However, the crystallinity index of NCC before and after acetylation decreased from 72% to 68%.

5.1.1.5 TGA

The weight loss characteristics of NCC as a function of temperature before and after acetylation was characterised using TGA. It was found that the thermal degradation of NCC shifts to a lower temperature after acetylation. This was from 270 ºC for the as-received NCC and 170 ºC for the acetylated NCC with a mass loss of 65% and 58%, respectively. The percentage residue for acetylated NCC also increase by approximately 6%.

5.1.1.6 Viscosity of NCC and NCC-Ac

The viscosity of NCC is 0.2 Pa.s at 25 ºC along with a shear rate of 1 s^{-1}. It increased slightly to 0.4 Pa.s after acetylation.

5.1.2 Acetylation of cellulose

The acetylation on cellulose was carried out with the same procedure as that the used for the acetylation on NCC. In other words, using acetic anhydride and pyridine as the acetylating agent and the catalyst, respectively, with a reaction time of 5 hours at 80 ºC. The properties of acetylated cellulose produced in this project was compared with commercially obtained cellulose acetate. A summary of the results is presented in the following sub-sections.

5.1.2.1 Morphology

The morphology of cellulose before and after acetylation was investigated using a SEM. It showed that a smooth surface for the as-received cellulose, which become rougher after acetylation. The morphology of commercial cellulose acetate was found to be smooth and in a powder state.

5.1.2.2 FTIR spectroscopy

The three main ester components used to confirm the success of the acetylation reaction are 1730 cm^{-1} (carbonyl C=O stretching of ester), 1371 cm^{-1} (C-H in –O(C=O)-CH_3 and 1232 cm^{-1} (C-O stretching of acetyl group). These three absorbance bands are much higher in intensity when compared to acetylated NCC. This is due to cellulose being more amorphous and therefore allowing for the acetyl groups to penetrate and substitute the hydroxyl groups more easily. However, these peaks are still lower compared to commercial cellulose acetate.

5.1.2.3 XRD

The form of native cellulose (cellulose-I) was observed for the as-received cellulose and acetylated cellulose with the crystallinity index 65% for the as-received cellulose and 58% for acetylated cellulose. However, the form of cellulose-I was not seen for the commercial cellulose acetate.

5.1.2.4 TGA

The thermal decomposition for the as-received cellulose starts at 300 ºC, the same pattern as seen for acetylated cellulose. Whilst commercial cellulose acetate starts to degrade at 310 ºC. The percentage residue for cellulose after acetylation is lower; 9.84% for the as-received cellulose, 4.07% for acetylated cellulose and 12.30% for commercial cellulose acetate.

5.1.3 Deacetylation of NCC-Ac

Deacetylation was carried out by immersing NCC-Ac in 0.1 N NaOH for 24 hours at room temperature. The properties of deacetylated NCC-Ac are summarised in the following sub-sections.

5.1.3.1 Morphology

The morphology of NCC-Ac after deacetylation changes from flake-like form to powder-like form. The appearance is almost similar to the as-received NCC.

5.1.3.2 FTIR spectroscopy

The main peak that characterises acetylated NCC is 1730 cm^{-1} (carbonyl C=O stretching of ester). This peak disappears after deacetylation.

5.1.3.3 XRD

From the XRD pattern, the crystalline form of native cellulose (cellulose-I) is seen for NCC-Ac before and after deacetylation. However, the crystallinity index of NCC-Ac and deacetylated NCC-Ac decreased from 68% to 62%. The decrease in the crystallinity is due to the treatment with sodium hydroxide during the regeneration of NCC-Ac.

5.1.3.4 TGA

NCC-Ac and deacetylated NCC-Ac started to decompose at 160 ºC with a mass loss of approximately 58%. The final temperature for TGA analysis was 900 ºC where the residue was 26.83% for NCC-Ac and 27.27% for deacetylated NCC-Ac.

5.1.4 Electro-spinning conductivity of cellulose acetate

Commercial cellulose acetate with a molecular weight (M_w) of 30,000 was spun successfully under different conditions at a concentration of 20% (w/v) in acetone and 20% (w/v) in acetone:DMSO (2:1). The first condition was at 15 ºC, whilst the following case was at room temperature. The collector used was also different: a flat aluminium grounded collector was used (for the experiments that were conducted at 15 ºC) and a paper drum collector at room temperature (25 ºC). The morphologies for both spun-fibres are summarised in the following section.

5.1.4.1 Morphology

The morphology of electro-spun fibres using cellulose acetate 20% (w/v) in acetone was found to be random and beaded-fibres produced. This is due the low conductivity of the solution, 3.45 µS/cm at 15 ºC. Using the binary solvent, acetone:DMSO (2:1), the conductivity of cellulose acetate was increased to 8.25 µS/cm at 25 ºC. From the ESEM result, bead-free and smooth fibres were obtained.

5.1.5 Mechano-electro-spinning of NCC with PAN

Electro-spinning of NCC using PAN as the 'carrier polymer' was carried out successfully by dispersing 9%, 17% and 21% of NCC. The presence of NCC in the polymer solution increased the conductivity of the solution. The conductivity of the PAN solution increased from 15.41 µS/cm to 17.73 µS/cm, 19.63 µS/cm and 21.59 µS/cm subsequence with the concentration above. However, the viscosity decreased from 13 Pa.s, to 6.5, 4 and 1 Pa.s.

5.1.5.1 Morphology

The diameter of PAN-NCC spun-fibre decreased from 500 µm to around 200 µm. However, the morphology of fibres containing NCC is rougher than those without NCC. This is due to the poor dispersion and compatibility of NCC with the polymer solution.

5.1.6 Carbonisation of wet-spun fibre

Wet-spun NCC and NCC-Ac using acetone as the coagulating bath was executed successfully. The properties of wet-spun fibres before and after carbonisation are summarised as follow.

5.1.6.1 Morphology

The morphology of wet-spun NCC and NCC-Ac was not circular containing pores. Introducing cellulose acetate to the suspension of NCC and NCC-Ac decreases the porosity of wet-spun fibres and produces circular fibre. Cellulose acetate spun-fibre reinforced with NCC-Ac is smoother than those reinforced with NCC. It was also seen that particles are found on the surface of the wet-spun fibre reinforced NCC. However, the particles are not found on the fibre reinforced with NCC-Ac. It indicates that the acetylation on NCC has improved its dispersion with cellulose acetate.

The carbonisation of wet-spun NCC and NCC-Ac is carried out at 900 ºC with a heating rate of 1 K.minute^{-1}. After carbonisation, the cross-section areas of carbon fibres are found to be compact and void free.

5.1.6.2 Raman spectroscopy

The sp^2 form of NCC and NCC-Ac-derived carbonised fibre were studied using Raman spectroscopy. It shows there are two peaks at 1350 cm^{-1} and 1580 cm^{-1} corresponding to the D band and G band respectively. The I_D/I_G of the carbon fibres is 0.83 - 0.84.

5.2 Future research

The aim of the thesis is to modify NCC through acetylation to improve its dispersibility with polymer matrix. However, many experiments and tests have been left for the future due to lack of time. There are several lines of research, which should be pursued:

i. It is highly recommended to acetylate NCC in a gel-form using either DMSO or acetic acid as the solvent instead of water. This preference is chosen due to NCC being highly dispersed with those substances. Increasing the concentration of acetylating agent is also recommended to produce higher acetyl content. Similarly, the calculation of reducing ends of NCC will be considered in determining the amount of acetylating agent needed to substitute the maximum number of hydroxyl groups of NCC. It is also suggested to consider the sulphur content of NCC and to remove this substance before acetylation.
ii. TEM characterisation of rod-like particle of NCC after acetylation is suggested. It is also recommended to dry NCC-Ac using freeze-drying to see the effect of drying for the acetylation.
iii. From sub-section 4.13, it can be seen that the acetylation of NCC improves its dispersibility with cellulose acetate as the ‘carrier polymer’. It may be possible to increase the concentration of NCC-Ac in the cellulose acetate solution. Further characterisations such as TEM and TGA should be carried out.

iv. In term of carbon fibre, it is recommended to investigate the crystallinity and the mechanical properties of NCC and NCC-Ac based carbonised fibre.

References

1. Fitzer E. Carbon fibre filaments and composites. Figueiredo J., editor. Dordrecht: Kluwer academic; 1990.
2. Edie DD. The effect of processing on the structure and properties of carbon fibers. Carbon N Y. 1998;36(4):345–62.
3. Toray composite materials America, inc. T700S Technical Data Sheet. [internet]. 2018 [cited 2018 March]. Available from: http://www.toraycma.com/page.php?id=661.
4. Matmach. Material properties. [internet]. 2018 [cited 2018 March]. Available from: www.matmach.com.
5. Hoffman WP, Hurley WC, Liu PM, Owens TW. The surface topography of non-shear treated pitch and PAN carbon fibers as viewed by the STM. J Mater Res. 1991;6(8):1685–94.
6. Soutis C. Carbon fiber reinforced plastics in aircraft construction. Mater Sci Eng A. 2005;412(1–2):171–6.
7. Kühnel M, Kraus T. The global CFRP market 2015. Carbon composites e.V. 2016.
8. Holmes M. Global carbon fibre market remains on upward trend. Reinf Plast. 2014;58(6):38–45.
9. Minus ML, Kumar S. The processing, properties, and structure of carbon fibers. J Miner Met Mater Soc. 2005;57:52–8.
10. Osullivan AC. Cellulose: the structure slowly unravels. Cellulose. 1997;4(3):173–207.
11. Deng L, Young RJ, Kinloch IA, Zhu Y, Eichhorn SJ. Carbon nanofibres produced from electrospun cellulose nanofibres. Carbon N Y. 2013;58(0):66–75.
12. Dumanli AG, Windle AH. Carbon fibres from cellulosic precursors: A review. J Mater Sci. 2012;47(10):4236–50.
13. Silvério HA, Neto WPF, Dantas NO, Pasquini D. Extraction and characterization of cellulose nanocrystals from corncob for application as reinforcing agent in nanocomposites. Ind Crop Prod. 2013;44:427–36.

14. Ko FK, Wan Y. Introduction to Nanofibre Technology. United Kingdom: Cambridge University Press; 2014.
15. Peng BL, Dhar N, Liu HL, Tam KC. Chemistry and applications of nanocrystalline cellulose and its derivatives: A nanotechnology perspective. Can J Chem Eng. 2011;89(5):1191–206.
16. Heuser E, Shockley W, Adams A, Grunwald EA. Acetylation of Cellulose in Phosphoric Acid Solution. Ind Eng Chem Res. 1948;40(8):1500–6.
17. Barthel S, Heinze T. Acylation and carbanilation of cellulose in ionic liquids. Green Chem. 2006;8(3):301–5.
18. Regiani AM, Frollini E, Marson GA, Arantes GM, El Seoud OA. Some aspects of acylation of cellulose under homogeneous solution conditions. J Polym Sci Part A Polym Chem. 1999;37(9):1357–63.
19. Heinze T, Liebert TF, Pfeiffer KS, Hussain MA. Unconventional cellulose esters : synthesis, characterization and structure – property relations. Cellulose. 2003;10:283–96.
20. Sassi J-F, Tekely P, Chanzy H. Relative susceptibility of the Iα and Iβ phases of cellulose towards acetylation. Cellulose. 2000;7(2):119–32.
21. Rodionova G, Lenes M, Eriksen O, Gregersen O. Surface chemical modification of microfibrillated cellulose: Improvement of barrier properties for packaging applications. Cellulose. 2011;18(1):127–34.
22. Beck-Candanedo S, Roman M, Gray D. Effect of conditions on the properties behavior of wood cellulose nanocrystals suspensions. Biomacromolecules. 2005;6:1048–54.
23. Huang F, Wu X, Yu Y, Lu Y, Chen Q. Acylation of cellulose nanocrystals with acids/trifluoroacetic anhydride and properties of films from esters of CNCs. Carbohydr Polym. 2017;155:525–34.
24. Uschanov P, Johansson LS, Maunu SL, Laine J. Heterogeneous modification of various celluloses with fatty acids. Cellulose. 2011;18(2):393–404.
25. Çetin NS, Tingaut P, Özmen N, Henry N, Harper D, Dadmun M, et al. Acetylation of cellulose nanowhiskers with vinyl acetate under moderate conditions. Macromol Biosci. 2009;9(10):997–1003.

26. Raminez JAA, Fortunati E, Kenny JM, Torre L, Foresti ML. Simple citric acid-catalyzed surface esterification of cellulose nanocrystals. Carbohydr Polym. 2017;157:1358–64.
27. Fahma F, Takemura A, Saito Y. Acetylation and stepwise solvent-exchange to modify hydrophilic cellulose whiskers to polychloroprene-compatible nanofiller. Cellulose. 2014;21(4):2519–27.
28. Tang L, Huang B, Lu Q, Wang S, Ou W, Lin W, et al. Ultrasonication-assisted manufacture of cellulose nanocrystals esterified with acetic acid. Bioresour Technol. 2013;127:100–5.
29. Lin N, Huang J, Chang PR, Feng J, Yu J. Surface acetylation of cellulose nanocrystal and its reinforcing function in poly (lactic acid). Carbohydr Polym. 2011;83:1834–42.
30. Mikkola J-P, Kirilin A, Tuuf J-C, Pranovich A, Holmbom B, Kustov LM, et al. Ultrasound enhancement of cellulose processing in ionic liquids: from dissolution towards functionalization. Green Chem. 2007;9(11):1229.
31. Eichhorn SJ, Young RJ. The Young's modulus of a microcrystalline cellulose. Cellulose. 2001;8(3):197–207.
32. Timell, T.E and Wimmer, R, editor. Crystalline cellulose and derivates. Heidelberg, Berlin: Springer; 2008. Springer series in wood science. Series editors.
33. Klemm D, Heublein B, Fink HP, Bohn A. Cellulose: Fascinating biopolymer and sustainable raw material. Angew Chemie - Int Ed. 2005;44(22):3358–93.
34. Sun XF, Sun RC, Fowler P, Baird MS. Isolation and characterisation of cellulose obtained by a two-stage treatment with organosolv and cyanamide activated hydrogen peroxide from wheat straw. Carbohydr Polym. 2004;55(4):379–91.
35. Sun, XJ, Sun, XF, Zhao, H, Sun, RC. Isolation and characterization of cellulose from sugarcane bagasse. Polym Degrad Stab. 2004;84(2):331–9.
36. Liu CF, Ren JL, Xu F, Liu JJ, Sun JX, Sun RC. Isolation and characterization of cellulose obtained from ultrasonic irradiated sugarcane bagasse. J Agric Food Chem. 2006;54(16):5742–8.

37. Sun R, Tomkinson J. Separation and characterization of cellulose from wheat straw. Sep Sci Technol. 2004;39(2):391–411.
38. Zuluaga R, Putaux JL, Restrepo A, Mondragon I, Gañán P. Cellulose microfibrils from banana farming residues: Isolation and characterization. Cellulose. 2007;14(6):585–92.
39. Elanthikkal S, Gopalakrishnapanicker U, Varghese S, Guthrie JT. Cellulose microfibres produced from banana plant wastes: Isolation and characterization. Carbohydr Polym. 2010;80(3):852–9.
40. Wang X, Li H, Cao Y, Tang Q. Cellulose extraction from wood chip in an ionic liquid 1-allyl-3-methylimidazolium chloride (AmimCl). Bioresour Technol. 2011;102(17):7959–65.
41. Rosa SML, Rehman N, De Miranda MIG, Nachtigall SMB, Bica CID. Chlorine-free extraction of cellulose from rice husk and whisker isolation. Carbohydr Polym. 2012;87(2):1131–8.
42. Khalil HPSA, Bhat AH, Yusra AFI. Green composites from sustainable cellulose nanofibrils: A review. Carbohydr Polym. 2012;87:963–79.
43. Schenzel K, Fischer S. NIR FT Raman spectroscopy - a rapid analytical tool for detecting the transformation of cellulose polymorphs. Cellulose. 2001;8(1):49–57.
44. Ishikawa A, Okano T, Sugiyama J. Fine structure and tensile properties of ramie fibres in the crystalline form of cellulose I, II, III and IV. Polymer (Guildf). 1997;38(2):463–8.
45. Sugiyama J, Vuong R, Chanzy H. Electron-diffraction study on the 2 crystalline phases occurring in native cellulose from an algal cell-wall. Macromolecules. 1991;24(14):4168–75.
46. Langan P, Nishiyama Y, Chanzy H. X-ray structure of mercerized cellulose II at 1 A resolution X-ray sructure of mercerized cellulose II at 1 Å resolution. Cellulose. 2001;2:410–6.
47. Imai T, Sugiyama J. Nanodomains of I α and I β cellulose in algal microfibrils. Macromolecules. 1998;31(18):6275–9.

48. Chen S, Schueneman G, Pipes RB, Youngblood J, Moon RJ. Effects of crystal orientation on cellulose nanocrystals-cellulose acetate nanocomposite fibers prepared by dry spinning. Biomacromolecules. 2014;15(10):3827–35.
49. Zhuo X, Liu C, Pan R, Dong X, Li Y. Nanocellulose mechanically isolated from amorpha fruticosa Linn. ACS Sustain Chem Eng. 2017;5:4414–20.
50. Dufresne A. Nanocellulose: A new ageless bionanomaterial. Mater Today. 2013;16(6):220–7.
51. Mariano M, El Kissi N, Dufresne A. Cellulose nanocrystals and related nanocomposites: Review of some properties and challenges. J Polym Sci Part B Polym Phys. 2014;52(12):791–806.
52. Kargarzadeh H, Ahmad I, Abdullah I, Dufresne A, Zainudin SY, Sheltami RM. Effects of hydrolysis conditions on the morphology, crystallinity, and thermal stability of cellulose nanocrystals extracted from kenaf bast fibers. Cellulose. 2012;19(3):855–66.
53. De Souza Lima MM, Borsali R. Rodlike cellulose microcrystals: Structure, properties, and applications. Macromol Rapid Commun. 2004;25(7):771–87.
54. Araki J, Wada M, Kuga S, Okano T. Flow properties of microcrystalline cellulose suspension prepared by acid treatment of native cellulose. Colloids Surfaces A Physicochem Eng Asp. 1998;142(1):75–82.
55. Dong XM, Kimura T, Gray DG. Effects of ionic strength on the isotropic - chiral nematic phase transition of suspensions of cellulose crystallites. Langmuir. 1996;12(8):2076–82.
56. Pires W, Neto F, Alves H, Oliveira N, Pasquini D. Extraction and characterization of cellulose nanocrystals from agro-industrial residue – Soy hulls. Ind Crop Prod. 2013;42:480–8.
57. Fleming K, Gray DG, Matthews S. Cellulose crystallites. Chem - A Eur J. 2001;7(9):1831–5.
58. Corrêa AC, Teixeira EM, Pessan LA, Mattoso LHC. Cellulose nanofibers from curaua fibers. Cellulose. 2010;17(6):1183–92.
59. Espinosa SC, Kuhnt T, Foster EJ, Weder C. Isolation of thermally stable cellulose nanocrystals by phosphoric acid hydrolysis. Biomacromolecules. 2013;14:1223–30.

60. Gu J, Hu C, Zhong R, Tu D, Yun H, Zhang W, et al. Isolation of cellulose nanocrystals from medium density fiberboards. Carbohydr Polym. 2017;167:70–8.
61. Ahmadi M, Madadlou A, Sabouri AA. Isolation of micro- and nano-crystalline cellulose particles and fabrication of crystalline particles-loaded whey protein cold-set gel. Food Chem. 2015;174:97–103.
62. Kallel F, Bettaieb F, Khiari R, García A, Bras J, Chaabouni SE. Isolation and structural characterization of cellulose nanocrystals extracted from garlic straw residues. Ind Crops Prod. 2016;87:287–96.
63. Sofla MRK, Brown RJ, Tsuzuki T, Rainey TJ. A comparison of cellulose nanocrystals and cellulose nanofibres extracted from bagasse using acid and ball milling methods. Adv Nat Sci Nanosci Nanotechnol. 2016;7(3):35004.
64. Lamaming J, Hashim R, Leh CP, Sulaiman O. Properties of cellulose nanocrystals from oil palm trunk isolated by total chlorine free method. Carbohydr Polym. 2017;156:409–16.
65. Jiang F, Hsieh Y Lo. Cellulose nanocrystal isolation from tomato peels and assembled nanofibers. Carbohydr Polym. 2015;122:60–8.
66. Alves H, Pires W, Neto F, Oliveira N, Pasquini D. Extraction and characterization of cellulose nanocrystals from corncob for application as reinforcing agentin nanocomposites. Ind Crops Prod. 2013;44:427–36.
67. Siqueira G, Abdillahi H, Bras J, Dufresne A. High reinforcing capability cellulose nanocrystals extracted from Syngonanthus nitens (Capim Dourado). Cellulose. 2010;17(2):289–98.
68. Morais JPS, Rosa MDF, De Souza Filho MDSM, Nascimento LD, Do Nascimento DM, Cassales AR. Extraction and characterization of nanocellulose structures from raw cotton linter. Carbohydr Polym. 2013;91:229–35.
69. Cherian BM, Leão AL, Souza SF, Thomas S, Pothan LA, Kottaisamy M. Isolation of nanocellulose from pineapple leaf fibres by steam explosion. Carbohydr Polym. 2010;81(3):720–5.
70. Habibi Y, Lucia LA, Rojas OJ. Cellulose nanocrystals : chemistry , self-assembly , and applications. ChemRev. 2010;110:3479–500.

71. Lu P, Hsieh Y-L. Preparation and characterization of cellulose nanocrystals from rice straw. Carbohydr Polym. 2012;87(1):564–73.
72. Klemm D, Kramer F, Moritz S, Lindstrom T, Ankerfors M, Gray D, et al. Nanocelluloses: A new family of nature-based materials. Angew Chemie - Int Ed. 2011;50(24):5438–66.
73. Tang J, Sisler J, Grishkewich N, Tam KC. Functionalization of cellulose nanocrystals for advanced applications. J Colloid Interface Sci. 2017;494:397–409.
74. Jorfi M, Foster EJ. Recent advances in nanocellulose for biomedical applications. J Appl Polym Sci. 2015;132(14):1–19.
75. Hoeng F, Denneulin A, Bras J. Use of nanocellulose in printed electronics: A review. Nanoscale. 2016;8:13131–54.
76. Capadona JR, Shanmuganathan K, Trittschuh S, Seidel S, Rowan SJ, Weder C. Polymer nanocomposites with nanowhiskers isolated from microcrystalline cellulose. Biomacromolecules. 2009;10(4):712–6.
77. Kalia S, Boufi S, Celli A, Kango S. Nanofibrillated cellulose: Surface modification and potential applications. Colloid Polym Sci. 2014;292:5–31.
78. Wanasekara ND, Santos RPO, Douch C, Frollini E, Eichhorn SJ. Orientation of cellulose nanocrystals in electrospun polymer fibres. J Mater Sci. 2016;51(1):218–27.
79. Rojas OJ, Montero GA, Habibi Y. Electrospun nanocomposites from polystyrene loaded with cellulose nanowhiskers. J Appl Polym Sci. 2009;113:927–35.
80. Sheng L, Jiang R, Zhu Y, Ji Y. Electrospun cellulose nanocrystals/polycaprolactone nanocomposite fiber mats. J Macromol Sci Part B. 2013;53(5):820–8.
81. Dong H, Strawhecker KE, Snyder JF, Orlicki JA, Reiner RS, Rudie AW. Cellulose nanocrystals as a reinforcing material for electrospun poly(methyl methacrylate) fibers: Formation, properties and nanomechanical characterization. Carbohydr Polym. 2012;87(4):2488–95.

82. Ago M, Okajima K, Jakes JE, Park S, Rojas OJ. Lignin-based electrospun nanofibers reinforced with cellulose nanocrystals. Biomacromolecules. 2012;13(3):918–26.
83. Peresin MS, Habibi Y, Zoppe JO, Pawlak JJ, Rojas OJ. Nanofiber composites of polyvinyl alcohol and cellulose nanocrystals: Manufacture and characterization. Biomacromolecules. 2010;11(3):674–81.
84. Enayati MS, Behzad T, Sajkiewicz P, Bagheri R, Ghasemi-Mobarakeh L, Lojkowski W, et al. Crystallinity study of electrospun poly (vinyl alcohol) nanofibers: effect of electrospinning, filler incorporation, and heat treatment. Iran Polym J English Ed. 2016;25(7):647–59.
85. Herrera NV, Mathew AP, Wang LY, Oksman K. Randomly oriented and aligned cellulose fibres reinforced with cellulose nanowhiskers, prepared by electrospinning. Plast Rubber Compos. 2011;40(2):57–64.
86. Huang J, Liu L, Yao J. Electrospinning of Bombyx mori silk fibroin nanofiber mats reinforced by cellulose nanowhiskers. Fibers Polym. 2011;12(8):1002–6.
87. Kampeerapappun P. The electrospun polyhydroxybutyrate fibers reinforced with cellulose nanocrystals: Morphology and properties. J Appl Polym Sci. 2016;133(20):1–7.
88. Naseri N, Mathew AP, Girandon L, Frohlich M, Oksman K. Porous electrospun nanocomposite mats based on chitosan-cellulose nanocrystals for wound dressing: effect of surface characteristics of nanocrystals. Cellulose. 2015;22(1):521–34.
89. Shi Q, Zhou C, Yue Y, Guo W, Wu Y, Wu Q. Mechanical properties and in vitro degradation of electrospun bio-nanocomposite mats from PLA and cellulose nanocrystals. Carbohydr Polym. 2012;90(1):301–8.
90. Lee J, Deng Y. Increased mechanical properties of aligned and isotropic electrospun PVA nanofiber webs by cellulose nanowhisker reinforcement. Macromol Res. 2012;20(1):76–83.
91. Li Y, Ko FK, Hamad WY. Effects of emulsion droplet size on the structure of electrospun ultrafine biocomposite fibers with cellulose nanocrystals. Biomacromolecules. 2013;14:3801–7.

92. Lu P, Hsieh Y-L. Cellulose nanocrystal-filled poly(acrylic acid) nanocomposite fibrous membranes. Nanotechnology. 2009;20(41):415604.
93. Vallejos ME, Peresin MS, Rojas OJ. All-cellulose composite fibers obtained by electrospinning dispersions of cellulose acetate and cellulose nanocrystals. J Polym Environ. 2012;20(4):1075–83.
94. Klemm D, Philipp B, Heinze T, Heinze U, Wagenknecht W. Comprehensive cellulose chemistry fundamental and analytical methods, Germany: Wiley-VCH Verlag GmbH; 1998, Volume 1.
95. Edgar KJ, Buchanan CM, Debenham JS, Rundquist PA, Seiler BD, Shelton MC, et al. Advances in cellulose ester performance and application. Prog Polym Sci. 2001;26(9):1605–88.
96. Jonoobi M, Harun J, Mathew AP, Hussein MZB, Oksman K. Preparation of cellulose nanofibers with hydrophobic surface characteristics. Cellulose. 2010;17:299–307.
97. Burk RE, Grummit O. The chemistry of large molecules. New York: Interscience publisher, inc.; 1943, Volume 1.
98. Sun XF, Sun R, Sun JX. Acetylation of rice straw with or without catalysts and its characterization as a natural sorbent in oil spill cleanup. J Agric Food Chem. 2002;50(22):6428–33.
99. Tosh B, Saikia CN, Dass NN. Homogeneous esterification of cellulose in the lithium chloride-N,N-dimethylacetamide solvent system: Effect of temperature and catalyst. Carbohydr Res. 2000;327(3):345–52.
100. Agustin MB, Nakatsubo F, Yano H. The thermal stability of nanocellulose and its acetates with different degree of polymerization. Cellulose. 2016;23(1):451–64.
101. Ifuku S, Nogi M, Abe K, Handa K, Nakatsubo F. Surface modification of bacterial cellulose nanofibers for property enhancement of optically transparent composites: dependence on acetyl-group DS. Biomacromolecules. 2007;8:1973–8.
102. Marsh J, Wood F. An introduction to the chemistry of cellulose. Great Britain: London and Norwich Press; 1942.

103. Huang ZM, Zhang YZ, Kotaki M, Ramakrishna S. A review on polymer nanofibers by electrospinning and their applications in nanocomposites. Compos Sci Technol. 2003;63(15):2223–53.
104. Formhals A. Process and apparatus for preparing artificial threads. 1934;US Patent.
105. Kalayci VE, Patra PK, Kim YK, Ugbolue SC, Warner SB. Charge consequences in electrospun polyacrylonitrile (PAN) nanofibers. Polymer (Guildf). 2005;46(18):7191–200.
106. Jayesh D, Reneker DH. Electrospinning process and application of electrospun fibres. J Electrostat. 1995;35:151–60.
107. Rutledge GC, Fridrikh S V. Formation of fibers by electrospinning. Adv Drug Deliv Rev. 2007;59(14):1384–91.
108. Zhang B, Kang F, Tarascon JM, Kim JK. Recent advances in electrospun carbon nanofibers and their application in electrochemical energy storage. Prog Mater Sci. 2015;76:319–80.
109. Subbiah T, Bhat GS, Tock RW, Parameswaran S, Ramkumar SS. Electrospinning of nanofibers. J Appl Polym Sci. 2005;96(2):557–69.
110. Baji A, Mai YW, Wong SC, Abtahi M, Chen P. Electrospinning of polymer nanofibers: Effects on oriented morphology, structures and tensile properties. Compos Sci Technol. 2010;70(5):703–18.
111. Maitra T, Sharma S, Srivastava A, Cho YK, Madou M, Sharma A. Improved graphitization and electrical conductivity of suspended carbon nanofibers derived from carbon nanotube/polyacrylonitrile composites by directed electrospinning. Carbon N Y. 2012;50(5):1753–61.
112. Liao Y, Li X-G, Hoek EMV, Kaner RB. Carbon nanotube/polyaniline nanofiber ultrafiltration membranes. J Mater Chem A. 2013;1(48):15390.
113. Agarwal S, Wendorff JH, Greiner A. Use of electrospinning technique for biomedical applications. Polymer (Guildf). 2008;49(26):5603–21.
114. Liu HQ, Tang CY. Electrospinning of cellulose acetate in solvent mixture N,N-dimethylacetamide (DMAc)/acetone. Polym J. 2007;39(1):65–72.

115. Deitzel J., Kleinmeyer J, Harris D, Beck Tan N. The effect of processing variables on the morphology of electrospun nanofibers and textiles. Polymer (Guildf). 2001;42(1):261–72.
116. Koski A, Yim K, Shivkumar S. Effect of molecular weight on fibrous PVA produced by electrospinning. Mater Lett. 2004;58(3):493–7.
117. Guerrini LM, Branciforti MC, Canova T, Bretas RES. Electrospinning and characterization of polyamide 66 nanofibers with different molecular weights. Mater Res. 2009;12(2):181–90.
118. Pant HR, Nam KT, Oh HJ, Panthi G, Kim HD, Kim B Il, et al. Effect of polymer molecular weight on the fiber morphology of electrospun mats. J Colloid Interface Sci. 2011;364(1):107–11.
119. Fong H, Chun I, Reneker DH. Beaded nanofibers formed during electrospinning. Polymer. 1999; 40(16): 4585–92.
120. Yang Q, Zhenyu LI, Hong Y, Zhao Y, Qiu S, Wang CE, et al. Influence of solvents on the formation of ultrathin uniform poly(vinyl pyrrolidone) nanofibers with electrospinning. J Polym Sci Part B Polym Phys. 2004;42(20):3721–6.
121. Uyar T, Besenbacher F. Electrospinning of uniform polystyrene fibers : The effect of solvent conductivity. Polymer (Guildf). 2008;49(24):5336–43.
122. Mit-uppatham C, Nithitanakul M, Supaphol P. Ultrafine electrospun polyamide-6 fibers: Effect of solution conditions on morphology and average fiber diameter. Macromol Chem Phys. 2004;205(17):2327–38.
123. Megelski S, Stephens JS, Bruce Chase D, Rabolt JF. Micro- and nanostructured surface morphology on electrospun polymer fibers. Macromolecules. 2002;35(22):8456–66.
124. Liu H, Hsieh YL. Ultrafine fibrous cellulose membranes from electrospinning of cellulose acetate. J Polym Sci Part B Polym Phys. 2002;40(18):2119–29.
125. Yördem OS, Papila M, Menceloğlu YZ. Effects of electrospinning parameters on polyacrylonitrile nanofiber diameter: An investigation by response surface methodology. Mater Des. 2008;29(1):34–44.
126. Zhang C, Yuan X, Wu L, Han Y, Sheng J. Study on morphology of electrospun poly(vinyl alcohol) mats. Eur Polym J. 2005;41(3):423–32.

127. Beachley V, Wen X. Effect of electrospinning parameters on the nanofiber diameter and length. Mater Sci Eng C. 2009;29(3):663–8.
128. Tungprapa S, Puangparn T, Weerasombut M, Jangchud I, Fakum P, Semongkhol S, et al. Electrospun cellulose acetate fibers: Effect of solvent system on morphology and fiber diameter. Cellulose. 2007;14(6):563–75.
129. Zargham S, Bazgir S, Tavakoli A, Rashidi AS, Damerchely R. The effect of flow rate on morphology and deposition area of electrospun nylon 6 nanofiber. J Eng Fiber Fabr. 2012;7(4):42–9.
130. Sill TJ, von Recum HA. Electrospinning: Applications in drug delivery and tissue engineering. Biomaterials. 2008;29(13):1989–2006.
131. Yuan XY, Zhang YY, Dong C, Sheng J. Morphology of ultrafine polysulfone fibers prepared by electrospinning. Polym Int. 2004;53(11):1704–10.
132. Zhang S, Shim WS, Kim J. Design of ultra-fine nonwovens via electrospinning of Nylon 6: Spinning parameters and filtration efficiency. Mater Des. 2009;30(9):3659–66.
133. De VS, Van CT, Nelvig A, Hagström B, Westbroek P, De CK. The effect of temperature and humidity on electrospinning. J Mater Sci. 2009;44(5):1357–62.
134. Pelipenko J, Kristl J, Janković B, Baumgartner S, Kocbek P. The impact of relative humidity during electrospinning on the morphology and mechanical properties of nanofibers. Int J Pharm. 2013;456(1):125–34.
135. Tripatanasuwan S, Zhong Z, Reneker DH. Effect of evaporation and solidification of the charged jet in electrospinning of poly(ethylene oxide) aqueous solution. Polymer (Guildf). 2007;48(19):5742–6.
136. Kim GT, Lee JS, Shin JH, Ahn YC, Hwang YJ, Shin HS, et al. Investigation of pore formation for polystyrene electrospun fiber: Effect of relative humidity. Korean J Chem Eng. 2005;22(5):783–8.
137. McClure MJ, Wolfe PS, Simpson DG, Sell SA, Bowlin GL. The use of air-flow impedance to control fiber deposition patterns during electrospinning. Biomaterials. 2012;33(3):771–9.
138. Wang X, Lin T, Wang X. Use of airflow to improve the nanofibrous structure and quality of nanofibers from needleless electrospinning. J Ind Text. 2015;45(2):310–20.

139. Torres-Rendon JG, Schacher FH, Ifuku S, Walther A. Mechanical performance of macrofibers of cellulose and chitin nanofibrils aligned by wet-stretching: A critical comparison. Biomacromolecules. 2014;15(7):2709–17.
140. Lundahl MJ, Cunha AG, Rojo E, Papageorgiou AC, Rautkari L, Arboleda JC, et al. Strength and water interactions of cellulose I filaments wet-spun from cellulose nanofibril hydrogels. Sci Rep. 2016;6(February):30695.
141. Iwamoto S, Isogai A, Iwata T. Structure and mechanical properties of wet-spun fibers made from natural cellulose nanofibers. Biomacromolecules. 2011;12(3):831–6.
142. Phillips DM, Drummy LF, Naik RR, Long HCD, Fox DM, Trulove PC, et al. Regenerated silk fiber wet spinning from an ionic liquid solution. J Mater Chem. 2005;15(39):4206.
143. Håkansson KMO. Online determination of anisotropy during cellulose nanofibril assembly in a flow focusing device. RSC Adv. 2015;5(24):18601–8.
144. Lundahl MJ, Klar V, Wang L, Ago M, Rojas OJ. Spinning of cellulose nanofibrils into filaments: A review. Ind Eng Chem Res. 2017;56(1):8–19.
145. Yan J, Zhou G, Knight DP, Shao Z, Chen X. Wet-spinning of regenerated silk fiber from aqueous silk fibroin solution: Discussion of spinning parameters. Biomacromolecules. 2010;11(1):1–5.
146. Um IC, Kweon HY, Lee KG, Ihm DW, Lee JH, Park YH. Wet spinning of silk polymer: I. Effect of coagulation conditions on the morphological feature of filament. Int J Biol Macromol. 2004;34(1–2):89–105.
147. Frank E, Hermanutz F, Buchmeiser MR. Carbon fibers: Precursors, manufacturing, and properties. Macromol Mater Eng. 2012;297(6):493–501.
148. Chung DDL. Carbon fibres, nanofibres, and nanotubes [Internet]. Elsevier; 2017. p. 1-87. Available from: http://dx.doi.org/10.1016/B978-0-12-804459-9/00001-4
149. Peng S, Shao H, Hu X. The effect of precursor properties on the strength of carbon fiber. Int J Polym Mater Polym Biomater. 2004;53(7):601–8.
150. Newcomb BA. Processing, structure, and properties of carbon fibers. Compos Part A [Internet]. 2016;91:262–82. Available from: http://dx.doi.org/10.1016/j.compositesa.2016.10.018

151. Mora E, Blanco C, Prada V, Santamaría R, Granda M, Menéndez R. A study of pitch-based precursors for general purpose carbon fibres. Carbon N Y. 2002;40(14):2719–25.
152. Sevilla M, Fuertes AB. Graphitic carbon nanostructures from cellulose. Chem Phys Lett. 2010;490(1–3):63–8.
153. Tang M., Bacon R. Carbonization of cellulose fibers—I. Low temperature pyrolysis. Carbon N Y. 1964;2(3):211–20.
154. Ishida O, Kim DY, Kuga S, Nishiyama Y, Brown RM. Microfibrillar carbon from native cellulose. Cellulose. 2004;11(3):475–480.
155. Kim DY, Nishiyama Y, Wada M, Kuga S. Graphitization of highly crystalline cellulose. Carbon N Y. 2001;39(7):1051–6.
156. Titirici MM, White RJ, Brun N, Budarin VL, Su DS, Del MF, et al. Sustainable carbon materials. Chem Soc Rev. 2015;44:250–90.
157. Rahaman MSA, Ismail AF, Mustafa A. A review of heat treatment on polyacrylonitrile fiber. Polym Degrad Stab. 2007;92(8):1421–32.
158. Goodhew PJ, Clarke AJ, Bailey JE. A review of the fabrication and properties of carbon fibres. Mater Sci Eng. 1975;17(1):3–30.
159. Mayes HB, Broadbelt LJ. Unraveling the reactions that unravel cellulose. J Phys Chem A. 2012;116(26):7098–106.
160. Frank E, Steudle LM, Ingildeev D, Spoorl JM, Buchmeiser MR. Carbon fibers: Precursor systems, processing, structure, and properties. Angew Chemie - Int Ed. 2014;53(21):5262–98.
161. Ma X, Yuan C, Liu X. Mechanical, microstructure and surface characterizations of carbon fibers prepared from cellulose after liquefying and curing. Materials (Basel). 2014;7(1):75–84.
162. Peng S, Shao H, Hu X. Lyocell fibers as the precursor of carbon fibers. J Appl Polym Sci. 2003;90(7):1941–7.
163. Wu QL, Gu SY, Gong JH, Pan D. SEM/STM studies on the surface structure of a novel carbon fiber from lyocell. Synth Met. 2006;156(11–13):792–5.
164. Zhang H, Guo L, Shao H, Hu X. Nano-carbon black filled lyocell fiber as a precursor for carbon fiber. J Appl Polym Sci. 2006;99(1):65–74.

165. Zhou X, Wang P, Zhang Y, Zhang X, Jiang Y. From Waste Cotton Linter: A renewable environment-friendly biomass based carbon fibers preparation. ACS Sustain Chem Eng. 2016;4(10):5585–93.
166. Segal L, Creely JJ, Martin AE, Conrad CM. An empirical method for estimating the degree of crystallinity of native cellulose using the X-ray diffreactometer. Text Res J. 1959;29:786–94.
167. Celluforce. Product specification. [internet]. 2016 [cited 2016 September 9]. Available from: http://www.celluforce.com.
168. Moharram MA, Mahmoud OM. FTIR spectrocopic study of the effect of microwave heating on the transformation of cellulose I into cellulose II during mercerization. J Appl Polym Sci. 2008;107:30–6.
169. Ashori A, Babaee M, Jonoobi M, Hamzeh Y. Solvent-free acetylation of cellulose nanofibers for improving compatibility and dispersion. Carbohydr Polym. 2014;102(1):369–75.
170. Zepic V. Effect of drying pretreatment on the acetylation of nanofibrillated cellulose. Bioresources. 2015;10(4):8148–67.
171. Moran JI, Alvarez VA, Cyras VP, Vazquez A. Extraction of cellulose and preparation of nanocellulose from sisal fibers. Cellulose. 2008;15:149–59.
172. Karande VS, Bharjmajja AK, Hadge G.B, Mhaske ST. Nanofibrillation of cotton fibres by disc refiner and its characterization. Fibers Polym. 2011;12(3):399–404.
173. Oh SY, Yoo DI, Shin Y, Seo G. FTIR analysis of cellulose treated with sodium hydroxide and carbon dioxide. Carbohydr Res. 2005;340(3):417–28.
174. Barud HS, Araújo JAM, Santos DB, Assunção RMN, Meireles CS, Cerqueira DA, et al. Thermal behavior of cellulose acetate produced from homogeneous acetylation of bacterial cellulose. Thermochim Acta. 2008;471(1–2):61–9.
175. Tomé LC, Freire MG, Rebelo LPN, Silvestre AJD, Neto CP, Marrucho IM, et al. Surface hydrophobization of bacterial and vegetable cellulose fibers using ionic liquids as solvent media and catalysts. Green Chem. 2011;13(9):2464.
176. Shaikh HM, Pandare KV, Nair G, Varma AJ. Utilization of sugarcane bagasse cellulose for producing cellulose acetates: Novel use of residual hemicellulose as plasticizer. Carbohydr Polym. 2009;76(1):23–9.

177. Frisoni G, Baiardo M, Scandola M, Lednická D, Cnockaert MC, Mergaert J, et al. Natural cellulose fibers: Heterogeneous acetylation kinetics and biodegradation behavior. Biomacromolecules. 2001;2(2):476–82.
178. Eyley S, Thielemans W. Surface modification of cellulose nanocrystals. R Soc Chem. 2014;6:7764–79.
179. Berlioz S, Molina-boisseau S, Nishiyama Y, Heux L. Gas-phase surface esterification of cellulose microfibrils and whiskers. Biomacromolecules. 2009;10:2144–51.
180. Liu D, Zhong T, Chang PR, Li K, Wu Q. Starch composites reinforced by bamboo cellulosic crystals. Bioresour Technol. 2010;101(7):2529–36.
181. Jonoobi M, Mathew AP, Abdi MM. A comparison of modified and unmodified cellulose nanofiber reinforced polylactic acid (PLA) prepared by twin screw extrusion. J Polym Environ. 2012;20:991–7.
182. Wei L, Agarwal UP, Hirth KC, Matuana LM, Sabo RC, Stark NM. Chemical modification of nanocellulose with canola oil fatty acid methyl ester. Carbohydr Polym. 2017;169:108–16.
183. Tomé LC, Brandão L, Mendes AM, Silvestre AJD, Neto CP, Gandini A, et al. Preparation and characterization of bacterial cellulose membranes with tailored surface and barrier properties. Cellulose. 2010;17(6):1203–11.
184. Yang Z, Xu S, Ma X, Wang S. Characterization and acetylation behavior of bamboo pulp. Wood Sci Technol. 2008;42(8):621–32.
185. Ávila RJA, Gómez HC, Arroyo S, Cerrutti P, Foresti ML. Acetylation of bacterial cellulose catalyzed by citric acid: Use of reaction conditions for tailoring the esterification extent. Carbohydr Polym. 2016;153:686–95.
186. Yin C, Li J, Xu Q, Peng Q, Liu Y, Shen X. Chemical modification of cotton cellulose in supercritical carbon dioxide: Synthesis and characterization of cellulose carbamate. Carbohydr Polym. 2007;67(2):147–54.
187. Agustin MB, Nakatsubo F, Yano H. The thermal stability of nanocellulose and its acetates with different degree of polymerization. Cellulose. 2016;23(1):451–64.

188. Taib MNAM, Yehye WA, Julkapli NM, Hamid SBOAA. Influence of hydrophobicity of acetylated nanocellulose on the mechanical performance of nitrile butadiene rubber (NBR) composites. Fibers Polym [Internet]. 2018;19(2):383–92. Available from: http://link.springer.com/10.1007/s12221-018-7591-z
189. Dong F, Yan M, Jin C, Li S. Characterization of type-II acetylated cellulose nanocrystals with various degree of substitution and its compatibility in PLA films. Polymers (Basel). 2017;9(8):1–14.
190. Kang KS, Cho KY, Lim HK, Kim J. Investigation of surface morphology of cellulose acetate micro-mould after deacetylation. J Phys D Appl Phys. 2008;41(19).
191. Son W, Youk J, Lee TS, Park W. Electrospinning of ultrafine cellulose acetate fibers: Studies of a new solvent system and deacetylation of ultrafine cellulose acetate fibres. Polym Sceiences. 2003;5–11.
192. Ahmed F, Arbab AA, Jatoi AW, Khatri M, Memon N, Khati Z, Kim IS. Ultrasonic-assited deacetylation of cellulose acetate nanofibres: A rapid method to produce cellulose nanofibres. Ultrasonic Chemistry. 2017; 36: 319-325.
193. Hansen CM. Hansen Solubility Parameters A User's Handbook. Second Edi. Boca Raton: CRC Taylor & Francis Group; 2007.
194. Seo JM, Arumugam GK, Khan S, Heiden PA. Comparison of the effects of an ionic liquid and triethylbenzylammonium chloride on the properties of electrospin fibers, 1-poly(lactic acid). Macromol Mater Eng. 2009;(294):35–44.
195. Qin XH, Yang EL, Li N, Wang SY. Effects of different salts on electrospinning of polyacrylonitrile (PAN) polymer solution. J Polym Sci. 2007;103:3865–70.
196. Heikkilä P, Harlin A. Electrospinning of polyacrylonitrile (PAN) solution: Effect of conductive additive and filler on the process. Express Polym Lett. 2009;3(7):437–45.
197. Farsani RE, Raissi S, Shokuhfar A, Sedghi A. FTIR study of stabilized PAN fibers for fabrication of carbon fibers. World Acad Sci Eng Technol. 2009;3(2):430–3.

198. Escribano R, Sloan JJ, Siddique N, Sze N, Dudev T. Raman spectroscopy of carbon-containing particles. Vib Spectrosc. 2001;26(2):179–86.
199. Melanitis N, Tetlow PL, Galiotis C. Characterization of PAN-based carbon fibres with laser Raman spectroscopy. J Mater Sci. 1996;31(4):851–60.
200. Tuinstra F, Koenig JL. Raman spectrum of graphite. J Chem Phys [Internet]. 1970;53(3):1126–30. Available from: http://aip.scitation.org/doi/10.1063/1.1674108
201. Mottershead B, Eichhorn SJ. Deformation micromechanics of model regenerated cellulose fibre-epoxy/polyester composites. Compos Sci Technol. 2007;67(10):2150–9.
202. Ioelovich M. Optimal conditions for isolation of nanocrystalline cellulose particles. Nanosci Nanotechnol [Internet]. 2012;2(2):9–13. Available from: http://article.sapub.org/10.5923.j.nn.20120202.03.html
203. Abraham E, Deepa B, Pothan LA, Jacob M, Thomas S, Cvelbar U, et al. Extraction of nanocellulose fibrils from lignocellulosic fibres: A novel approach. Carbohydr Polym. 2011;86(4):1468–75.

Appendices

Appendix 1 Properties of cellulose and nano-crystalline cellulose.

The comparison of cellulose and nano-crystalline cellulose is described in Table A.

Table A Properties of cellulose and nano-crystalline cellulose [15].

Cellulose	**Nano-crystalline cellulose**
Semi-crystalline	Crystalline regions
Isotropic phase	Anisotropic phase
	Dispersed readily in water due to abundant charge sulphate ester on the surface of NCC obtained during acid hydrolysis
	Nano-scale dimension
Strength (2.6 GPa) [201]	High specific strength (7.5 GPa) [202]
Modulus (25 $\pm$ 4 GPa) [31]	High modulus 138 GPa [203]

Appendix 2 Acetylation of nano-crystalline cellulose.

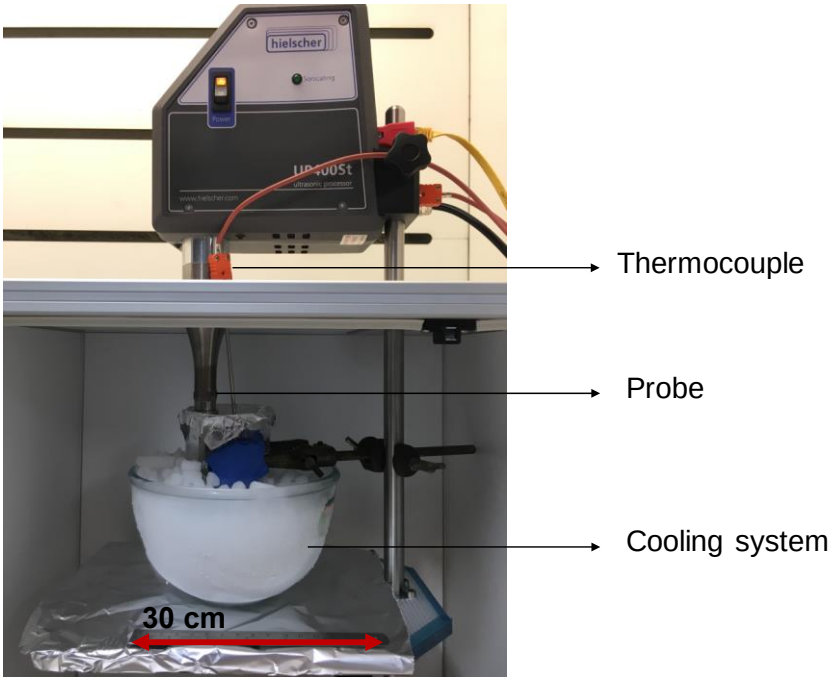

Figure A Ultrasonic set up.

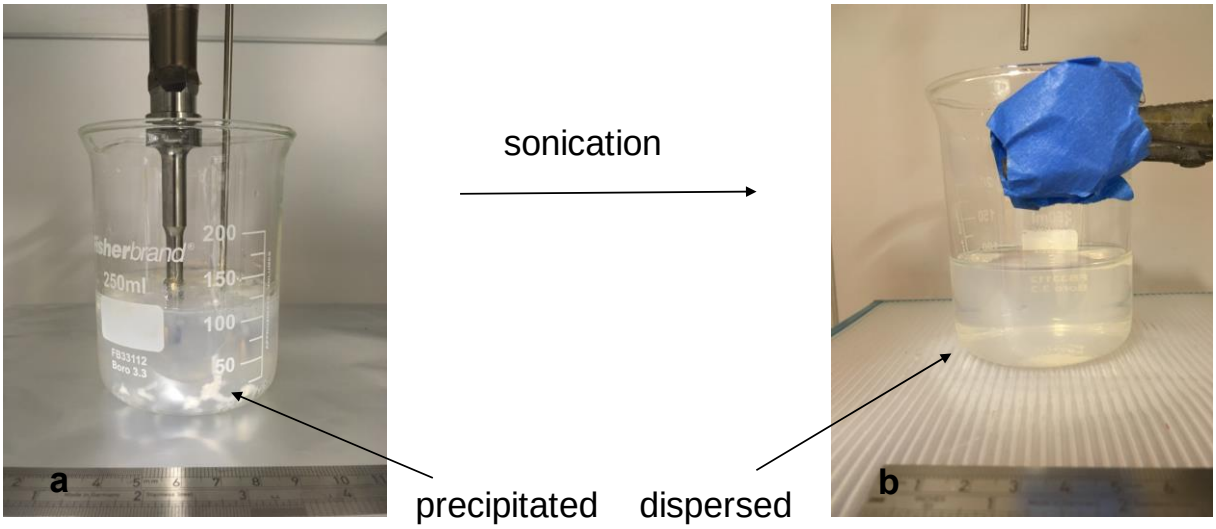

Figure B Illustration of dispersing NCC in DI water (a) before and (b) after sonication.

Figure C Acetylation of NCC under constant reflux in a nitrogen atmosphere.


Figure D Rotarievaporator set up.

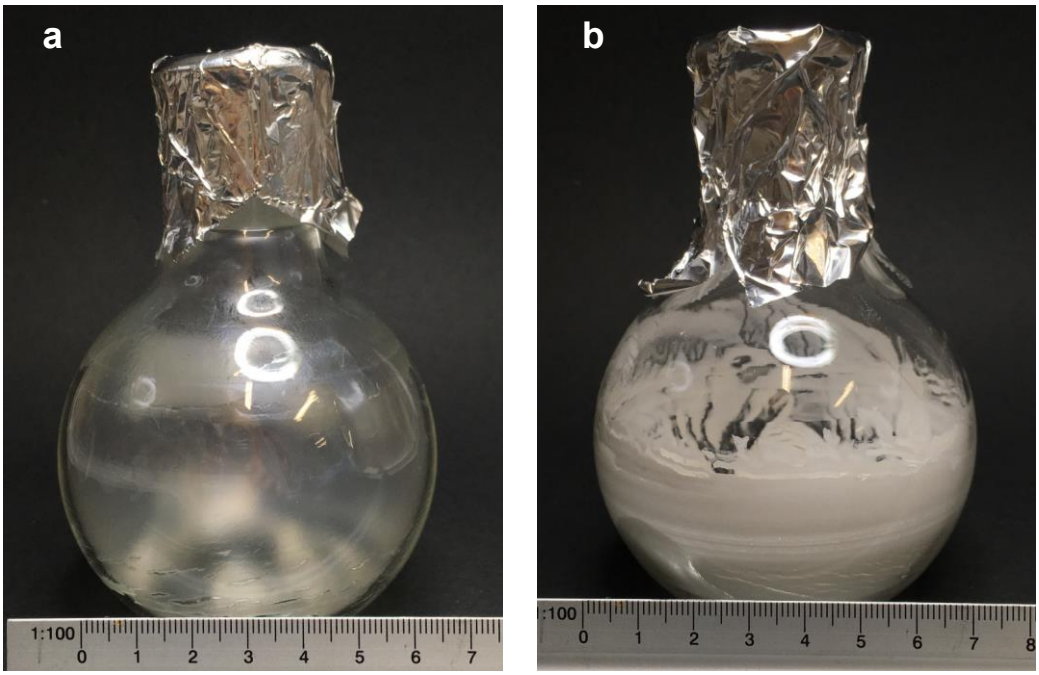

Figure E (a) NCC-Ac after drying, (b) acetylated cellulose after drying.

Appendix 4 TEM micrographs of as-received NCC.

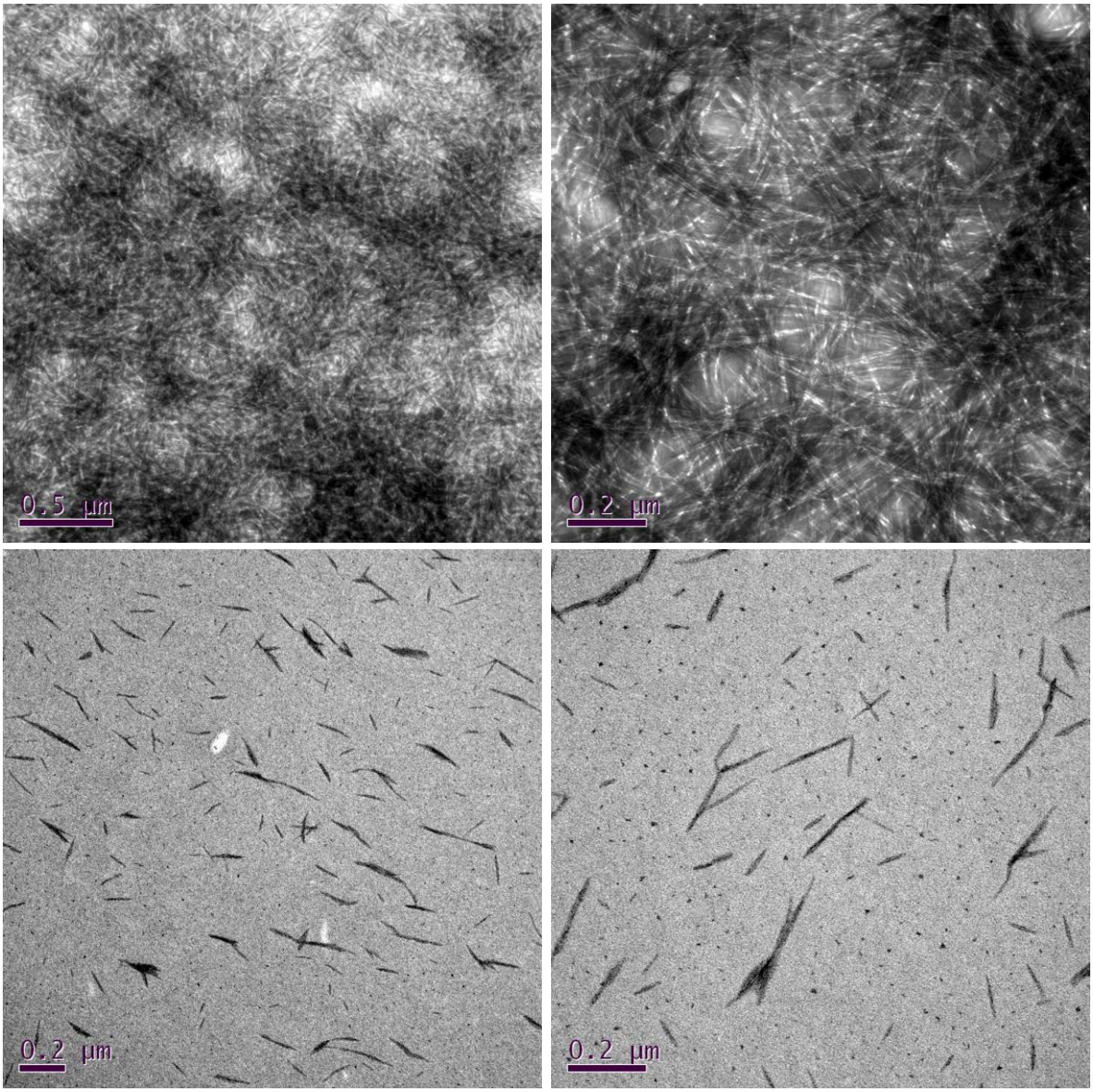

Figure A (a-d) TEM micrograph of as-received NCC.

Appendix 5 TEM micrographs of cryomilled NCC.

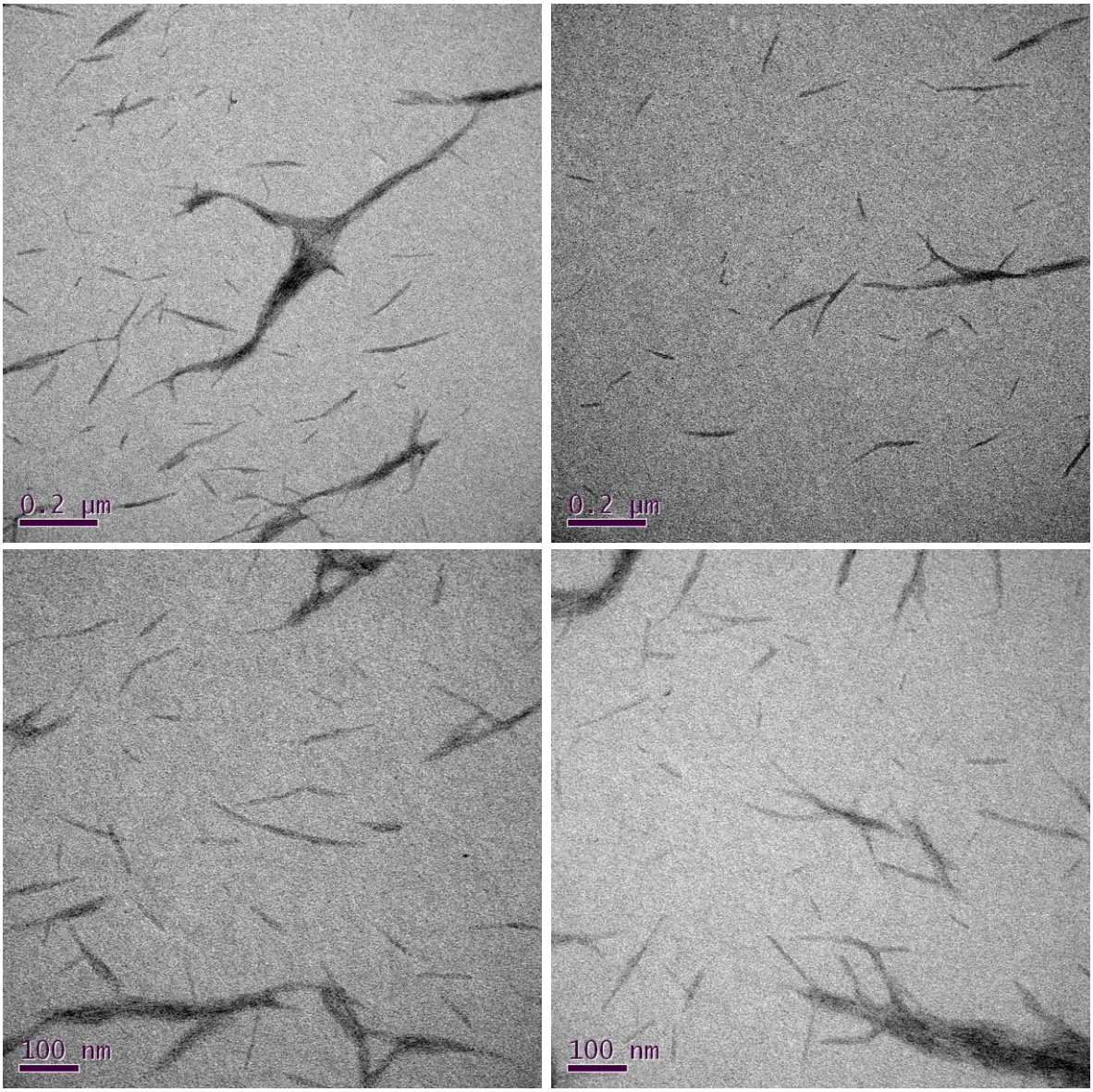

Figure A (a-d) TEM micrograph of cryomilled NCC.

Appendix 6 NMR spectrum of acetylated nano-crystalline cellulose dispersed and gel-form.

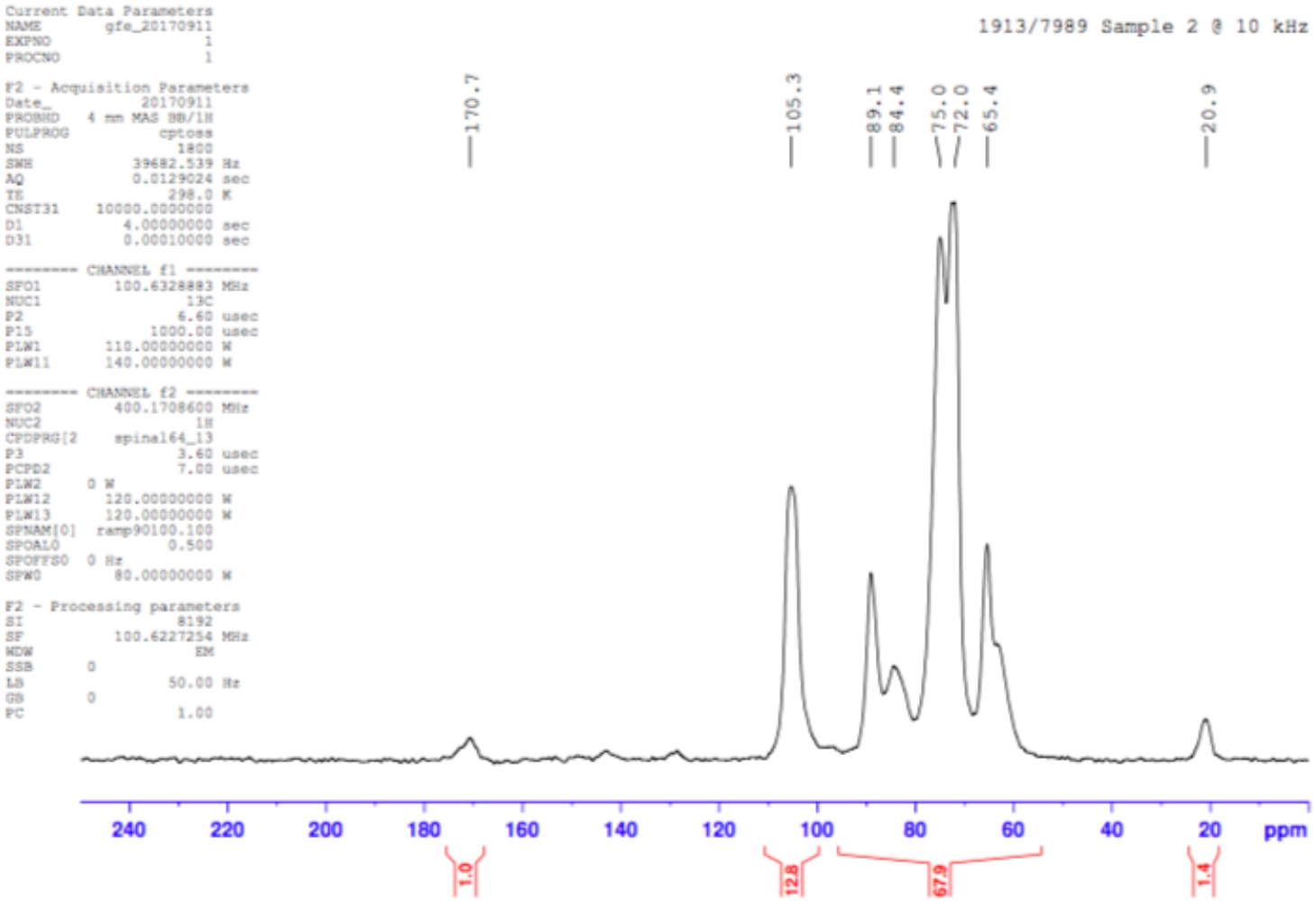

Figure A CP ^{13}C Solid-state NMR spectrum of NCC-Ac dispersed.

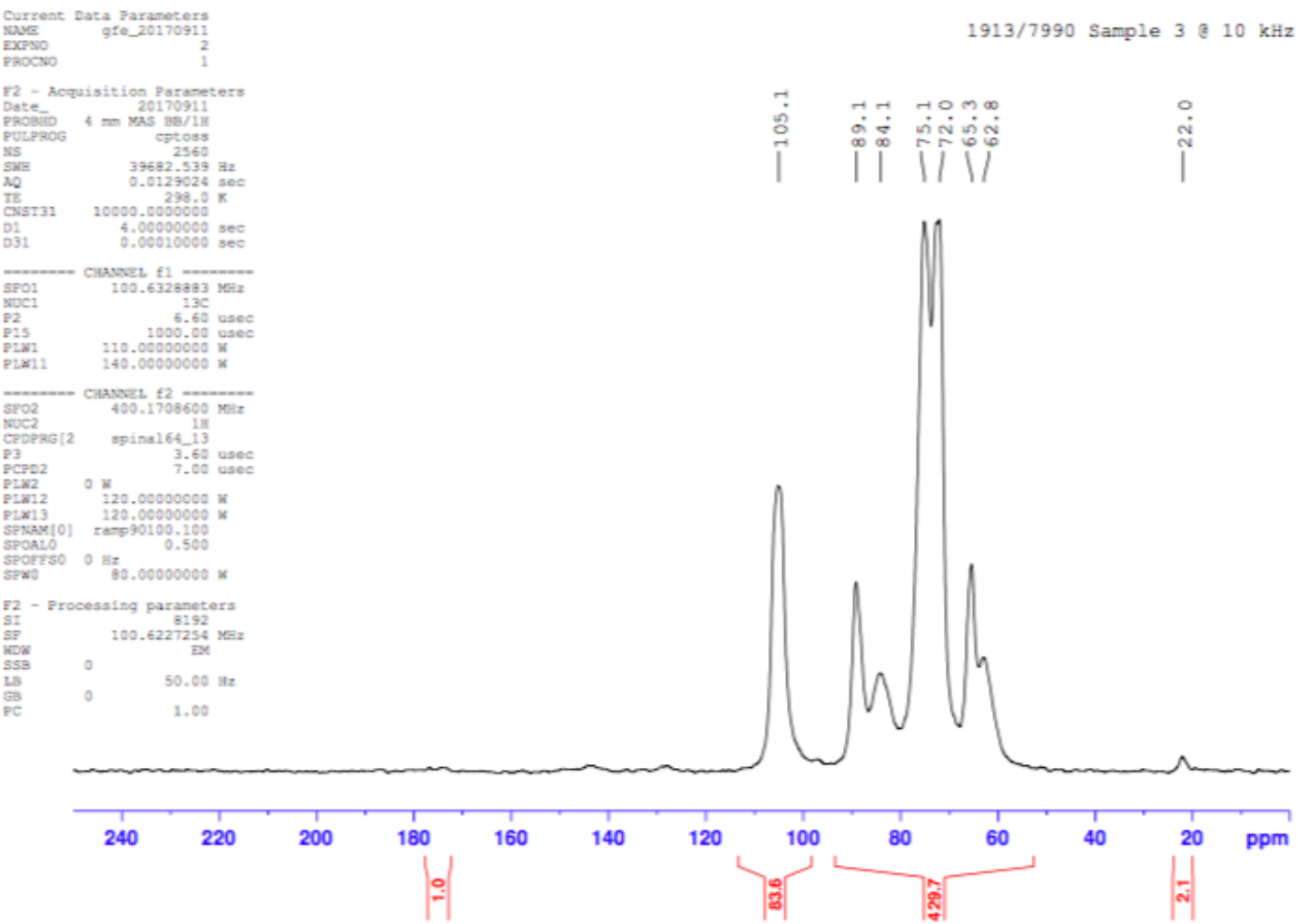

Figure A CP ^{13}C Solid-state NMR spectrum of NCC-Ac gel-py.

Appendix 7 The properties of NCC

625, President-Kennedy avenue
Office 1501
Montreal (Quebec)
Canada H3A 1K2
514-360-1023
www.celluforce.com

Product Specification

Product Name: NanoCrystalline Cellulose (NCC™)
Product Code: CelluForce NCV100
Chemical Name: Cellulose hydrogen sulphate sodium salt
CAS No.: 9005-22-5

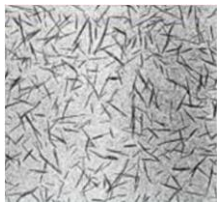

PARAMETER	SPECIFICATION
Product form	Spray dried powder
Appearance (color)	White
Product bulk density	0.7 g/cm^3
Molecular formula	[($C_6O_5H_{10}$)22-28 SO_3 Na]4-6
Specific surface area	400 m^2/g
Gram molecular weight	14,700-27,850
Moisture content (powder)	4-6%
Particle size (powder)	1-50 µm
Particle diameter (crystallite)*	2.3-4.5 nm (by AFM)
Particle length (crystallite)*	44-108 nm (by AFM)
Crystalline fraction*	0.88 (by XRD)
Crystallite density	1.5 g/cm^3
Sulfur content*	0.86-0.89 %
Sulfate content*	246-261 mmol/kg
pH (dispersed in water)	6-7
Hydrodynamic diameter*	70 nm (by DLS)
Ionic strength	230-270 mmol/kg
Zeta potential*	-37 mV

CelluForce warrants that at the time of the quality release or subsequent retest date this product conformed to the information contained in this publication. Purchaser must determine the suitability of the product for its particular use. For further inquiries, or for ordering information, please visit **www.celluforce.com**.

*Parameters marked with an asterisk measured by the National Research Council of Canada.

Date of issue: 09 September 2016 1 of 1